Reducing the air quality impacts of aircraft activity at airports

by
Akshay Ashok

B.S. Aeronautical and Astronautical Engineering, Purdue University, 2009
S.M. Aeronautics and Astronautics, Massachusetts Institute of Technology, 2011

SUBMITTED TO THE DEPARTMENT OF AERONAUTICS AND ASTRONAUTICS
IN PARTIAL FULFILLMENT OF THE REQUIREMENTS FOR THE DEGREE OF

DOCTOR OF PHILOSOPHY IN AERONAUTICS AND ASTRONAUTICS

AT THE
MASSACHUSETTS INSTITUTE OF TECHNOLOGY

JUNE 2016

Signature of Author...
Department of Aeronautics and Astronautics
June 2016

Certified by...
Steven R.H. Barrett
Associate Professor of Aeronautics and Astronautics
Chair, Thesis Committee

Certified by...
Hamsa Balakrishnan
Associate Professor of Aeronautics and Astronautics
Member, Thesis Committee

Certified by...
Ian A. Waitz
Dean of Engineering
Jerome C. Hunsaker Professor of Aeronautics and Astronautics
Member, Thesis Committee

Accepted by..
Paulo C. Lozano
Associate Professor of Aeronautics and Astronautics
Chair, Graduate Program Committee

Reducing the air quality impacts of aircraft activity at airports

by Akshay Ashok

Abstract

Air transportation is an integral part of the economy and the transportation infrastructure. However, aircraft activity at airports generates CO_2 emissions that affect the climate and other pollutants that affect air quality and human health. The focus of this thesis is to enable the reduction of the air quality impacts of aircraft operations at airports by (1) advancing the understanding of the relationship between aircraft activity and its air quality impacts and (2) evaluating the air quality benefits of controlling aircraft operations.

There are atmospheric conditions where decreasing fuel burn (which is directly proportional to CO_2 emissions) results in increased population exposure to fine particulate matter ($PM_{2.5}$) and ozone (O_3). This thesis quantifies the duration and magnitude of the tradeoffs between CO_2 emissions and population exposure. The research complements current studies that optimize aircraft operations at airports for CO_2 emissions but have not quantified the air quality implications of doing so. This raises the possibility of reducing the air quality impacts of airports beyond focusing only on minimizing fuel burn.

Next, this thesis characterizes the atmospheric conditions that give rise to tradeoffs between emissions and population exposure to ozone. The ozone exposure response to nitrogen oxide (NO_x) and Volatile Organic Compound (VOC) emissions is quantified as a function of ambient NO_x and VOC concentrations using ozone exposure isopleths. This is the first time that ozone exposure isopleths are created for all locations in the US, using emission sensitivities from the adjoint of an air quality model. Metrics are calculated based on the isopleths which can be used to determine whether NO_x and VOC emission reductions will improve ozone exposure or be counter-productive and the optimal NO_x/VOC reduction ratio.

Finally, this thesis calculates, for the first time, the air quality and climate benefits of pushback control and de-rated takeoffs for simulated aircraft operations at the Detroit Metropolitan Wayne County Airport (DTW). Operations are also optimized for minimum air quality, environmental and fuel combustion-related costs. The results show that the gate holding strategy is effective in mitigating the environmental impacts of taxi operations at airports, reducing CO_2 emissions and air quality impacts by 35-40% relative to a baseline without gate holds. De-rated takeoffs at 75% thrust are effective in

reducing the air quality impacts of takeoff operations by 19% but increase fuel burn by 3% relative to full-thrust takeoffs. Environmental costs are minimized with average optimal thrust setting of 81%, while maintenance cost savings are estimated to be 2 orders of magnitude larger than the increase in fuel costs from de-rated takeoffs.

Thesis supervisor: Steven R.H. Barrett
Title: Associate Professor of Aeronautics and Astronautics

Thesis committee member: Hamsa Balakrishnan
Title: Associate Professor of Aeronautics and Astronautics

Thesis committee member: Ian. A. Waitz
Title: Dean of Engineering, Jerome C. Hunsaker Professor of Aeronautics and Astronautics

Thesis reader: R. John Hansman
Title: Professor of Aeronautics and Astronautics

Thesis reader: Raymond L. Speth
Title: Research Scientist at the Laboratory for Aviation and the Environment

Acknowledgements

I express my sincerest gratitude to Prof. Steven Barrett, my thesis advisor. Through the past five years, his guidance and mentorship have groomed me to become a more mature researcher, a more effective educator and a better communicator (no more waffle!). I am honored to have completed this PhD under his advisement and am inspired by his unwavering determination to tackle large and impactful problems.

I thank Prof. Hamsa Balakrishnan for the many discussions we've had on airport operations that I have thoroughly enjoyed, in large part due to her enthusiasm for the research. Her guidance was instrumental in enabling me to complete this thesis. Dean Ian Waitz has had a profound influence on me during my time at MIT. He has provided encouragement when needed, sage advice when appropriate and insightful perspectives when it mattered. For that, I am truly grateful.

I have had the privilege of receiving encouragement, support, deep discussions and camaraderie from members of the lab, and I convey my deepest thanks to them. Fabio, for whom I'll always be the IT guy, was my brother-in-arms throughout classes and research at MIT. Sergio brought forth a fascinating new perspective to life. Philip contributed many ideas that were just at the edge of my reach, including those on good eats around town. Steve remains a good friend and colleague, inspiring discussions scientific, technical and otherwise. Chris is a true companion for coffee and snack breaks who continues to immerse me in local culture. I have enjoyed Philosophical Fridays (and other such alliterations), thanks to Irene who smiled politely at all the random things I professed and bade me a good noon afterwards. I thank Lawrence for many intriguing conversations, especially ones where we just take it, and go. The enthusiasm and positive energy of Luis has renewed my spirits time and again, both inside and outside of lab. Pooja is an unparalleled source of motivation, some of which I tapped into during the final steps of the thesis. I appreciate the random (yet refreshing) surprise visits of Parth and Jamin, keeping me guessing as to the next visit to Penang. I am thrilled to have shared my aviation geekiness with several in the lab, chief amongst whom are Robert and Florian.

I must make mention of the tireless efforts of Jennie, Melanie, Beth and Robin for their assistance on numerous occasions, prompt and always with a smile. This journey was so much smoother thanks to your efforts.

I would like to thank NASA for providing financial assistance for the majority of my PhD, and especially acknowledge William Chan and Dr. Banavar Sridhar for stimulating discussions and pleasant hospitality during my visits to NASA Ames.

I now acknowledge the bedrock of my thesis effort, my family members: Appa, Amma, Abhishek and Anubhav. Also included in the team is my good friend, Shahid. There is no one better to fulfil the roles you have played, and I am blessed to have your support.

Contents

List of Figures

List of Tables

Chapter 1

Introduction

Air transportation is an integral part of the economy and the transportation infrastructure, generating an annual economic output of USD 1.6 trillion in the US in 2015 (EDR Group et al., 2015) and moving ~800 million passengers (BTS, 2016a). However, aircraft operations are responsible for a number of environmental externalities, including noise impacts on near-airport population as well as air quality and climate impacts that affect people regionally and globally (Mahashabde et al., 2011; Wolfe et al., 2014; Yim et al., 2015). Air quality impacts are a public health concern as population exposure to particulate matter less than 2.5 micrometers in aerodynamic diameter ($PM_{2.5}$) and ozone (O_3) is associated with increased risk of mortality and morbidity (USEPA, 2011; WHO, 2008, 2006). Premature mortalities due to aircraft emissions near airports (i.e. emissions within 3000ft of airports, referred to as the Landing and Take-Off (LTO) cycle) have been most recently estimated at 650 early deaths in North America, accounting for 43% of total aviation-attributable health impacts in the region with monetized damages of 2006 USD 3.07 bn (Yim et al., 2015).

There is growing pressure on US airlines and airports to mitigate aviation's environmental and particularly human health impacts. The Federal Aviation Administration (FAA) has set forth goals as part of the development of the Next Generation Transportation System (NextGen) to mitigate the effect of aviation operations on significant adverse air quality and health impacts by 2025, to halve aviation-attributable health impacts by 2018 relative to a 2005 baseline and be on a

trajectory for carbon-neutral growth by 2018 (FAA, 2012). Furthermore, airports located within non-attainment areas in the US – i.e. where pollution levels exceed the US National Ambient Air Quality Standards (NAAQS) – are required by the US Environmental Protection Agency (US EPA) to implement measures that bring pollution levels into compliance (40 C.F.R. §51.110, (FAA, 2010)). This task may become more challenging in future for two reasons. First, air traffic in the US is forecast to grow at ~3% per year over the next 20 years (The Boeing Company, 2013). Second, the health impacts of aviation in the future are expected to approximately double as a result of anticipated changes in non-aviation anthropogenic emissions (Levy et al., 2012). The latter is attributed to increased availability of free ammonia in the atmosphere, which results in increased ammonium nitrate $PM_{2.5}$ formation from aviation NO_x emissions (Woody et al., 2011).

This thesis is focused on enabling the reduction of the air quality impacts of aircraft operations at airports. First, previous research is reviewed in section 1.1 pertaining to current assessments of aviation's air quality impacts and improving the environmental impacts of aircraft operations at airports. Section 1.2 outlines the core contributions of this thesis towards reducing the air quality impacts of aircraft operations at airports. Finally, section 1.3 provides the organization of the remainder of this thesis.

1.1 Background and review of previous research

1.1.1 Aircraft operations at airports

A brief narrative of typical aircraft operations at US airports is provided here, paraphrased from Belobaba et al. (2009) and Lee and Balakrishnan (2010). Readers are referred to these sources for a more detailed description of aircraft operations. When a flight is ready to depart, the flight crew requests for clearance to push back from ramp control or air traffic control (ATC). The controller may issue a gate hold or expected takeoff time in response to airport congestion, routing conflicts or adverse weather. Once pushed out of the gate area, the engines are started and the flight crew requests for taxi-out clearance and a routing to the departure runway. The aircraft may experience taxi

delays en-route to the runway due to surface congestion or if there are many departures ahead of it in the takeoff queue.

Once cleared, the pilot applies takeoff thrust and the aircraft begins its ground roll. The takeoff may be accomplished at reduced or "de-rated" thrust (up to 25% from the maximum setting) to reduce engine wear and mitigate noise impacts (FAA, 1988; Lee, 2005). The decision to de-rate is subject to takeoff safety limits, aircraft performance margins, runway availability and meteorological factors. Once airborne, the aircraft climbs to the thrust reduction altitude where it accelerates to its low-altitude climb speed and continues the climb-out.

Arriving aircraft, after touching down and vacating the runway, establish contact with ground control for their taxi-in route. The flight may incur delays if its gate is occupied by a delayed departure. Once parked at the gate, the aircraft shuts its engines down and the disembarkation process begins. Departures and arrivals occur simultaneously, share the airport resources, and interact with each other on the taxiways.

1.1.2 Improving the environmental impacts of aircraft operations at airports

Efforts to reduce the environmental impacts of airport operations have been coupled to the goal of reducing ground delays during taxi. This is based on the understanding that reducing taxi times would reduce fuel burn and emissions, and thereby reduce air quality and climate impacts. Departure metering strategies have been proposed that reduce taxi delays by regulating the number of aircraft on the airport taxiways (Carr et al., 2002; Idris et al., 2002, 1998; Pujet et al., 1999; Simaiakis and Balakrishnan, 2009). Balakrishnan and Jung (2007) developed an integer programming formulation to optimize throughput of airports and minimize delays incurred by taxiing aircraft through taxi re-routing and pushback scheduling (i.e. holding departing aircraft at their gates to reduce surface congestion instead of pushing back immediately). The results showed up to an 18% reduction in average taxi-out time at the Dallas/Fort-Worth International Airport (DFW). Burgain et al. (2008) proposed a pushback control strategy ("N-control") and showed that it could reduce average passenger delays by up to 15% during congested conditions. Lee and Balakrishnan (2010) extended the work of

Balakrishnan and Jung (2007) to include additional operational constraints that exist in practice, and showed reductions in departure taxi times of 55% using a simulation of taxi operations at the Detroit Metropolitan Wayne County Airport (DTW). Simaiakis and Balakrishnan (2010) estimated that the elimination of taxi delays at New York John F. Kennedy International Airport (JFK), Newark Liberty International Airport (EWR), Boston Logan International Airport (BOS) and Philadelphia International Airport (PHL) in 2007 could theoretically achieve ~50% reduction in fuel burn and emissions from taxi operations.

Other research studies have had the explicit goal of minimizing aircraft fuel burn and emissions. An analysis of the N-control pushback control strategy at BOS showed 1-5% reduction in fleet-wide fuel burn and emissions for 4 frequently used runway configurations, and up to 20% reduction during congested periods (Simaiakis and Balakrishnan, 2010b). Nikoleris et al. (2011) developed a fuel burn and emissions model for estimating aircraft fuel burn and emissions from taxi operations at DFW using aircraft position data and assumed thrust levels. Applying this model, Jung et al. (2011) quantified the reductions in taxi delay, fuel burn and emissions of a departure scheduling algorithm at DFW and found a 66% reduction in departure delay and a ~38% reduction in fuel consumption and hydrocarbon (HC), carbon monoxide (CO) and nitrogen oxide (NO_x) emissions. Levine and Gao (2007) found a 43% reduction in NO_x, HC and CO emissions from schedule de-peaking (spreading out departure demand evenly throughout the day) at EWR. Deonandan and Balakrishnan (2010) estimated a 25-60% reduction in fuel burn and emissions from single-engine taxiing, operational tow-outs and advanced queue management techniques. King and Waitz (2005) found that de-rated takeoffs (i.e. taking off with less than 100% thrust) reduce LTO NO_x emissions by 0.7% and increase fuel burn by 0.6% for every percent de-rate in thrust for B777 aircraft.

Pushback control and departure metering strategies have been tested in field trials. Simaiakis et al. (2011) implemented a pushback rate control strategy during eight four-hour field trials conducted at BOS and found reduced taxi-out times by 4-5 minutes on

average (compared to an average taxi-out time of ~20 minutes) and 12-15 tonnes of fuel savings (50-60 kg per flight). In another field trial at BOS, the authors calculated optimal pushback rates using a dynamic programming approach accounting for random delays and periodic updates. They estimated a reduction of ~8 tonnes of fuel burn (~57 kg per flight) (Simaiakis and Balakrishnan, 2012). Departure metering trials at New York's John F. Kennedy International airport reduced taxi-out times by 14800 hours, reduced fuel consumption by ~19 million liters and lowered CO_2 emissions by 48,000 tonnes (Nakahara et al., 2011). As a point of comparison, Deonandan and Balakrishnan (2010) estimated an average fuel burn per flight of 521 kg at JFK and 270 kg at BOS using flight activity data from the Bureau of Transportation Statistics (BTS) and Federal Aviation Administration's Airspace System Performance Metrics (FAA ASPM) databases for 2007.

1.1.3 Aviation's impact on air quality

Aircraft engines produce gaseous emissions of carbon dioxide (CO_2), water vapor, carbon monoxide (CO), sulfur dioxide (SO_2), volatile organic compounds (VOCs; also referred to as unburned hydrocarbons, HC) and oxides of nitrogen (NO_x). Aircraft engines also emit volatile particulate matter in the form of organic carbon (OC) and sulfates ($SO_4^=$), as well as non-volatile particulate black carbon (BC). The majority of particulates are emitted in the form of $PM_{2.5}$ (Stettler et al., 2011). Primary $PM_{2.5}$ (BC, OC, $SO_4^=$) which are emitted from the engine directly contribute to ambient $PM_{2.5}$ concentrations through atmospheric dispersion (Barrett et al., 2013; Barrett and Britter, 2008). Emissions of gaseous species of NO_x, SO_2, CO and HC are precursors to secondary $PM_{2.5}$ and O_3 concentrations via chemical reactions in the atmosphere (Ashok et al., 2013; Barrett et al., 2010; Seinfeld and Pandis, 2006). A number of epidemiological studies have found chronic (long term) exposure to elevated levels of $PM_{2.5}$ or O_3 to be positively correlated with increased premature mortality and morbidity (Dockery et al., 1993; Jerrett et al., 2009; Krewski et al., 2009; Pope et al., 2002). These form the basis for the assessment of the public health impacts of air pollution by regulatory agencies in the US and Europe (USEPA, 2011; WHO, 2008, 2006).

Several works have quantified the contribution of aircraft activities at selected airports to near-airport concentrations of $PM_{2.5}$, O_3 and other gaseous species via modeling and measurement campaigns (Adamkiewicz et al., 2010; Carruthers et al., 2011; Carslaw et al., 2006; Diez et al., 2012; Dodson et al., 2009; Hsu et al., 2013, 2012; Hu et al., 2009; Lobo et al., 2012; Schürmann et al., 2007; Unal et al., 2005; Westerdahl et al., 2008; Yu et al., 2004). Regional- and global-scale impacts of aviation have been calculated using 3-dimensional chemical-transport and dispersion models. For instance, regional impacts in the US, considering only LTO emissions, are estimated to be 75-650 premature mortalities from aviation in 2005 (Ashok et al., 2013; Brunelle-Yeung et al., 2014; Levy et al., 2012; Mahashabde et al., 2011; Yim et al., 2015) with monetized damages between 2006 USD 1.5 bn - 3.1 bn (Brunelle-Yeung et al., 2014; Wolfe et al., 2014; Yim et al., 2015). Regional-scale impacts of aviation in Europe and Asia as well as global scale impacts of aviation have also been quantified in the literature (Barrett et al., 2010; Koo et al., 2013; Yim et al., 2015, 2013).

A limited number of research studies have investigated the air quality benefits of operational mitigation strategies. Yim et al. (2013) found up to 65% of premature mortalities from airport emissions in the UK could be avoided by using ground electric power, electrification of ground support equipment, single-engine taxiing and desulfurizing jet fuel. Barrett et al. (2012) estimate that global implementation of desulfurized jet fuel could reduce aviation-attributable premature mortalities by 900-4000 incidences. Dorbian et al. (2011) estimate annual air quality damages of $230 per tonne of fuel burned within the LTO cycle at US airports.

1.1.4 Tradeoffs between air quality and climate impacts

Aircraft activity has adverse impacts on air quality, as shown by the literature reviewed in the previous section. Emissions from aircraft activity also impact the climate: CO_2 emissions exert a warming effect on the atmosphere, while aerosols affect the radiative balance of the Earth directly and indirectly (Lee et al., 2010). In the mitigation of these environmental impacts, however, tradeoffs can exist where a reduction in one of CO_2

emissions or $PM_{2.5}/O_3$ population exposure corresponds to an increase in the other. Prior research on such tradeoffs (mostly from a non-aviation context) is reviewed below.

Tradeoffs between greenhouse gas emissions and air quality impacts have been identified with the introduction of alternative technologies and fuels. For example, shifts in household fuel choice and woodstove technology that lead to health benefits may have increased GHG impacts (Bailis, 2005; Freeman and Zerriffi, 2012; Grieshop et al., 2011). Power-plants with carbon capture technologies emit less CO_2 emissions but could incur an efficiency penalty that increases emissions of NO_x and other gases (Koornneef et al., 2010; Tzimas et al., 2007). The use of alternative fuels and engine technology has also been studied in the context of automobiles by MacLean and Lave (2000), who found direct-injection diesel engines may not be able to meet strict emission standards without lowering efficiency. Aircraft engine technologies, under consideration by International Civil Aviation Organization's Committee on Aviation Environmental Protection (ICAO CAEP) to meet stringencies on NO_x emissions were shown by Mahashabde et al. (2011) to reduce air quality impacts but emit more CO_2 due to engine efficiency penalties.

Sulfate particles have a cooling effect on the atmosphere due to their reflectivity of sunlight but also contribute to adverse human health impacts. Regulating emissions of sulfate particulate emissions or precursor gases could lead to climate-air quality tradeoffs. For example, Barrett et al. (2012) identified a climate-air quality tradeoff relevant to cruise emissions – that of desulfurizing jet fuel. They estimated that reduced aerosol loading resulting from global desulfurization of jet fuel would result in a net climate warming equivalent to ~10% of the warming from aviation CO_2 emissions. Similar tradeoffs involving de-sulfurized marine bunker oil have also been reported (Lack et al., 2011; Partanen et al., 2013). Aardenne et al. (2009) studied global climate change policies for future years targeted at fuel and technology shifts and energy savings. They found that ambitious air pollution controls would lead to an almost doubling of the overall radiative forcing relative to a scenario without these controls, due to the reduction of sulfate aerosols.

Tradeoffs between air quality and climate could arise when emissions reductions – associated with reduced fuel consumption and therefore reduced CO_2 emissions – lead to air quality degradation instead of improvements. An example of this is the ozone weekend effect in major cities (Cleveland et al., 1974; Cleveland and McRae, 1978; Lebron, 1975), where elevated ozone concentrations were seen during weekends relative to weekdays. This is attributed to larger reductions in NO_x relative to VOC emissions within the city as a result of lowered diesel traffic during weekends (Heuss et al., 2003), where the nonlinearity of NO_x-VOC-O_3 chemistry leads to increases in O_3 due to NO_x reductions in polluted urban environments. Emissions reductions may also increase $PM_{2.5}$ concentrations. For instance, a NO_x control strategy in Europe was found to increase $PM_{2.5}$ concentrations during the winter (Megaritis et al., 2013). This was found to be the result of increased availability of oxidants to convert SO_2 and VOCs into $PM_{2.5}$. Reductions in sulfate aerosols due to NO_x emissions have been noted (Ashok et al., 2013; Mahashabde et al., 2011; Pinder et al., 2008; Zhang and Wu, 2013), attributed to competition for free ammonia in the atmosphere. Increases in nitrate PM due to sulfur emission controls have been observed (Barrett et al., 2012; West et al., 1999), as a result of increased transfer of nitric acid to the aerosol phase.

1.2 Thesis contributions

This thesis is focused on the mitigation of the air quality impacts of aircraft operations at airports, and presents research that addresses this objective in two ways. First, this research furthers the understanding of the links between aircraft activity and its air quality impacts by quantifying tradeoffs between fuel burn (and associated emissions) and air quality impacts. Second, this thesis evaluates the air quality benefits achievable via the control of aircraft operations at airports. These goals are accomplished via the three core contributions of this thesis listed below:

1. **Assessment of the air quality-CO_2 tradeoff potential at US airports.** Current approaches to reducing the environmental impacts of aircraft operations are based upon reducing fuel burn and emissions. While the potential for optimizing aircraft surface movements to minimize CO_2 emissions has been assessed in the

literature, the implications of CO_2 emissions minimization for air quality have not previously been quantified. The work presented in this thesis is the first to quantify the extent of the tradeoff between CO_2 emissions and air quality impacts at US airports. This raises the possibility of reducing the air quality impacts of airports beyond minimizing fuel burn as well as optimizing for minimum net environmental impact.

2. **Characterization of the ozone exposure response to emissions reductions.** Efforts to mitigate population exposure to ozone involve reducing emissions of NO_x and VOCs. However, nonlinearities in the NO_x-VOC-O_3 chemistry could result in increased O_3 exposure from reductions in NO_x emissions depending on ambient NO_x and VOC concentrations (e.g. in polluted urban environments). This thesis characterizes the ambient conditions in which this tradeoff occurs by quantifying the ozone exposure response to NO_x and VOC emissions as a function of ambient atmospheric VOC and NO_x concentrations at each location in the contiguous US. Metrics are developed which can be used to determine whether NO_x and VOC emission reductions will improve ozone exposure impacts or will be counter-productive and the optimal NO_x/VOC reduction ratio. This is the first research effort to perform such a quantification for all locations in the contiguous US.

3. **Quantification of the air quality benefits and associated tradeoffs of the pushback control and de-rated takeoff mitigation strategies.** Previous studies have evaluated the fuel burn and emissions reductions of environmental mitigation strategies, but few have related them to the resulting air quality impacts (Barrett et al., 2012; Yim et al., 2013). In this work, the air quality and climate benefits of the pushback control and de-rated takeoff emission reduction measures are quantified for aircraft operations at DTW. Aircraft operations are optimized for air quality, environmental and fuel combustion-related costs beyond fuel burn minimization, and tradeoffs between air quality impacts and fuel burn/CO_2 emissions are quantified. This is the first time that the air quality benefits of the pushback

control and de-rated takeoff strategies have been quantified and is also the first attempt at controlling aircraft movements at airports with the objective of minimizing air quality impacts.

1.3 Outline of thesis

The organization of this thesis mirrors the order of the core contributions defined in section 1.2. Chapter 2 quantifies the air quality-CO_2 tradeoff potential for airports. Chapter 3 characterizes ozone exposure response to emission reductions as a function of ambient conditions for all locations in the US. Chapter 4 presents an analysis of benefits and tradeoffs of pushback control and de-rated takeoffs. Each chapter includes a description of the methods used in that study, followed by a discussion of the results, and ends with a summary of the main findings and limitations of the study.

Chapter 2

Quantifying the air quality-CO_2 tradeoffs at airports

This chapter presents research that quantifies conditions in which there is a tradeoff between aircraft CO_2 emissions and population exposure to secondary $PM_{2.5}$ or O_3. A "tradeoff" is defined as where a reduction in one of CO_2 emissions or exposure corresponds to an increase in the other. As noted in section 1.1.4, tradeoffs can occur when the atmospheric response to emissions, associated with fuel burn and therefore CO_2 emissions, is negative. For example, NO_x emissions may reduce O_3 under certain conditions due to nonlinear O_3 photochemistry (Seinfeld and Pandis, 2006). Similarly, NO_x emissions may decrease $PM_{2.5}$ based on the availability of ammonia (Ashok et al., 2013).

There are two main goals of this work. The first is to identify time periods (at three-hourly intervals over a year) in which a tradeoff between CO_2 emissions (which are directly proportional to fuel burn) and population exposure to $PM_{2.5}$ and O_3 exists. The second goal is to identify airports with relatively high population exposure reduction potentials beyond CO_2 minimization– i.e. airports that have a relatively high magnitude and duration of tradeoff between fuel burn and population exposure.

This chapter is organized as follows. First, the methods used to assess tradeoffs between fuel burn and air quality impacts are described in section 2.1. An example of a CO_2 – air quality tradeoff condition is shown in section 2.2. The duration and magnitudes of these

tradeoffs are quantified in sections 2.3 and 2.4, respectively. Airports with relatively high reduction potentials are identified in section 2.6. Section 2.7 assesses the magnitude of aircraft and airport emissions relative to other near-airport anthropogenic emission sources. Finally, section 2.8 summarizes the results of this chapter.

2.1 Methods

In section 2.1.1 the estimation of aircraft emissions is described. Section 2.1.2 provides an overview of the air quality modeling that is used to quantify population exposure to $PM_{2.5}$ and O_3 attributable to aircraft emissions. The tradeoff between CO_2 emissions (directly proportional to fuel burn, F) and $PM_{2.5}$ and O_3 population exposure (P) is defined in section 2.1.3. The approach to quantifying the tradeoff at US airports is detailed in section 2.1.4.

2.1.1 Emissions modeling

The total mass of emissions of species i, M_i, from a given engine can be written as a product of an emission index (EI) (defined in aviation as grams of pollutant emitted per kilogram of fuel burned) and the fuel consumed, i.e. $M_i = F \cdot EI_i(\dot{m}_f)$, where the emission index is specific to an engine type and may be a function of the rate of fuel burn, $\dot{m}_f$. The rate of fuel burn is approximately proportional to engine thrust (Wey et al., 2007).

Emission species considered in this work include CO, HC, NO_x and SO_2, which are precursors for secondary $PM_{2.5}$ and O_3 formation. Population exposure to primary $PM_{2.5}$ (that is, BC, OC and $SO_4^=$ that are directly emitted from the engine) is proportional to emissions and therefore no tradeoffs occur. Furthermore, secondary $PM_{2.5}$ contributes to ~80% of total $PM_{2.5}$ population exposure from US LTO activity in 2018 (Ashok et al., 2013). Emissions are computed using the Aviation Emissions Inventory Code (AEIC) v2.1 (Simone et al., 2013; Stettler et al., 2011), with modifications. Emission indices are estimated according to the Boeing Fuel Flow Method 2 (BFFM2) (Baughcum et al., 1996). The BFFM2 method uses engine emission certification data from the International Civil Aviation Organization (ICAO), tabulated in the engine emissions databank (ICAO, 2012). Engines are certified at standard thrust settings of 7%, 30%,

85% and 100%, representing engine operation during the taxi/idle, approach, climb-out and takeoff phases of flight. For an arbitrary thrust setting, the BFFM2 method prescribes a log-linear interpolation for the NO_x emission index (EI_{NO_x}) and a log bi-linear interpolation for EI_{HC} and EI_{CO}. EI_{SO_2} is independent of thrust and is calculated assuming a fuel sulfur content (FSC) of 600 ppm with a S^{IV} - S^{VI} oxidation efficiency of 2% (Stettler et al., 2011). Uncertainty distributions are applied that account for variability and deviations in EIs from the ICAO emissions certification measurements upon which emissions estimates are based (Stettler et al., 2011).

The current work includes changes to emissions modeling at low thrust and modeling the dependence on ambient conditions beyond those presented in (Stettler et al., 2011). These are described in the following two sections.

Estimation of EIs at low thrust

Hydrocarbon and CO emission indices increase as thrust is decreased due to incomplete combustion of jet fuel at relatively low combustion temperatures. The BBFM2 over-predicts CO and HC emissions at thrust settings below the lowest certification measurement (7%) that is available for all engines. Based on new and existing experimental data, Herndon et al. (2012) propose the use of a linear relationship between EI_{HC} and fuel flow rate at thrusts below 7%. In particular, for thrust settings below 7% their suggested relation of

$$\frac{EI_{HC}(\dot{m}_f)}{EI_{HC}\left(\dot{m}_{f_{7\%}}\right)} = 1 - a_{HC}\left(\dot{m}_f - \dot{m}_{f_{7\%}}\right), \qquad \text{Eq. 2-1}$$

is adopted, where $a_{HC} = 52$ s kg^{-1}±23% is the fuel flow dependence parameter for EI_{HC}. A similar expression for EI_{CO} is derived using the experimental data included in the appendix A of Herndon et al. (2012), i.e.

$$\frac{EI_{CO}(\dot{m}_f)}{EI_{CO}\left(\dot{m}_{f_{7\%}}\right)} = 1 - a_{CO}\left(\dot{m}_f - \dot{m}_{f_{7\%}}\right), \qquad \text{Eq. 2-2}$$

where $a_{CO} = 29$ s kg^{-1}±23% is the fuel flow dependence parameter for EI$_{CO}$. The uncertainty in the fuel flow dependence parameters includes measurement errors and the spread in observed emission indices (Herndon et al., 2012).

Dependence on ambient conditions

The dependence of NO$_x$ emissions on ambient conditions is modeled according to the BFFM2 method. Ambient temperature, pressure and humidity are used to compute correction factors to the ICAO certification EIs, which assume sea level standard atmospheric conditions.

Temperature correction for HC emissions follow the approach of Herndon et al. (2012), who find a negative correlation between Volatile Organic Compounds (VOC) emissions and temperature at low thrust (<7%). No data is available for the influence of ambient temperature on CO emissions at low thrust. The same relative correction factors as for HC are assumed for CO, on the basis that ambient temperature influences the combustor inlet and operating conditions (Lyon et al., 1979) and the formation of both pollutants is determined by combustion efficiency.

GEOS-5 meteorological data from the NASA Global Modeling and Assimilation Office (GMAO) for the year 2006 is used to calculate EI correction factors at US airport locations. Across all airport locations considered in this study, the correction factors are found to be normally distributed with a standard deviation of 8% for EI$_{NO_x}$ and uniformly distributed between ±50% for EI$_{HC}$.

2.1.2 Regional air quality modeling

Population exposure to ozone is calculated using the adjoint of the GEOS-Chem model (GEOS-Chem Adjoint v33). GEOS-Chem is a tropospheric chemistry-transport model (Bey et al., 2001) that calculates transport, gas- and aerosol-phase chemistry, as well as wet and dry deposition. The standard GEOS-Chem simulation of HO$_x$-NO$_x$-VOC-O$_3$ chemistry including aerosols as described by Bey et al. (2001) is used, with updated chemical reactions and reaction rates from JPL/IUPAC. The modeling domain applied in this study encompasses the contiguous US between 140°W to 40°W and 10°N to 70°N.

The resolution of the horizontal grid is 0.5° × 0.667° (latitude × longitude, approximately 50 km resolution over North America), with 47 vertical layers up to 80 km and a surface layer depth of ~120m. Boundary conditions for the domain are obtained from a GEOS-Chem simulation for the global domain (at 4° × 5° resolution). Emission inputs include the 2005 National Emissions Inventory in the US, the BRAVO inventory for Mexico and 2005 CAC inventory for Canada.

Meteorological data for the year 2006 from the NASA GMAO GEOS-5 modeling system (Rienecker et al., 2008) is used to drive GEOS-Chem. The GEOS-5 Atmospheric General circulation Model (AGCM) has been evaluated against surface, upper-air and satellite observations for several years including 2006 (Decker et al., 2011; Jordan et al., 2010; Yi et al., 2011). Surface air temperatures are found to be well-correlated (*r>0.9*) to World Meteorological Organization observations for 2003-2006 (Yi et al., 2011) and observations from 33 flux towers in North America from 1991-2006 (Decker et al., 2011), with mean biases between 1-2.5 K. Decker et al. (2011) find surface wind speed to be positively biased by ~2 ms^{-1} on average with a correlation of 0.4 - 0.8 based on flux tower measurements in North America. Jordan et al. (2010) find planetary boundary layer (PBL) heights in GEOS-5 are within 25% of Cloud-Aerosol Lidar and Infrared Pathfinder Satellite Observations (CALIPSO) in 2006, with correlation coefficients between 0.47-0.73 in the Western hemisphere and Africa.

The GEOS-Chem model outputs for annual average $PM_{2.5}$, daily maximum O_3, NO_x and VOC species are validated against surface measurements from the US EPA AQS database (US EPA, 2015) for 2006. For O_3, an average annual bias of 7.0 ppb and a correlation coefficient of *R*=0.69 are calculated across all monitor sites (~1200 sites). This is comparable to the model performance reported in other studies (Fiore et al., 2014; Wang et al., 2009; Zhang et al., 2011). The biases are relatively higher near major cities, with 11.7 ppb in the New York Metropolitan Statistical Area (MSA), 8.6ppb in the Los Angeles MSA and 12.2ppb in the Chicago MSA. The high ozone bias would likely lead to overestimation of the magnitude of ozone exposure response predicted by the adjoint sensitivities.

GEOS-Chem predictions for annually-averaged $PM_{2.5}$ concentrations (corrected to include particle bound water for comparison purposes using the Aerosol Inorganic Model by Clegg et al. (1998) are ~40% lower on average than observed Federal Reference Method (FRM) $PM_{2.5}$ data from the EPA's Air Quality System (AQS) database for ~1,000 monitor locations in the US.

The AQS database contains VOC measurements at 6-50 monitor sites (depending on VOC species) across the contiguous US. Annual mean biases for isoprene, formaldehyde and acetone concentrations are -0.2 ppbC, 0.07 ppbC and 1.5 ppbC respectively with correlations between 0.31 and 0.47. Ethane and propane concentrations are under-predicted by 13.3 ppbC and 14.7 ppbC, respectively, likely due to emission plumes being unresolved by the GEOS-Chem model. When compared against measurements in 28 US cities from Baker et al. (2008), however, relatively smaller negative biases are found (-2.0 ppbC for ethane and -2.8 ppbC for propane). Surface NO_x concentrations in 2006 are under-predicted by 10.2ppb on average across ~330 monitor locations. This is driven by under-representation of NO_x near major urban areas, with mean biases of -19.1 ppb, -17.0 ppb and -10.8 ppb in the New York, Los Angeles and Chicago MSAs respectively. Low NO_x biases in GEOS-Chem have been observed in previous studies. For example, Zhang et al. (2012) find that the NO_2 tropospheric column over urban areas of the US in 2006 is under-represented by 15-40% relative to OMI satellite data. Fiore et al. (2002) find that peak NO values are underestimated in an urban area (Nashville, TN) in the summer of 1995 due to emission plumes from power plants being unresolved by the model. Bey et al. (2001) find that GEOS-Chem predicts global NO concentrations in 1994 to within a factor of 2 of observations. Furthermore, the validation does not consider NO_y (a combination of NO_x and its oxidation compounds) which could result in the model being biased low against NO_y measurements from AQS monitors.

The adjoint model of GEOS-Chem, originally developed by Henze et al. (2007) and Singh et al. (2009) and extended to the nested domain by Jiang et al. (2015), is used to compute receptor-oriented sensitivities of national population exposure to $PM_{2.5}$ or O_3 to aircraft emissions; that is, the sensitivity of population exposure with respect to

emissions of each of the modeled species at every location and time in the model domain (Henze et al., 2007; Koo et al., 2013; Sandu et al., 2005). It is based on the forward model described above, and the same grid.

An adjoint model is a computationally efficient way of calculating sensitivities, which are partial derivatives of a quantity of interest with respect to various control parameters. In the present study, annually averaged population exposure to $PM_{2.5}$ or O_3, i.e. $P_{PM_{2.5}}$ or P_{O_3} are the quantities of interest. They are defined as

$$P_{PM_{2.5}} = \frac{1}{N_{steps}} \sum_{k=1}^{N_{cells}} \sum_{t=1}^{N_{steps}} [p(k) \cdot C_{PM_{2.5}}(k,t)] \qquad \text{Eq. 2-3}$$

and

$$P_{O_3} = \frac{1}{N_{steps}} \sum_{k=1}^{N_{cells}} \sum_{t=1}^{N_{steps}} [p(k) \cdot C_{O_3}(k,t)], \qquad \text{Eq. 2-4}$$

respectively, where k indexes GEOS-Chem model surface layer grid cells from 1 to N_{cells}, t indexes model time steps from 1 to N_{steps}, $p(k)$ is the population in grid cell k, $C_{PM_{2.5}}(k,t)$ is the mass concentration (in ng/m^3) of $PM_{2.5}$ at grid cell k at time interval t, and $C_{O_3}(k,t)$ is the mixing ratio (in ppt) of O_3 at grid cell k at time step t. The population data was re-gridded from the 30 arc-second resolution data obtained from the GRUMP 2006 database (Balk et al., 2006). This study considers ozone exposure of the US population only, and therefore the population within grid cells outside the US is set to zero.

The control parameters in this case are the different aviation emission species, M_i. Therefore, the sensitivities computed by the nested grid GEOS-Chem adjoint model are

$$S_i(K,T) = \frac{\partial P}{\partial M_i(K,T)}, \qquad \text{Eq. 2-5}$$

which are computed separately for population exposure to $PM_{2.5}$ or O_3. The units of the sensitivities for each time step therefore are ppl·ngm^{-3}·kg^{-1} and ppl·ppt·kg^{-1} for $PM_{2.5}$ and O_3 respectively, and quantify the change in population exposure given a change in

any of the emission species M_i at each point in time. Note that in this case K is the location of emission (an airport) rather than the location of exposure (denoted by k), thus the sensitivity is for spatially-integrated exposure to emissions at location K. Similarly, while T is the time step of emission, t in Eq. 2-3 - Eq. 2-4 denotes the time step of exposure. The adjoint sensitivities are calculated relative to an emissions scenario which includes aircraft emissions. Second-order effects caused by aviation emissions on the adjoint sensitivities are expected to be negligible (Ashok et al., 2013; Koo et al., 2013). The adjoint simulations were for a 12-month period, with an additional period of 3 months used as the adjoint spin-up time to ensure that the complete impact of the emissions on air quality is captured, assuming that any emission event does not contribute significantly to exposure beyond 3 months after the event. The sensitivities are therefore interpreted as the partial derivatives of annual average total US population exposure with respect to emission of species i at any time and any location. These adjoint-calculated sensitivities are used to estimate exposure, i.e.

$$P(F, K, T, \dot{m}_f) = \sum_i S_i(K, T) \cdot M_i = F \cdot \sum_i S_i(K, T) \cdot \text{EI}_i(\dot{m}_f).$$

<div align="right">Eq. 2-6</div>

The sensitivities S_i are functions of location and time of emissions (in this case, emissions in time interval T at airport K). Thus, population exposure is a function of the total amount of fuel burn (F), the location and time of operation (K and T) as well as the thrust setting of the engine (equivalently the fuel burn rate, $\dot{m}_f$), which affects the EI.

2.1.3 Calculating the tradeoffs between CO_2 emissions and population exposure to $PM_{2.5}$ and O_3

The relationship between population exposure and CO_2 emissions (proportional to fuel burn) is obtained by taking the partial derivative of P with respect to F in Eq. 2-6, to yield

$$\frac{\partial P}{\partial F} = \sum_i S_i(K, T) \cdot \text{EI}_i(\dot{m}_f)$$

<div align="right">Eq. 2-7</div>

The partial derivative denotes the change in population exposure with respect to fuel burn, while holding thrust setting constant for a given time and airport.

It is typically expected that the relationship between aviation fuel burn and the resulting exposure to pollutants is positive. While this assumption may hold true for long-term impacts [for example, as demonstrated by Ashok et al. (2013) and Koo et al. (2013)], hourly atmospheric sensitivities S_i at a given airport location K and time of emissions T may be either positive or negative depending on atmospheric conditions. For example, O_3 formation is dependent on background NO_x and hydrocarbon concentrations, and under certain conditions aircraft emissions may lead to an O_3 reduction. Similarly, a reduction in sulfate $PM_{2.5}$, one of the main components of $PM_{2.5}$, may occur due to increased NO_x emissions based on the competition for free ammonia in the atmosphere. Thus, when combined with emissions indices as per Eq. 2-7, negative atmospheric sensitivities could result in a tradeoff between CO_2 emissions and air quality, i.e. $\partial P / \partial F < 0$.

2.1.4 Approach to quantify tradeoffs

The relationship between CO_2 and population exposure to $PM_{2.5}$ and O_3 is assessed for five commonly-used aircraft engines in the US aircraft fleet. Engines were selected based on activity data obtained from the FAA's Aviation Performance Metrics (APM) database for 2012 for 35 Operational Evolution Partnership (OEP) airports in the US (see section S3 of the SI). The OEP airports are among the busiest in the US, representing more than 70% of passenger traffic in the US (FAA, 2011) and account for 70% of US aviation LTO fuel burn (Ashok, 2011). Table 2-1 lists the engines, their abbreviations used in this paper, and an example aircraft within the US fleet that is powered by the engine.

Table 2-1: Top five aircraft engines (by activity) selected to quantify tradeoffs. The engine manufacturer, name, year of certification, ICAO unique identifier (UID) and abbreviation used in this work are tabulated. An example aircraft within the US fleet that is powered by the engine is also listed.

Engine	(abbrev.)	ICAO UID	Certification	Example aircraft
General Electric CF34-3B	(CF34)	5GE084	1991	Canadair CRJ-200
CFM Int'l. CFM56-7B24	(CFM56)	3CM032	1996	Boeing B737-800
Allison Engine Company AE3007A1	(AE3007)	6AL005	1994	Embraer ERJ-145
Rolls Royce RB211-535E4B	(RB211)	3RR034	1984	Boeing B757-200
Pratt & Whitney JT8D-219	(JT8D)	1PW019	1983	McDonnell Douglas MD88

Eq. 2-7 is evaluated for every set of atmospheric sensitivities over the course of a year (sampled every 3 hours) at all of the OEP airports except Honolulu International Airport, in order to capture spatial and temporal variations in sensitivities. Eight discrete thrust settings are used: 4%, 7%, 10% and 13% to span the range of taxi thrusts, and 85%, 90%, 95% and 100% to span the range of takeoff thrusts. These thrust settings were selected to reflect operational taxi thrust settings and reduced thrust takeoffs observed at airports, and are based on a review of literature from Stettler et al. (2011) and King and Waitz (2005).

2.2 Example of CO_2 – air quality tradeoff

The analysis method in section 2.1.4 results in a four-dimensional "lookup table" of relationships between fuel burn and population exposure indexed by engine type, thrust setting, airport location and time of emissions. As an example, Table 2-2 shows the change in population exposure to $PM_{2.5}$ and O_3 per kilogram fuel burn at Hartsfield-Jackson Atlanta International Airport (ATL), for two of the five engine types, and all eight thrust settings.

Table 2-2: Change in population exposure to $PM_{2.5}$ and O_3, per unit fuel burn at Atlanta's Hartsfield-Jackson airport (ATL). Values are shown for one specific hour (1500-1600 UTC on Jan 10, 2006) and annual average for the RB211 and CFM56 engines. Engine operation is assumed to be at one of the eight thrust settings studied: four taxi thrust settings (4, 7, 10 and 13%) and four takeoff thrust settings (85, 90, 95 100%).

$\partial P/\partial F$		$PM_{2.5}$ exposure [ppl·ngm^{-3}·kg^{-1}]							
Jan 10, 2006, 1500 UTC		**4%**	**7%**	**10%**	**13%**	**85%**	**90%**	**95%**	**100%**
	RB211	0.003	-0.01	-0.02	-0.02	-0.27	-0.30	-0.33	-0.36
	CFM56	0.02	-0.01	-0.02	-0.03	-0.14	-0.15	-0.16	-0.17
Annual average		**4%**	**7%**	**10%**	**13%**	**85%**	**90%**	**95%**	**100%**
	RB211	0.12	0.15	0.17	0.20	1.36	1.49	1.63	1.78
	CFM56	0.24	0.21	0.23	0.24	0.75	0.79	0.83	0.87

$\partial P/\partial F$		O_3 exposure [ppl·ppt·kg^{-1}]							
Jan 10, 2006, 1500 UTC		**4%**	**7%**	**10%**	**13%**	**85%**	**90%**	**95%**	**100%**
	RB211	0.04	-0.17	-0.24	-0.30	-2.65	-2.94	-3.22	-3.51
	CFM56	0.41	-0.11	-0.25	-0.34	-1.44	-1.52	-1.60	-1.67
Annual average		**4%**	**7%**	**10%**	**13%**	**85%**	**90%**	**95%**	**100%**
	RB211	0.40	0.33	0.38	0.46	3.61	3.99	4.37	4.77
	CFM56	1.28	0.65	0.57	0.57	1.78	1.87	1.97	2.06

The values shown in Table 2-2 represent the change in population exposure to $PM_{2.5}$ and O_3 per kilogram of fuel burn annually averaged and for a single hour. The annually averaged values are positive, implying that a unit of fuel burn every hour of the year causes a net increase in population exposure. However, considering the specific example hour shown, a unit increase in fuel burn causes a decrease in $PM_{2.5}$ and O_3 exposures at 7% thrust or higher. Thus there exists a tradeoff between the CO_2 and air quality impacts of emissions during these conditions, where minimizing CO_2 emissions leads to an increase in population exposure to $PM_{2.5}$ and O_3, all else held constant.

In section 2.3 the total duration of occurrence (over an annual period) of tradeoff conditions is quantified. In section 2.4, the magnitude of the tradeoff between CO_2

emissions and population exposure to $PM_{2.5}$ and O_3 is evaluated. Finally, in section 2.6 the magnitude and duration information are combined to identify airports with relatively high potential for exposure reduction.

2.3 Duration of occurrence of CO_2 – air quality tradeoff

The percentage of the year for which a CO_2–air quality tradeoff occurs is given in Figure 2-1 (a) and (b) for $PM_{2.5}$ and O_3 impacts, respectively. At the 4% taxi thrust setting, CO_2 is negatively correlated with $PM_{2.5}$ population exposure 2-3% of the year on average across all airports and is negatively correlated with O_3 population exposure 5-12% of the year on average across all airports, depending on the engine type. At the 100% takeoff thrust setting, the tradeoff duration increases to 14-18% of the year for $PM_{2.5}$ exposure, and ~60% of the year for O_3 exposure. For a given thrust setting, variability in annual tradeoff durations across engines arises due to differing emission characteristics amongst engines. For all engines, HC and CO emissions decline with increased thrust while NO_x emissions increase.
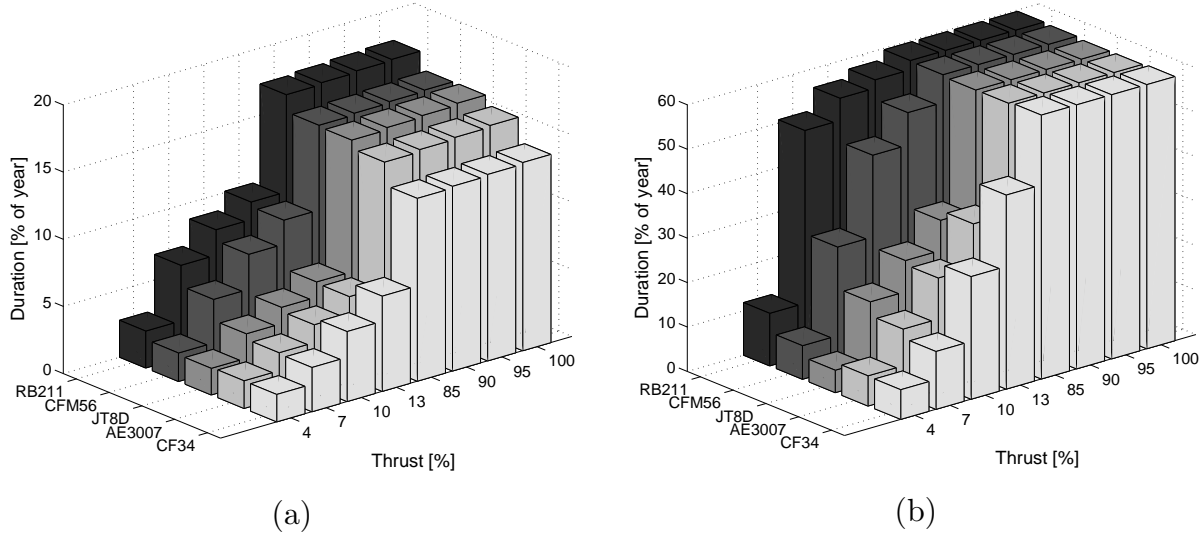
Figure 2-1: Annual duration of tradeoff, expressed as a fraction of the year, between fuel burn and population exposure to (a) $PM_{2.5}$ and (b) O_3, by each engine type and thrust setting. For each engine and thrust setting, annual durations are averaged over all 34 airports.

At high (takeoff) thrusts, the occurrence of tradeoff conditions is limited by the presence of negative atmospheric NO_x sensitivities, i.e. occasions where $S_{NO_x} = \partial P / \partial M_{NO_x} < 0$. This is because, as thrust increases, the ratio between EI_{NO_x} and other species becomes

larger. For example for the CFM56 engine, increasing thrust from 4% to 100% increases EI_{NO_x}/EI_{HC} from ~1/3 to ~256, EI_{NO_x}/EI_{CO} from ~1/20 to ~53 and EI_{NO_x}/EI_{SO_2} from ~2.4 to ~22. This trend holds for all other engines. As a result, tradeoff conditions are more dependent on S_{NO_x} at high thrust settings relative to low thrusts. As EI_{NO_x} is a positive quantity, the atmospheric sensitivities of $PM_{2.5}$ and O_3 exposures to NO_x have to be negative for $\partial P/\partial F < 0$ (as will be discussed further in the next section). At takeoff thrusts, therefore, the fractions of the year that tradeoff conditions occur for all engines (14-18% for $PM_{2.5}$ and ~60% for O_3 exposures, as seen in Figure 2-1) approximately equals the annual duration of negative NO_x sensitivity (~19% for $PM_{2.5}$ exposure and 60% for O_3 exposure across all airports).

Engine operations at maximum thrust result in CO_2 emissions – O_3 exposure tradeoff conditions 5-12 times more frequently than operations at 4% thrust. This suggests that minimizing fuel burn during taxi operations is less likely to result in an O_3 exposure tradeoff than reducing fuel burn at takeoff. To explain this, it is noted that over all airports, engines and thrust settings, less than 5% of the magnitude of CO_2 – O_3 exposure tradeoff is attributable to CO emissions, while <0.4% of the magnitude of CO_2 – O_3 exposure tradeoff is attributed to SO_2 emissions. Therefore Eq. 2-7 is simplified as

$$\frac{\partial P}{\partial F} \approx S_{NO_x} \cdot EI_{NO_x} + S_{HC} \cdot EI_{HC}. \qquad \text{Eq. 2-8}$$

Taking the CFM56 engine as an example, at 100% thrust, EI_{NO_x} is ~256 times larger than the EI_{HC} for the CFM56 engine. In order to create a tradeoff between fuel burn (CO_2 emissions) and population exposure, $\partial P/\partial F$ has to be less than zero and it follows from Eq. 2-8 that the condition

$$S_{NO_x} < -(1/256) \cdot S_{HC} \qquad \text{Eq. 2-9}$$

must be satisfied. At the 4% thrust setting, EI_{HC} is ~3 times as larger than that of NO_x for the CFM56 engine. For tradeoff conditions to occur in this regime, the inequality

$$S_{NO_x} < -3\, S_{HC} \qquad \text{Eq. 2-10}$$

must be fulfilled. For a given S_{HC}, atmospheric NO_x sensitivities must be ~770 times more negative to create tradeoff conditions at 4% thrust than to do so at 100% thrust. Conversely, for a given negative S_{NO_x}, atmospheric sensitivity to HC should be relatively smaller in magnitude or negative. Over all airports, the combination of sensitivities required to satisfy Eq. 2-10 occurs less frequently than the occurrence of negative NO_x sensitivities (~8.6 times less frequently, in the case of the CFM56 engine). As a result, for the CFM56 engine, O_3 exposure tradeoff conditions occur ~8 times less frequently at the 4% thrust setting relative to the 100% setting.

Engine operations at maximum thrust result in CO_2 emissions – $PM_{2.5}$ exposure tradeoff conditions 6-8 times more frequently than operations at 4% thrust. Compared to tradeoffs between CO_2 emissions and O_3 exposure, SO_2 emissions contribute to a larger percentage of the magnitude of CO_2 emissions – $PM_{2.5}$ exposure tradeoff (up to 11% for $PM_{2.5}$ c.f. <0.4% for O_3, over all airports and engines). $PM_{2.5}$ concentrations have been observed to increase with a reduction in sulfates under ammonia-rich conditions, due to a transfer of nitric acid from the gas phase to the aerosol phase (West et al., 1999). While Eq. 2-8 - Eq. 2-10 do not include the contribution of SO_2 emissions to population exposure, they qualitatively describe the trends in $PM_{2.5}$ tradeoff duration across thrust settings. For the CFM56 engine, the inequality in Eq. 2-10 is satisfied less frequently than the occurrence of negative $PM_{2.5}$ exposure sensitivity to NO_x (~9 times less frequently, for the CFM56 engine), which is congruent with durations of tradeoff between CO_2 emissions and $PM_{2.5}$ exposure occurring ~7.7 times less frequently at 4% trust than at 100% thrust.

The duration of the tradeoff between CO_2 emissions and population exposure to $PM_{2.5}$ and O_3 also varies according to time of year, occurring more frequently in the fall and winter months than the summer months. Figure 2-2 shows the percentage of each month for which a CO_2 – air quality tradeoff is seen for operations at 7% thrust setting. Over three quarters of CO_2 – $PM_{2.5}$ exposure tradeoffs occur within October to March. For O_3 the duration of occurrence is highest at 33% of the month during February, becoming relatively less frequent in July (~17%).
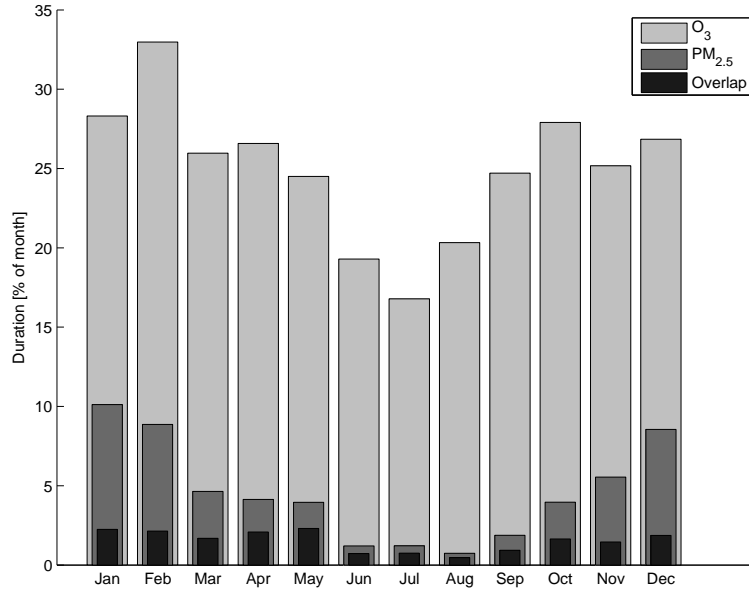
Figure 2-2: Occurrence of tradeoff conditions as a fraction of each month, aggregated over all engines at 7% thrust across all airports. Overlap denotes conditions when a tradeoff exists between fuel burn and both $PM_{2.5}$ and O_3 exposures.

The variation across airports in occurrence of tradeoff conditions between CO_2 emissions and population exposure to $PM_{2.5}$ and O_3 is shown in Figure 2-3 for operations at 7% thrust setting. For $PM_{2.5}$ impacts, the tradeoff situations occur between 0-12% depending on the airport. Airports in the Eastern US experience tradeoff conditions for a greater fraction of the year than airports in the Central and Western portions of the country. For O_3 impacts, the duration of occurrence varies between 7-45%, with airports in the Southern and Mountain regions of the country experiencing relatively fewer tradeoff conditions than other airports in the US.
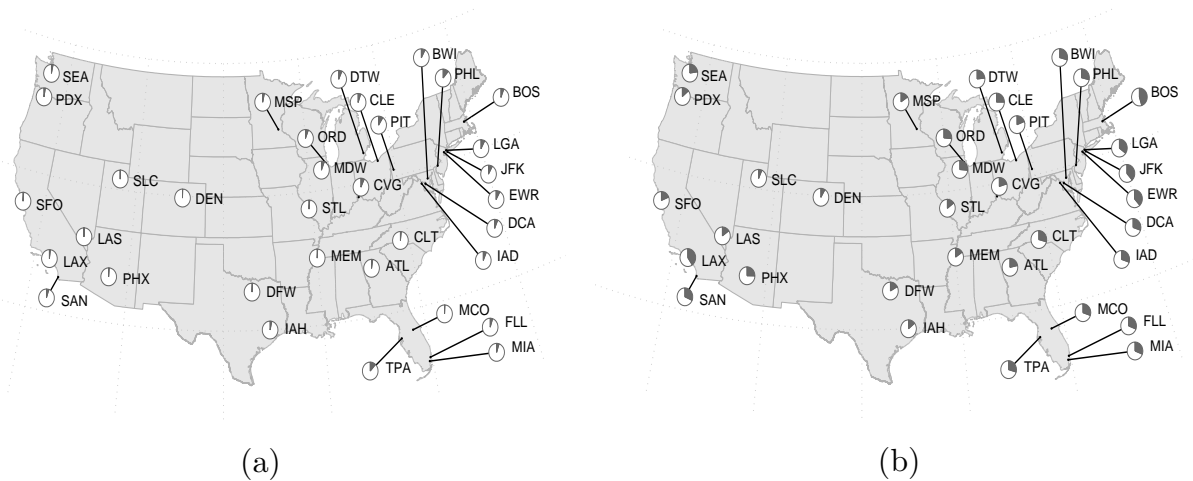
Figure 2-3: Spatial variation in percentage of the year when tradeoffs occur between CO_2 (fuel burn) and (a) $PM_{2.5}$ exposures and (b) ozone exposures. The duration of year at each airport is averaged over all engine types operating at 7% thrust.

2.4 Negative sensitivity of $PM_{2.5}$ and O_3 exposure to NO_x

Negative $PM_{2.5}$ and O_3 exposure sensitivity to NO_x emissions is an important determinant in the occurrence of tradeoff conditions, as discussed in the previous section. In this section, the physical mechanisms responsible for the negative NO_x sensitivities are discussed.

First, the mechanisms that give rise to negative ozone sensitivity to NO_x emissions are described. Figure 2-4 shows the chemical mechanisms involved in the production of ozone and oxidation of CO within the troposphere, adapted from Chapter 11 of Jacob (1999). This process is representative of the key features of the oxidation of more complex VOCs in the troposphere (Seinfeld and Pandis, 2006), and is used here to illustrate the dependence of ozone formation on NO_x emissions as a function of ambient NO_x and VOC (CO) concentrations.
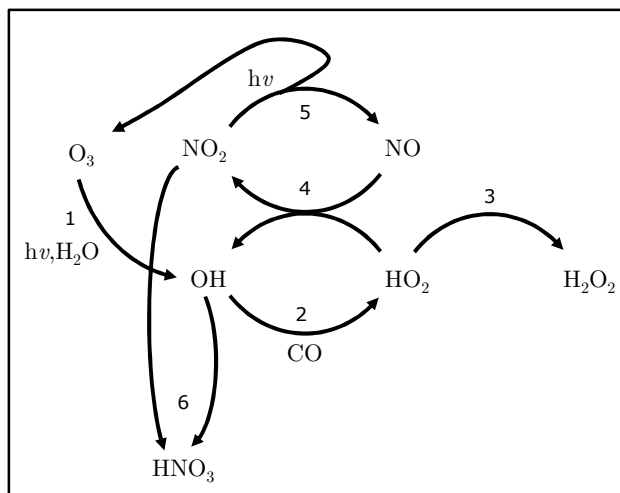
Figure 2-4: Mechanism for O_3-NO_x-CO chemistry in the troposphere, adapted from Chapter 11 of Jacob (1999). Individual reactions, indicated by reaction number, are listed in Table 2-3.

Table 2-3: Set of chemical reactions representing the mechanism for O_3-NO_x-CO chemistry in the troposphere as described in Figure 2-4.

Reaction	Formula
(1)	$O_3 + h\nu \rightarrow O_2 + O^1(D)$
	$O^1(D) + H_2O \rightarrow 2OH$
(2)	$CO + OH \xrightarrow{O_2} CO_2 + HO_2$
(3)	$HO_2 + HO_2 \rightarrow H_2O_2 + O_2$
(4)	$HO_2 + NO \rightarrow OH + NO_2$
(5)	$NO_2 + h\nu \xrightarrow{O_2} NO + O_3$
(6)	$NO_2 + OH \rightarrow HNO_3$

The reaction chain is initiated by the production of the hydroxyl radical (OH) from photolysis of O_3 (reaction 1). The OH molecule oxidizes CO (reaction 2) which results in the formation of the hydroperoxyl radical (HO_2). In the presence of NO, HO_2 is converted back to OH (reaction 4). This reaction oxidizes NO to NO_2, which is undergoes photolysis to form O_3 via reaction 5. The rate of ozone production is therefore governed by the rate of production of NO_2 from NO as per reaction 4,

$$P_{O_3} = k_4 [HO_2][NO],$$

Eq. 2-11

Assuming chemical equilibrium of the HO_x ($OH + HO_2$) family (Seinfeld and Pandis, 2006), the rate of reaction 2 and 4 can be set equal to each other,

$$k_2[CO][OH] = k_4[HO_2][NO],$$

Eq. 2-12

which implies that the rate of ozone production, P_{O_3}, is also a function of CO and OH concentrations.

The reaction chain is terminated when HO_x is removed from the system, accomplished via reactions 3 and 6. At high NO_x concentrations relative to CO, the termination reaction 6 dominates whereby NO_2 is converted to nitric acid by OH and the steady-state HO_x balance is given by

$$P_{HO_x} \cong k_6[NO_2][OH],$$

Eq. 2-13

where P_{HO_x} is the rate of production of OH via photolysis of O_3 (i.e. the rate of reaction 1) and k_6 is the rate constant for reaction 6.

Solving Eq. 2-13 for OH and substituting into Eq. 2-12,

$$k_4[HO_2][NO] = P_{O_3} = \frac{k_2[CO]P_{HO_x}}{k_6[NO_2]}.$$

Eq. 2-14

At the high NO_x limit, therefore, the rate of ozone production is proportional to CO (and VOC) concentrations but is inversely proportional to NO_2 concentrations. This means that an increase in NO_2 concentrations (for example, via increased NO_x emissions) decreases the amount of O_3 that can be formed. The removal of OH from the system inhibits the conversion between OH and HO_2 via reaction (2), which limits the conversion of NO to NO_2 via reaction (4) thereby reducing the rate of O_3 production.

The threshold for high NO_x concentrations is specified in proportion to ambient CO (or more generally, VOC) concentrations via a critical VOC/NO_x ratio. This ratio is studied in further detail in Chapter 3 (referred to as the ozone isopleth ridge line VOC/NO_x ratio) and quantified for all locations in the US.

The negative sensitivity of $PM_{2.5}$ concentrations to NO_x emissions is also explained by changes in atmospheric oxidant levels. Several works have reported increased $PM_{2.5}$

concentrations from NO_x controls, mainly during the winter (Konovalov, 2003; Megaritis et al., 2013; Pinder et al., 2008; Tsimpidi et al., 2008; Zhao et al., 2015). The growth in total $PM_{2.5}$ is attributed to increased formation of sulfate and organic $PM_{2.5}$, in spite of reduced nitrate $PM_{2.5}$. This occurs due to the increase in HO_x radicals with NO_x emissions reductions at relatively high NO_x concentrations relative to VOCs (via the mechanisms described in Figure 2-4), which in turn promotes the oxidation of sulfur dioxide and other $PM_{2.5}$ precursors into secondary $PM_{2.5}$ (Konovalov, 2003; Megaritis et al., 2013; Tsimpidi et al., 2008). Furthermore, the reduced formation of nitric acid increases the amount of free ammonia available to condense sulfuric acid to sulfate $PM_{2.5}$ (Ashok et al., 2013; Pinder et al., 2008). Thus, reduction in nitrate aerosol mass due to NO_x emissions reductions may be offset by the increase in mass of other $PM_{2.5}$ components (such as sulfates), thereby leading to an overall increase in $PM_{2.5}$ exposure in some conditions.

2.5 Magnitude of CO_2 emissions – air quality tradeoff

In this section the magnitude of tradeoff between CO_2 emissions and population exposure to $PM_{2.5}$ and O_3 are quantified. For a given airport and time of emissions, population exposure is affected by engine operation in two ways: total fuel consumed and thrust setting (see Eq. 2-6) – the two main factors controlling emissions. First, the reduction in population exposure to $PM_{2.5}$ and O_3 per kilogram increase in fuel burn at constant thrust during tradeoff conditions is shown. Second, the relationship between thrust setting and population exposure is quantified, as in some operational cases thrust setting can be altered. Finally, airports are ranked according to their exposure reduction potentials, i.e. the combination of magnitude and duration of tradeoff between CO_2 emissions and population exposure to $PM_{2.5}$ and O_3.

2.5.1 Tradeoff between CO_2 emissions and population exposure to $PM_{2.5}$ and O_3 at constant thrust

The distribution of $PM_{2.5}$ and O_3 population exposure reductions per kilogram fuel burned at constant thrust is shown in Figure 2-5 (a) and (b), respectively. As an example, 1 kg of fuel burned by an RB211 engine at 7% thrust causes a median [25th –

75th percentile] reduction in $PM_{2.5}$ population exposure of 1.21 [0.33 - 3.64] $\times$ 10^{-2} ppl·ngm^{-3} during tradeoff conditions (the distribution reflects conditions across all hours of tradeoffs and at all 34 airports).

At 7% thrust, the median reductions in $PM_{2.5}$ exposure per kilogram fuel burn is ~0.016 ppl·ngm^{-3}·kg^{-1} for all engines, while at 100% thrust the reductions are greater in magnitude and relatively more varied between 0.06 and 0.27 ppl·ngm^{-3}·kg^{-1} across the five engines. This trend is also observed in O_3 exposure reductions, which are ~0.25 ppl·ppt·kg^{-1} at 7% thrust and 0.98-4.44 ppl·ppt·kg^{-1} at 100% thrust. Relative to the annual average (positive) $PM_{2.5}$ exposure per unit fuel burn, the median reductions in population exposure to $PM_{2.5}$ during tradeoff conditions at 7% and 100% thrust are 6-8% and 11-13% respectively, depending on the engine. For O_3 exposure, the relative magnitudes are 32-1060% and 265-314% for fuel burn at 7% and 100%, respectively. The large variability in relative magnitudes across engines means that the potential improvements in O_3 exposure at airports, though significant relative to the annual average, may be sensitive to the fleet composition of airport traffic.

The variation in magnitude of tradeoff at 100% thrust (grey bars in Figure 2-5) amongst the engines is explained by differences in the NO_x EI. At high thrusts, reductions in population exposure are more sensitive to variations in EI_{NO_x} than other species, in part as EI_{NO_x} exceeds that of other species by 1-2 orders of magnitude. Thus for a given (negative) atmospheric sensitivity to NO_x, engines with larger EI_{NO_x} lead to relatively greater reductions in population exposure to O_3 and $PM_{2.5}$ per unit fuel burn than engines with smaller EI_{NO_x}. This means that the tradeoff is greater for older engines and engines with higher pressure ratios, in general.
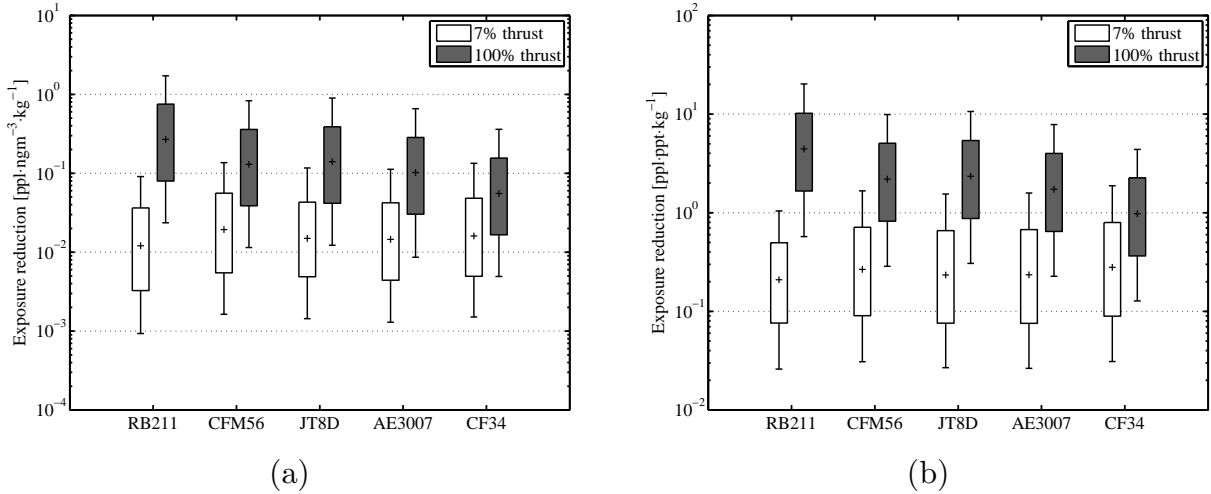
Figure 2-5: Reduction in population exposure to (a) $PM_{2.5}$ and (b) O_3 due to 1 kg of (additional) fuel burned at a constant thrust setting of 7% (white bars) and 100% (grey bars). The marker within the box plot for each engine represents the median value across all airports and tradeoff durations; the box extents are the interquartile range; and the whiskers, the 10th and 90th percentile values.

2.5.2 Negative dependence of air quality on thrust setting

The operating thrust setting of an engine influences population exposure via two pathways. Firstly, thrust setting affects emission indices and consequently the value of $\partial P/\partial F$, as shown in Eq. 2-7 and Table 2-2. The second pathway is by affecting fuel burn itself. Assuming a fixed duration of operation, changing the thrust from some reference condition $\dot{m}_{f,ref}$ to $\dot{m}_{f,1}$ scales the reference fuel burn F_{ref} according to $F_1 = F_{ref} \cdot \dot{m}_{f,1}/\dot{m}_{f,ref}$.

In this section, the analysis assumes that the duration of operation is held constant as the engine thrust setting is varied. This assumption is revised in Chapter 4 where thrust setting is coupled to aircraft activity models for airport surface movements and takeoff activity. For example, King and Waitz (2005) find that reduced-thrust takeoffs lead to increased airborne climb durations up to 3000 ft (~1 km). (However, the study by King and Waitz (2005) did not account for the fact that reduced-thrust takeoffs covered relatively more ground track distance than a takeoff at full thrust, which is accounted for in the analysis presented in Chapter 4.)

The tradeoff between thrust setting and air quality is defined as the condition where there is a monotonic decrease in population exposure with increasing thrust. An example of such a condition is shown in Table 2-4, which tabulates the gradient of $PM_{2.5}$ exposure with respect to fuel burn, $\Delta P/\Delta F$, between successive thrust settings at ATL. All gradients are negative, implying that population exposure is progressively lowered as thrust setting is increased for a constant operation time. Furthermore, population exposure depends nonlinearly on thrust, as gradients in the takeoff (85-100%) thrust regime are an order of magnitude larger than those in the taxi (4-13%) thrust regime. The nonlinearity arises from the power-law trends of NO_x, HC and CO EIs with thrust.

The reduction in population exposure from fuel burn (and CO_2 emissions) increase from thrust setting is quantified by computing an average gradient over the taxi and takeoff thrust regimes separately. Over all airports and engine types, negative trends between thrust and population exposure to $PM_{2.5}$ and O_3 occur 13% and 59% of the year, respectively.

Table 2-4: Change in $PM_{2.5}$ exposure per unit fuel burn increased due to thrust setting for the RB211 engine at ATL on 1 Jan 2006, 0600 – 0700 UTC. Units are ppl·ngm^{-3}·kg^{-1}. Changes in population exposure and fuel burn are calculated between each consecutive pair of thrust settings.

Thrust setting range	4%-7%	7%-10%	10%-13%	85%-90%	90%-95%	95%-100%
$\Delta P/\Delta F$ (ppl·ngm^{-3}·kg^{-1})	-0.058	-0.049	-0.059	-0.57	-0.62	-0.68
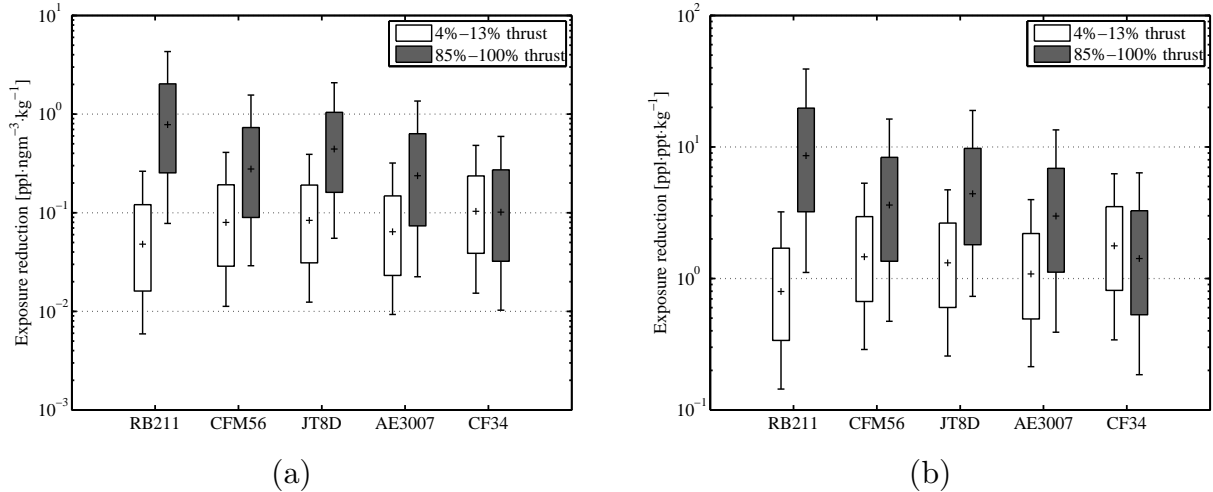
Figure 2-6: Reduction in population exposure to (a) $PM_{2.5}$ and (b) O_3 per kilogram of fuel burn increased via thrust setting, over the taxi thrust (white bars) and takeoff thrust (grey bars) regimes. The marker within the box plot for each engine represents the median value across all airports and tradeoff durations; the box extents, the interquartile range; and the whiskers, the 10th and 90th percentile values.

$PM_{2.5}$ and O_3 exposure reductions per kilogram fuel burn (or per 3.16 kg of CO_2 emissions) increased via thrust setting are shown in Figure 2-6 (a) and (b) (as before, the distribution reflects conditions across all hours and airports). Median $PM_{2.5}$ exposure reductions (over all airports) for the five engines are 0.05-0.10 ppl·ngm^{-3}·kg^{-1} for thrust changes within the taxi thrust regime, and 0.10-0.78 ppl·ngm^{-3}·kg^{-1} for changes in thrust over the takeoff thrust regime. Median ozone reductions are 0.80-1.77 ppl·ppt·kg^{-1} and 1.42-8.59 ppl·ppt·kg^{-1} for thrust increments in the taxi and takeoff regimes, respectively. Similar to section 2.5.1, the median magnitudes of tradeoffs are compared relative to the annual average change in population exposure per kilogram fuel burn (i.e. the average change in population exposure when fuel burn is increased via thrust setting during all times of the year). The median $PM_{2.5}$ population exposure reductions are 15-54% and 15-23% of the annually averaged $PM_{2.5}$ exposure per kilogram fuel burn, over the taxi and takeoff thrust regimes respectively. Median ozone reductions are 114-218% and 263-320% of the annually averaged O_3 exposure per kilogram fuel burn, over the taxi and takeoff thrust regimes respectively.

For all except the CF34 engine, increasing fuel burn in the takeoff thrust regime causes a greater reduction in exposure than the same increase in the taxi thrust regime. For the CF34 engine, EI_{NO_x} grows at a slower rate with respect to thrust than the other engines

(e.g. EI_{NO_x} at 100% thrust is ~3 times larger than that at 7%, while the ratio is ~15 for the RB211 engine). As a result, the tradeoff magnitudes for the CF34 engine are similar across thrust setting while those of the other engines vary. The reductions in $PM_{2.5}$ and O_3 exposure are both 1.5-6.4 times larger if fuel burn is increased due to thrust as opposed to increased fuel burn at a constant thrust.

2.6 Potential for population exposure reduction at airports

The potential for reduction of population exposure to $PM_{2.5}$ and O_3 at airports at the cost of increasing CO_2 emissions is assessed by considering both the magnitude of tradeoff as well as the frequency of occurrence. An airport with high potential for exposure reduction has a combination of relatively high magnitude of tradeoff for a relatively large fraction of the year, compared to an airport with relatively low exposure reduction potential. Figure 2-7 plots the mean reduction in $PM_{2.5}$ and O_3 exposure per kilogram fuel burn at 7% thrust (i.e. taxi operations) against the fraction of the year tradeoff conditions occur, for each airport. The airport locations with the highest and lowest exposure reduction potentials are highlighted and labeled in black. Note that the Los Angeles (LAX) airport has been excluded from Figure 2-7 (a) for clarity, as it has a relatively high $PM_{2.5}$ exposure reduction magnitude of 1.58 $ppl \cdot ngm^{-3} \cdot kg^{-1}$. The Philadelphia (PHL), Cincinnati (CVG) and Seattle (SEA) airports have a higher $PM_{2.5}$ exposure reduction potential than the Orlando (MCO) and Salt Lake City (SLC) airports. For ozone impacts, it is seen that the Los Angeles (LAX), New York's JFK, Newark (EWR) and La Guardia (LGA) airports have a higher reduction potential relative to the Lambert – St. Louis (STL), Salt Lake City (SLC) and Denver (DEN) airports.
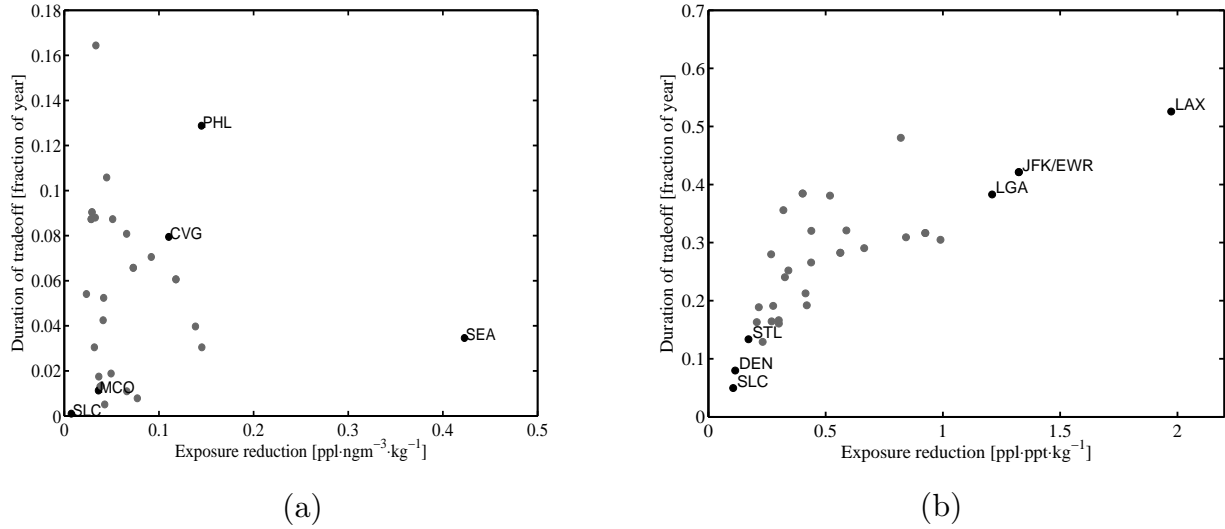
Figure 2-7: Annual duration of tradeoff plotted against mean exposure reduction due to 1 kg fuel burn (or 3.16 kg of CO_2 emissions) at 7% thrust for each airport. Panel (a) plots $PM_{2.5}$ impacts while panel (b) plots O_3 impacts. The three airport locations with the highest and lowest reduction potentials – the product of duration and magnitude of O_3 exposure tradeoff with fuel burn – are highlighted in black and labeled, while all other airports are shown as grey markers and not labeled for clarity. The Los Angeles (LAX) airport is not shown in panel (a) for clarity due to its relatively high exposure reduction magnitude of 1.58 ppl·ngm^{-3}·kg^{-1}.

The average magnitude of tradeoff is multiplied by the annual duration of occurrence to quantify the $PM_{2.5}$ and O_3 exposure reduction potentials at each airport. Reduction potentials are calculated for four engine operation scenarios: increased fuel burn at constant thrust settings of 7% and 100%, as well as thrust increments over the taxi and takeoff thrust regimes. Airport-specific tradeoff magnitudes and annual durations for $PM_{2.5}$ and O_3 exposures are tabulated in Appendix A. The top 5 airports, ranked according to their reduction potentials under each of the four engine operation scenarios, are given in Table 2-5. The LAX, Philadelphia (PHL) and Cincinnati (CVG) airports are observed to have consistently high $PM_{2.5}$ exposure reduction potentials across all four scenarios. For O_3 exposures the LAX, EWR, JFK, LGA and PHL airports consistently have the highest reduction potentials.

46

Table 2-5: Top five airports (identified by IATA airport code) ranked by reduction potential, the product of duration and magnitude of CO_2 emissions – exposure tradeoff. Reductions in both $PM_{2.5}$ and O_3 exposure are computed for fuel burn increases at constant thrust of 7% and 100%, as well as increases due to thrust setting over the taxi and takeoff thrust regimes. The parenthesis below each airport lists, in order, the mean magnitude (in ppl ngm^{-3}·kg^{-1} or ppl ppt·kg^{-1}) and duration (as a fraction of year) of the fuel burn – population exposure tradeoff at that airport. Airports are grouped where they fall in the same ~50 km nested GEOS-Chem adjoint grid cell.

	$PM_{2.5}$ exposure reduction				O_3 exposure reduction			
	Increased fuel burn (constant thrust)		Increased thrust		Increased fuel burn (constant thrust)		Increased thrust	
Ranking	7%	100%	Taxi range	Takeoff range	7%	100%	Taxi range	Takeoff range
1	LAX (1.58,0.03)	LAX (3.56,0.09)	LAX (1.60,0.08)	LAX (6.76,0.08)	LAX (1.97,0.53)	LAX (17.09,0.83)	LAX (8.36,0.83)	LAX (28.17,0.83)
2	PHL (0.14,0.13)	PHL (0.68,0.25)	CVG (0.27,0.30)	PHL (1.21,0.23)	JFK/EWR (1.32,0.42)	JFK/EWR (7.20,0.76)	JFK/EWR (3.39,0.76)	JFK/EWR (11.86,0.76)
3	SEA (0.42,0.03)	SAN (0.48,0.31)	PIT (0.24,0.34)	SAN (0.99,0.25)	LGA (1.21,0.38)	LGA (6.99,0.71)	LGA (3.52,0.71)	LGA (11.50,0.71)
4	CVG (0.11,0.08)	CVG (0.46,0.30)	PHL (0.31,0.23)	CVG (0.79,0.30)	BOS (0.82,0.48)	BOS (4.90,0.76)	ORD/MDW (2.54,0.82)	BOS (8.07,0.77)
5	ORD/MDW (0.12,0.06)	PIT (0.36,0.35)	SEA (0.89,0.05)	PIT (0.65,0.34)	PHL (0.99,0.30)	PHL (5.08,0.67)	PHL (2.75,0.67)	PHL (8.37,0.67)

2.7 Magnitude of aircraft and airport emissions relative to near-airport sources

In this section, aircraft emissions are compared to those from other airport sources that are airside – i.e. auxiliary power units (APUs) and ground support equipment (GSEs) – as well as other anthropogenic sources in the vicinity of the airport. This quantifies the relative order of magnitude of emission perturbations applied to the adjoint emissions sensitivities, which represent the linearized atmospheric response to emissions.

Emission inventories for aircraft LTO emissions, APU and GSE are obtained from the US EPA 2011 National Emissions Inventory (NEI) (US EPA, 2014a) for 200 airports in

the US accounting for ~99% of passenger enplanements. A gridded inventory of the 2011 NEI, with a resolution of $0.1° \times 0.1°$ (approximately 10 km × 10 km) is used to provide emission estimates for non-airport sources. The gridded inventory includes emissions from all anthropogenic sources including airport airside sources. The comparison is performed for NO_x, SO_2, CO, primary $PM_{2.5}$ (comprising BC, OC and $SO_4^=$) and two VOC emission species (species with paraffinic carbon bonds, PAR, and formaldehyde, FORM).
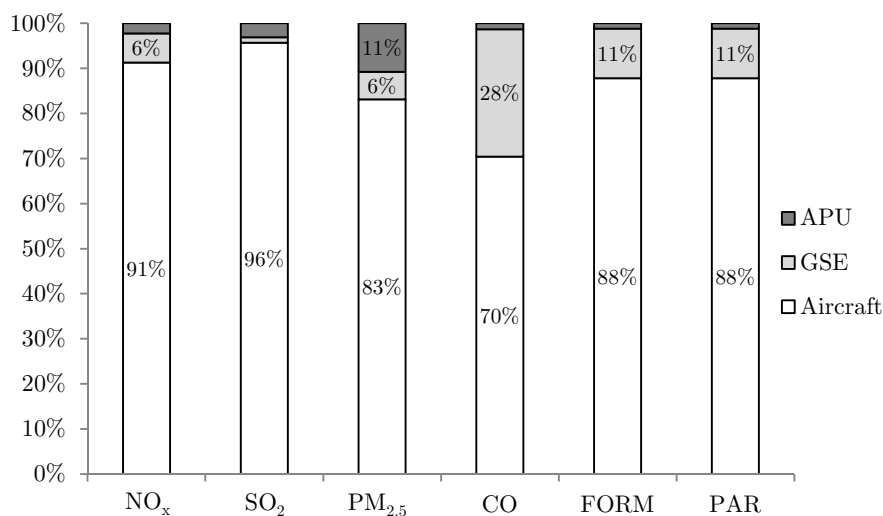
Figure 2-8: Relative contribution of aircraft, APU and GSE sources to airport airside emissions. Data from the US EPA NEI 2011 is used for ~200 airports in the US.

Figure 2-8 shows the relative contribution of aircraft, APUs and GSEs to airport emissions at all the airports considered. Aircraft and APUs are responsible for 72-99% of airport emissions, with the proportion varying across emission species. GSEs contribute 11% of airport VOC emissions and 28% of airport CO emissions.

The magnitude of total airport airside emissions (i.e. aircraft, APU and GSE emissions) is compared relative to emissions from all anthropogenic sources in the vicinity of airports. Figure 2-9 plots the proportion of anthropogenic emissions that is attributed to airport airside emissions as a function of radial distance from airports, averaged across all airports. Here, the proximity to the airport is defined by the radius from the center of the airport grid cell, which starts at 15 km (i.e. cells adjacent to the airport grid cell)

48

and goes up to 55 km (covering approximately five grid cells in all directions). The proportion of anthropogenic emissions attributable to airside aviation activity is largest when within 15km of the airports (ranging from 0.6-4.7%), decreasing to 0.1-1.1% when within 55 km of the airports. The airport-attributable fraction varies depending on airport location – for instance, at a radius of 15 km, the upper bound of airport-attributable emissions is ~2-26% depending on emission species (where the upper bound is calculated as the 95th percentile across all airports studied).
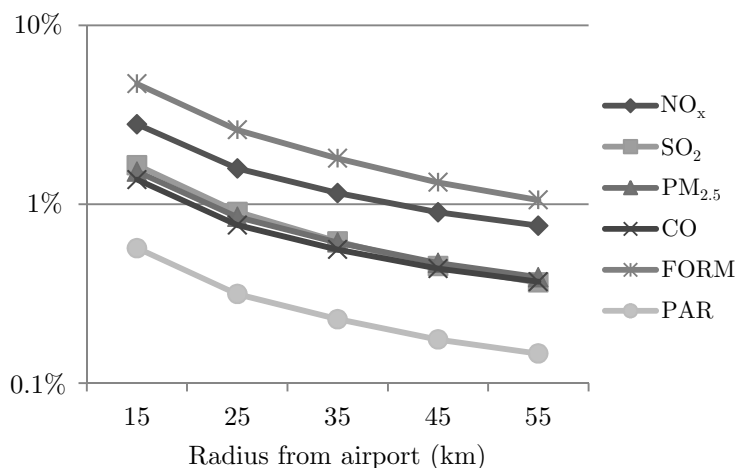
Figure 2-9: The proportion of anthropogenic emissions that is attributed to airport airside emissions as a function of radial distance from airports. Data from the US EPA NEI 2011 is used to obtain emission inventories for ~200 airports in the US as well as for all anthropogenic sources.

2.8 Summary

This work has identified tradeoffs between CO_2 emissions and population exposure to $PM_{2.5}$ and O_3 – conditions when exposure decreases with an increase in fuel burn (directly proportional to CO_2 emissions). The analysis is performed for five commonly-used engines operating at taxi and takeoff thrust levels and for the top 34 US airports by passenger traffic. Emission sensitivities from the GEOS-Chem adjoint model are employed to model secondary $PM_{2.5}$ and O_3 population exposure. Key findings from the study are summarized below:

1) A tradeoff between CO_2 emissions and $PM_{2.5}$ population exposure occurs during 2-18% of the year, and a tradeoff between CO_2 and O_3 population exposure

49

occurs for 5-60% of the year across all airport locations, depending on engine and thrust setting.

2) Engine operations at takeoff thrust settings lead to more frequent occurrence of tradeoff conditions than when the engine is operated at taxi thrust settings (e.g. 6-8 times more frequently for $PM_{2.5}$ and 5-12 times more frequently for O_3 when operated at 100% thrust c.f. 4% thrust).

3) When fuel burn in increased at a constant thrust setting, the median reduction (across all airports) in $PM_{2.5}$ and O_3 exposure during tradeoff conditions per kilogram fuel burn are 6-13% and 32-1063% of the annually averaged exposure per unit fuel burn.

4) When fuel burn in increased by changing the thrust setting, the median reduction (across all airports) in $PM_{2.5}$ and O_3 exposure during tradeoff conditions per kilogram fuel burn are 15-54% and 114-320% of the annually averaged exposure per unit fuel burn.

5) Exposure reduction potentials beyond fuel burn minimization– i.e. a combination of high duration and magnitude of tradeoffs – are highest at the LAX, PHL and CVG airports for $PM_{2.5}$ exposure, and at the LAX, EWR/JFK, LGA and PHL for O_3 exposure.

6) Aircraft and APU emissions constitute 72-99% of airport emissions, while total airport airside emissions are 0.1-1.1% of total anthropogenic emissions (depending on emission species) when within 55km of the airports.

It is noted that the climate impact of aviation is affected not only by CO_2 emissions, but also other emissions that simultaneously impact air quality. For example, the mean global warming potential (GWP) for NO_x (North America, time horizon of 100 years) is -8.2 (Myhre et al., 2013). For the RB211 engine at takeoff thrust, this results in a (negative) CO_2-equivalent emission that is ~14% relative to CO_2. It is, however, out of the scope of this thesis to conduct further numerical simulations to quantify the total climate impacts in detail. Furthermore, it is noted that the uncertainty of the GWP value is ±10.3 (Myhre et al., 2013) which suggests that more research is required to improve the understanding of the climate impacts of NO_x emissions.

This study has identified airports with relatively high population exposure reduction potentials beyond fuel burn minimization, but has not explained the spatial differences in exposure reduction potentials across airport locations in the US. Spatial differences in duration and magnitude of tradeoffs between emissions and O_3 exposure are quantified in Chapter 3. A similar quantification for $PM_{2.5}$ exposure reduction potentials at airports, while not done in this thesis, would require further numerical simulations which consider population exposure to speciated components of $PM_{2.5}$ (e.g. ammonium nitrate and ammonium sulfate $PM_{2.5}$).

The findings show that at the airports and engines studied, there are times during the year where population exposure to both $PM_{2.5}$ and O_3 can be improved (in some cases, significantly relative to the annual mean), with an increase in fuel burn. This raises the possibility of reducing the air quality impacts of airports beyond minimizing fuel burn as well as the possibility of optimizing operations for minimum net environmental impact (considering air quality and climate together). This is the subject of Chapter 4, where aircraft operations at DTW are optimized for minimum environmental and air quality impact.

The next chapter, Chapter 3, characterizes the ozone exposure response to NO_x and VOCs emission reductions as a function of ambient VOC and NO_x concentrations. This is done for emissions at all locations in the US. This research effort is motivated by the prevalence of tradeoff conditions between CO_2 and O_3 exposure (e.g. up to 60% of the year as shown in Figure 2-1) and the magnitude of tradeoffs (reductions in O_3 exposure up to a factor of 10 of the annual mean exposure per unit fuel burn, as calculated in section 2.4). The knowledge of when and where emissions reductions are counter-productive to O_3 exposure enables the implementation of effective control strategies to mitigate the O_3 exposure impacts of aircraft emissions at airports.

Chapter 3

Characterizing ozone exposure response to emissions reductions

Population exposure to ozone has been quantitatively associated with an increased risk of premature mortality and morbidity (Bell, 2004; Jerrett et al., 2009; WHO, 2008). In the US, premature mortality due to ozone in 2005 has been estimated at 4700-19,000 early deaths by Fann et al. (2012) and 10,000 early deaths by Caiazzo et al. (2013) with 155 of these attributable to aviation in North America. Efforts to mitigate population exposure to ozone involve reducing emissions of NO_x and VOCs by the Clean Air Act (USEPA, 2011), NO_x cap-and-trade policies such as in the eastern US (Mesbah et al., 2013) and other state-based emission controls (Cohan et al., 2006).

Ozone is formed via photochemical reactions of NO_x with VOCs (Seinfeld and Pandis, 2006; Sillman, 1999). Variations in emissions of these precursors as well as meteorological factors affecting the photochemistry (e.g. cloud cover) can result in nonlinear changes in O_3 concentrations with respect to emissions (Ainslie and Steyn, 2006; Sillman, 1999). For instance, increased ozone concentrations in cities were observed when larger reductions in NO_x relative to VOC emissions occurred during the weekend due to a reduction in diesel vehicular traffic into cities (Cleveland and McRae, 1978; Heuss et al., 2003; Lebron, 1975). In addition, the response of ozone concentrations to changes in electricity generation emissions (Mesbah et al., 2013) and future anthropogenic emissions in the US (Tao et al., 2007) have also been shown to vary with location and time.

The nonlinear dependence of O_3 concentrations on NO_x and VOC is commonly captured by an ozone exposure response surface (usually presented as isopleth diagram). Figure 3-1, adapted from Figure 6.10 of Seinfeld and Pandis (2006), shows an example of an isopleth diagram for Atlanta. The isopleth diagram depicts the response of maximum ozone concentrations with respect to NO_x and VOC concentrations and is useful in assessing the potential outcome of proposed changes in NO_x and/or VOC emissions. The ozone ridge line on the isopleth diagram identifies the local maximum in ozone with respect to NO_x concentration at each VOC level. In regions where the VOC/NO_x ratio is lower than that of the ridge line (denoted as 'VOC-limited'), reducing NO_x emissions increases O_3 concentrations whereas reducing VOC emissions lowers ozone. In regions of higher VOC/NO_x ratios than that of the ridge (denoted as 'NO_x-limited'), reducing NO_x emissions decreases O_3 while VOC emissions have little effect on O_3.
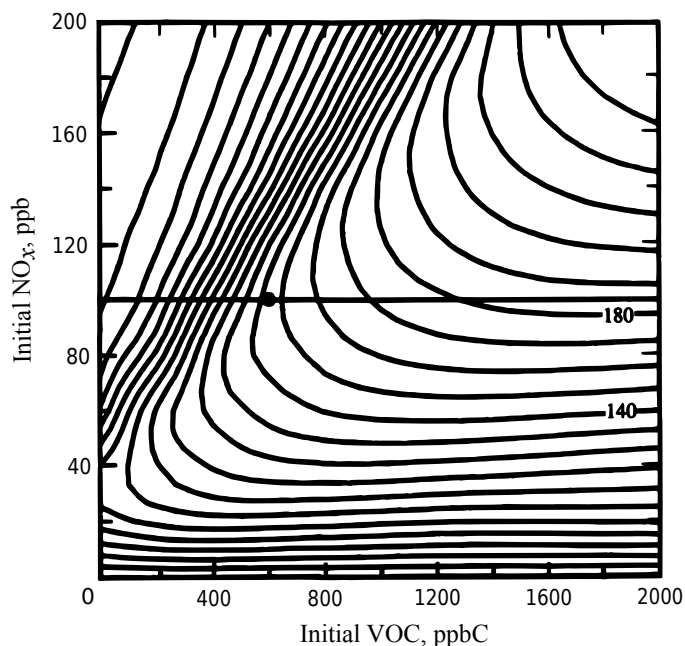
Figure 3-1: Example of an ozone concentration isopleth diagram for Atlanta, taken from Figure 6.10 of Seinfeld and Pandis (2006) and based on chemistry simulations along air trajectories. Each isopleth represents 10ppb increments in O_3 concentration upward and toward the right of the plot.

The work presented in this chapter quantifies the impacts of NO_x and VOC emissions on national population exposure to ozone as a function of their ambient concentrations through isopleth diagrams. Isopleth diagrams are constructed for every location in the US, and are used to calculate three metrics that quantify the impact of emissions on

national ozone exposure: duration of the year that VOC-limited conditions occur, the VOC/NO$_x$ ratio of the ridge line on the isopleth diagram and the ozone exposure-neutral VOC/NO$_x$ emissions ratio. It is noted that VOC-limited conditions may not necessarily occur during a continuous period of time during the year, and therefore the duration of VOC-limited conditions calculated here refers to the fraction of time during the year where such conditions occur. The ozone exposure-neutral ratio is the ratio of VOC/NO$_x$ emissions that neither increases nor decreases ozone exposure during VOC-limited conditions. When used together with measured or modeled NO$_x$ and VOC concentrations, this information allows the determination of whether emissions from a particular source will increase or decrease national population exposure to ozone.

This chapter is organized as follows: section 3.1 discusses previous research on ozone isopleths and the contributions of the present work to the current literature. Section 3.2 presents the methods used to calculate ozone exposure isopleths and the associated emission impact metrics. Section 3.3 discusses the results including ozone exposure isopleths for the three largest cities in the US. These ozone exposure isopleths are validated in section 3.4. Section 3.5 and 3.6 describe the spatial distribution of the three isopleth metrics and emission sensitivities. Section 3.7 presents a summary of the characterization of ozone exposure response to emissions reductions.

3.1 Background on ozone isopleths

Isopleth diagrams have been generated from photochemical simulations using a matrix of different combinations of VOC and NO$_x$ emissions. Kinosian (1982) employed the Empirical Kinetic Modeling Approach (EKMA) together with the ozone isopleth plotting package (OZIP) to generate city-specific isopleths for a city in the Central Valley of California and the South Coast Air Basin. Other studies have calculated the ozone response to a range of emission perturbations at specific locations using multiple runs of 3-dimensional chemistry transport models (CTMs) (Milford et al., 1989; Reynolds et al., 2004; Sierra et al., 2013; Wagner et al., 1992; Zavala et al., 2009) and box models (Chameides et al., 1992; Menut et al., 2000). Menut (2003) showed isopleths of ozone as a function of meteorological parameters (wind speed, reaction rate,

atmospheric stability and temperature) and emissions (NO_x and VOC) over Paris using multiple runs of a CTM. Apart from simulations, ozone isopleths have also been constructed based on measured VOC, NO_x and O_3 concentrations at a rural and urban site in Italy (Thielmann et al., 2001).

Hakami et al. (2004) employed the higher-order decoupled direct method (HDDM) to compute third-order source-oriented sensitivities of ozone with respect to domain-wide NO_x and VOC emissions. They used the sensitivities together with a third-order Taylor expansion to construct ozone isopleths assuming NO_x and VOC emissions perturbations of $\pm 70\%$ in the San Joaquin Valley in central California. A similar approach was used to create an ozone isopleth in the Houston region (Koo et al., 2008). The HDDM method was also applied by Cohan et al. (2005) to characterize ozone response to large perturbations in emissions over Georgia.

Studies have been conducted to parameterize the ozone isopleth based on a dimensional scaling analysis (Ainslie and Steyn, 2006) and non-linear regression (Chang and Rudy, 1993) and were found to compare well with simulated ozone concentrations.

This work develops isopleths of population exposure to ozone as a function of ambient VOC and NO_x concentrations using emissions sensitivities from the adjoint of the GEOS-Chem air quality model (Henze et al., 2007). Adjoint sensitivities are receptor-oriented, meaning that they relate, in this case, the integrated ozone exposure to emissions at every location and time. Adjoint methods have been extensively used to constrain sources of emissions using measurements of atmospheric concentrations (Chai et al., 2009; Kopacz et al., 2009; Zhu et al., 2013) and also to calculate the dependence of ozone and aerosols on precursor emissions (Henze et al., 2009, 2007; Parrington et al., 2012; Walker et al., 2012). They have been applied in the context of aviation's air quality impact (Gilmore et al., 2013; Koo et al., 2013), sectoral attribution of emissions impacts (Dedoussi and Barrett, 2014; Pappin and Hakami, 2013a, 2013b), vegetative exposure to ozone in the US (Lapina et al., 2014) and optimal air quality management strategies (Hakami et al., 2006; Mesbah et al., 2013, 2012).

This work is the first to generate ozone exposure using sensitivities from the adjoint of an air quality model to calculate national-level exposure to ozone concentrations. The adjoint method overcomes a limitation of the previous studies in that multiple model simulations with emissions perturbations were required to calculate the sensitivity of ozone to NO_x and VOC emissions. Furthermore, the adjoint method provides sensitivities to emissions at every location and time, and a single simulation is sufficient to calculate isopleths of national ozone exposure for every location in the domain, instead of one simulation per location (e.g. the HDDM approach). Ozone exposure isopleths have been researched in prior literature (Hayes et al., 1991; Wagner et al., 1992), though they have been created only for specific locations or regions of emissions. For the first time, this work presents ozone exposure isopleths for all locations nationwide. By calculating population exposure to ozone in the contiguous U.S., the spatial distribution of ozone is accounted for and the human health implications of changing NO_x or VOC emissions at every location are assessed.

3.2 Methods

This section presents the methods used to calculate ozone exposure isopleths. First, modifications to the air quality model from section 2.1.2 are discussed. Next, the computation of ozone exposure isopleths from the adjoint sensitivities and modeled NO_x and VOC mixing ratios is described. Finally, three quantitative metrics derived from the exposure isopleths that are used to describe the ozone response to changes in NO_x and VOC emissions are described.

3.2.1 Adjoint of GEOS-Chem

Population exposure to ozone is calculated using the adjoint of the GEOS-Chem model (GEOS-Chem Adjoint v33) as described in section 2.1.2. An adjoint model calculates sensitivities, which are partial derivatives of a quantity of interest with respect to various control parameters. The quantity of interest here is annually averaged population exposure to one-hour daily maximum O_3 (denoted Z). This is defined as

$$Z = \frac{1}{N_{\text{days}}} \sum_{k=1}^{N_{\text{cells}}} \sum_{d=1}^{N_{\text{days}}} [p(k) \cdot C_{\text{O}_3}(k,d)], \qquad \text{Eq. 3-1}$$

where k indexes the GEOS-Chem model surface layer grid cells from 1 to N_{cells}, d indexes the number of days from 1 to N_{days} (365), $p(k)$ is the population in grid cell k, $C_{\text{O}_3}(k,d)$ is the mixing ratio (in ppb) of daily maximum O_3 at grid cell k on day d. The population data is re-gridded from the 30 arc-second resolution obtained from the GRUMP 2006 database (Balk et al., 2006). Ozone exposure of the US population only is considered, and therefore the population within grid cells outside the US is set to zero.

Population exposure to one-hour daily maximum O_3 was chosen as the adjoint objective function given that the six-month mean of one-hour daily maximum O_3 is the exposure metric most strongly linked to increased risk of premature mortality (Jerrett et al., 2009). It is noted that premature mortality accounts for > 90% of health costs related to ozone exposure (Hubbell et al., 2005; Levy et al., 2001) and is therefore the most significant health impact. A correction factor can be applied to convert between one-hour maximum ozone and the regulatory metric of eight-hour maximum ozone, if needed (Thurston and Ito, 2001).

The control parameters in this study are hourly emission rates of NO_x (E_N) and VOC (E_V). Therefore, the adjoint sensitivities calculated by GEOS-Chem are

$$Z_N = \partial Z / \partial E_N(K,T), \qquad \text{Eq. 3-2}$$

and

$$Z_V = \partial Z / \partial E_V(K,T), \qquad \text{Eq. 3-3}$$

with units of ppl·ppb·(kg/hr/box)$^{-1}$ and are specified for every grid box (K) and hour of the year (T).

VOCs are a combination of several hydrocarbons and in this work an average emissions speciation profile – i.e. the amount of each species emitted per unit of VOC – from the US EPA's SPECIATE database (US EPA, 2014b) is applied to the adjoint model outputs. The sensitivity of ozone exposure to VOC emissions is calculated by weighting

the individual hydrocarbon sensitivities by the speciation coefficients. Appendix B contains details on the VOC speciation factors as well as the weighting of sensitivities. Use of an average VOC speciation profile is justified in grid cells where there are multiple sources of anthropogenic VOC emissions; however, this may over- or under-estimate VOC sensitivity where VOC emissions are dominated by a single source (for example, coal-fired power plants). It is noted that the emission inputs to the GEOS-Chem forward model include source-specific speciation profiles.

3.2.2 Construction of the ozone exposure isopleth

The ozone exposure isopleths developed in this work quantify the effects of emissions in a grid cell (or multiple grid cells, in the case of city-level isopleths) to annual-average daily maximum ozone exposure in the US as a function of the ambient NO_x and VOC mixing ratios. The approach of using adjoint sensitivities to create ozone exposure isopleths is based upon using the sensitivities to describe the ozone exposure response at the NO_x and VOC mixing ratios occurring at the same time step and location.

Time-varying adjoint sensitivities (at hourly time resolution) over an annual period from the GEOS-Chem adjoint model are used together with hourly concentrations of NO_x and VOC as calculated by the GEOS-Chem forward model. The hourly adjoint sensitivities are first sorted according to their corresponding VOC and NO_x concentrations. The resulting VOC-NO_x (V-N) space is discretized into equally-sized bins and the sensitivities within each bin of VOC-NO_x concentration pairs are averaged. The adjoint sensitivities are weighted by a time-varying mapping between emissions and concentrations before averaging (discussed below). This results in a vector field of ozone exposure gradients – i.e. a gradient vector $\mathbf{V}=[\overline{Z_V},\overline{Z_N}]$ defined at every V-N coordinate, that represents the average VOC and NO_x sensitivity within the bin (denoted $\overline{Z_V}$ and $\overline{Z_N}$).

An example of the gradient vector field is shown in Figure 3-4(a). The VOC and NO_x axes are curtailed at the 85th percentiles of the hourly VOC and NO_x concentrations in order to ensure that the ozone exposure gradients are well-represented everywhere

58

within the *V-N* space. The vector field **V** represents the average sensitivity of ozone exposure to emissions at each *V-N* coordinate, and variations in sensitivities within each *V-N* coordinate (e.g. due to meteorology) are not explicitly captured.

The gradient vector field is integrated to obtain a surface of population exposure to daily maximum O_3. The integration is performed with respect to NO_x and VOC mixing ratios, whereas the adjoint sensitivities relate changes in ozone exposure, dZ, to perturbations in hourly NO_x and VOC emission rates (dE_N and dE_V respectively),

$$dZ = (\partial Z / \partial E_N) \cdot dE_N + (\partial Z / \partial E_V) \cdot dE_V = Z_N \cdot dE_N + Z_V \cdot dE_V. \qquad \text{Eq. 3-4}$$

Perturbations in emissions are related to an equivalent change in hourly mixing ratios within each grid cell via a box model (Seinfeld and Pandis, 2006), which describes the relationship between the emissions rate perturbation (dE, kg·hr^{-1}·box^{-1}) and concentration of NO_x or VOC (χ) within the box,

$$\frac{d}{dt}(\epsilon \chi \, L \, W \, H) = dE + R \cdot (L \, W \, H) - S + u \, W \, H \cdot \epsilon(\chi^0 - \chi). \qquad \text{Eq. 3-5}$$

Here, ϵ is the conversion between mixing ratio units (ppb or ppbC) and mass units (kg/km^3 or kgC/km^3) for NO_x or VOC, L is the length of the box in km, W is its width (assumed to be 50km in this case), H its height in km, R is the chemical production rate, S is the deposition removal rate, u is the wind speed across the box in km·hr^{-1} and χ^0 is the background concentration of NO_x or VOC in ppb or ppbC. Note that the background concentration is assumed to be constant within the box and therefore the sub-grid convection is assumed to occur due to advection (i.e. no concentration gradients).

The contribution of chemistry and deposition processes (R and S in Eq. 3-5) are assumed to be small relative to emissions rate on the spatial and time scale of interest (local mixing ratios on an hourly time scale), and are therefore neglected. This is justified since chemistry and deposition processes occur on relatively longer time scales, with the typical lifetime of NO_x being 1-2 days and those of VOCs being on the scale of

several hours to days at the surface (Seinfeld and Pandis, 2006). Assuming steady state conditions (i.e. the time derivative is set to zero), Eq. 3-5 simplifies to

$$\chi - \chi^0 = d\chi = \frac{dE}{uWH\epsilon},$$

Eq. 3-6

The box height, H, is taken to be the depth of the mixed layer; this is consistent with the boundary layer mixing assumption used in the version of the GEOS-Chem model employed in this study, but could over-estimate mixing when the planetary boundary layer (PBL) is weakly unstable or stable (Lin and McElroy, 2010).

Through Eq. 3-6, changes in NO_x and VOC emission rates (dE_N and dE_V) are related to changes in their local mixing ratios (dN and dV),

$$dN \cdot \epsilon_N = dE_N/uWH$$

Eq. 3-7

and

$$dV \cdot \epsilon_V = dE_V/uWH,$$

Eq. 3-8

Solving Eq. 3-7 and Eq. 3-8 for dE_N and dE_V and substituting into Eq. 3-4 yields

$$dZ = Z_N \cdot uWH\epsilon_N \cdot dN + Z_V \cdot uWH\epsilon_V \cdot dV,$$

Eq. 3-9

which enables the integration of the sensitivities with respect to mixing ratios. The PBL height and wind speed at each location are interpolated for every hour from 3-hourly GEOS-5 meteorology fields and are applied to the hourly adjoint sensitivities before averaging (i.e. $\overline{Z_N} = \langle Z_N \cdot uWH\epsilon_N \rangle$ and $\overline{Z_V} = \langle Z_V \cdot uWH\epsilon_V \rangle$).

The gradient vector field is numerically integrated to obtain a surface of population exposure to daily maximum O_3, denoted as $\hat{Z}$. The gradient vector field may not be conservative (i.e. numerical integration is path-dependent) since the adjoint sensitivities that comprise the vector field have been averaged within each VOC-NO_x bin. This path-dependency is overcome by solving for an exposure surface $\hat{Z}$ such that the sum of squared differences between its gradient, $\nabla\hat{Z}(V,N)$, and the adjoint-based gradient vector field, $\mathbf{V}(V,N)$ is minimized. The sum of squared errors between $\nabla\hat{Z}$ and $\mathbf{V}$ is written as,

$$\varepsilon = \sum_{V,N} \left(\hat{Z}_V(V,N) - \overline{Z_V}(V,N)\right)^2 + \left(\hat{Z}_N(V,N) - \overline{Z_N}(V,N)\right)^2. \qquad \text{Eq. 3-10}$$

Here, the partial derivatives of $\hat{Z}$, $\hat{Z}_N$ and $\hat{Z}_V$, are expressed in terms of $\hat{Z}$ through a first-order finite difference – for example, $\hat{Z}_N(V,N) = \left(\hat{Z}(V,N+\Delta N) - \hat{Z}(V,N)\right) \cdot (\Delta N)^{-1}$. The exposure surface $\hat{Z}$ that minimizes the sum of squared errors ε is then solved for. Similar approaches are used in surface reconstruction from shadows in the field of image processing (Harker and O'Leary, 2008; Horn, 1990). The arbitrary integration constant – i.e. the value of $\hat{Z}(0,0)$ – is set such that the ozone exposure surface is never negative inside in the V-N domain. The integration constant does not have an effect if the ozone exposure isopleth is used to quantify changes in ozone exposure resulting from changing emissions. The isopleths quantify the ozone exposure response from hourly emissions perturbations, since hourly sensitivities are used in the integration.
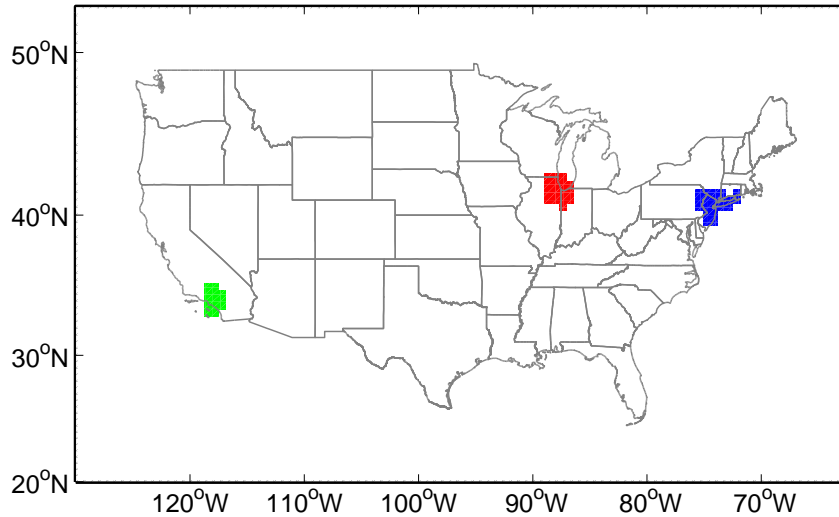
Figure 3-2: Grid cells belonging to one of the three most populous metropolitan statistical areas (MSAs) in the US. Blue grid cells are part of the New York MSA, red grid cells belong to the Chicago MSA and green cells belong to the Los Angeles MSA.

Ozone exposure isopleths are developed for each grid cell in the US. City-level isopleths for the three most populous cities in the US – New York, Los Angeles, and Chicago – are computed by aggregating sensitivity and concentration data from all the grid cells within the respective Metropolitan Statistical Areas (MSAs). MSA boundaries are obtained from the US Census Bureau 2010 Core-based Statistical Areas (US CENSUS,

2010), and are mapped onto the GEOS-Chem model grid cells using the ArcGIS mapping software. The spatial coverage of each MSA is plotted in Figure 3-2.

3.2.3 Calculating ozone exposure isopleth metrics

Information from the ozone exposure isopleths is summarized by extracting three metrics that describe the ozone response to changes in NO_x and VOC emissions. First, the VOC/NO_x ratio of the ridge line of the isopleth diagram is quantified, which provides information on the chemical regime that governs ozone exposure for emissions in each grid cell. Second, the ozone exposure-neutral concentration ratio in the VOC-limited exposure regime is calculated – that is, the ratio of VOC and NO_x concentration perturbations that neither increases nor decreases ozone exposure. Finally, the duration of the year during which VOC-limited exposure conditions prevail in each grid cell is quantified. The calculation of these three metrics is explained in the following sections. These metrics are depicted graphically on a notional isopleth diagram shown in Figure 3-3, and are described in detail in the following sections.
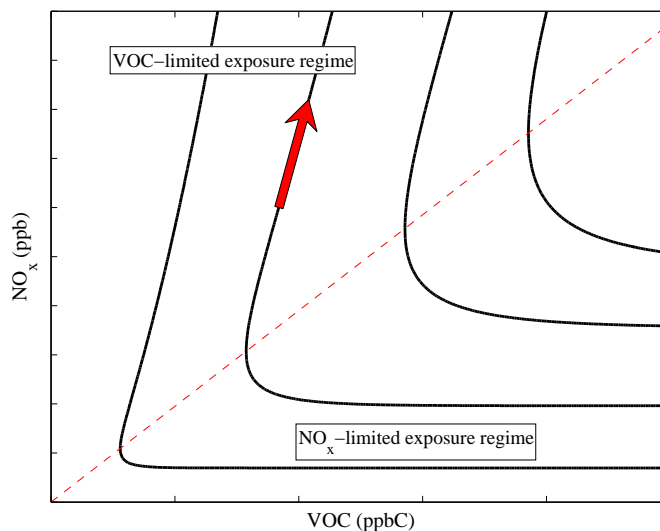
Figure 3-3: Notional ozone exposure isopleth diagram. Contours represent ozone exposures and increase in value towards the top-right of the figure. VOC- and NO_x-limited exposure regimes are labeled on the plot. The red dashed line represents the ridge line of the ozone exposure isopleth diagram, which is defined as the local maximum ozone level with respect to variations in NO_x at a fixed VOC level (the slope of the ridge line is quantified in this study). The red arrow represents a vector of VOC and NO_x emissions that neither increases nor decreases ozone exposure and is its slope is quantified in this study as an ozone exposure-neutral VOC/NO_x emission ratio.

VOC/NO$_x$ ratio of the ridge line of the ozone exposure isopleth diagram

The ridge line on an isopleth diagram separates the NO$_x$-limited and VOC-limited exposure regimes. The ridge line for ozone isopleths typically has a constant VOC/NO$_x$ ratio (Sillman, 1999). In this case, the ridge line is used to determine whether additional NO$_x$ emissions increase or decrease population exposure to ozone under a given ambient NO$_x$ and VOC concentration.

The ozone ridge is defined as the local maximum ozone level with respect to variations in NO$_x$ at a fixed VOC level (Ainslie and Steyn, 2006; Seinfeld and Pandis, 2006; Tonnesen and Dennis, 2000). The ozone exposure ridge line is estimated from the surface $\hat{Z}$ by first calculating the VOC/NO$_x$ ratio of the ozone exposure maximum for every VOC bin. Then, the individual VOC/NO$_x$ ratios are averaged over all VOC bins to estimate the VOC/NO$_x$ ratio of the ridge line.

Ozone exposure-neutral concentration ratio

In a VOC-limited exposure regime, ozone exposure is reduced with increasing NO$_x$ concentrations and increased with increasing VOC concentration. The slope of the ozone exposure isopleths in this regime indicates the ratio of VOC/NO$_x$ concentration that is exposure-neutral. This indicates a ratio of concentrations that neither increases nor decreases ozone exposure. It is noted that an ozone-neutral VOC/NO$_x$ concentration ratio implies an ozone-neutral emissions ratio, since changes in emissions result in changes to ambient concentrations via Eq. 3-7 and Eq. 3-8.

The ozone exposure-neutral concentration ratio is calculated numerically via the discretized ozone exposure surface $\hat{Z}$. First, lines of constant exposure are calculated over each discrete panel of $\hat{Z}$ (e.g. see Figure 3-4(b)) using the geometry of the panel (i.e. by evaluating the cross product of the surface normal and vertical unit vectors). These lines are isopleths, by definition, and therefore their slopes indicate the VOC/NO$_x$ concentration ratio that result in a constant ozone exposure level. This calculation is performed for each panel in the VOC-limited exposure regime and the median slope over all panels is reported for each ozone exposure surface. The ozone exposure-neutral ratios are calculated only in the VOC-limited exposure regime as ozone exposure is negatively

sensitive to NO_x emissions and more sensitive to VOC emissions in this regime than the NO_x-limited regime.

Annual duration of VOC-limited exposure conditions

The ridge line VOC/NO_x ratio is used to quantify the percentage of the year that the exposure is VOC-limited at each location. This metric is calculated by identifying the times when the ambient VOC/NO_x ratio, obtained from the forward GEOS-Chem simulation for 2006, is less than that of the ridge line.

3.3 Ozone exposure isopleths at the three most populous US cities

Figure 3-4(a) shows the gradient vector field described in Section 3.2.2 for the Los Angeles MSA, calculated from the hourly adjoint sensitivities over a full year. The vector field represents the gradient of the ozone exposure surface, $\hat{Z}$, i.e. the vectors point in the direction of increasing ozone exposure. The nonlinear dependence of ozone exposure on ambient NO_x and VOC levels are observed from this vector field. For VOC/NO_x concentration ratios larger than ~10.1 ppbC/ppb, the atmosphere is NO_x-limited and increasing NO_x emissions leads to greater population exposure to ozone. For relatively lower VOC/NO_x ratios, the atmosphere is in a VOC-limited exposure regime and the effect of increasing NO_x is a decrease in ozone exposure. Ozone exposure increases with VOC emissions in the VOC-limited exposure regime, while in the NO_x-limited exposure regime, ozone exposure is relatively less sensitive to VOC.

The result of numerically integrating the gradient field from Figure 3-4(a) is shown in Figure 3-4(b). Contours of the exposure surface for Los Angeles are shown in Figure 3-5(d). The isopleths developed in this work relate the national population exposure to ozone with NO_x and VOC ambient conditions that occur at the location and time of emissions, i.e. the characteristic concentrations on the axes of the isopleth diagram are the grid cell of emission, while the isopleths are the lines of constant population ozone exposure integrated over all grid cells in the US.
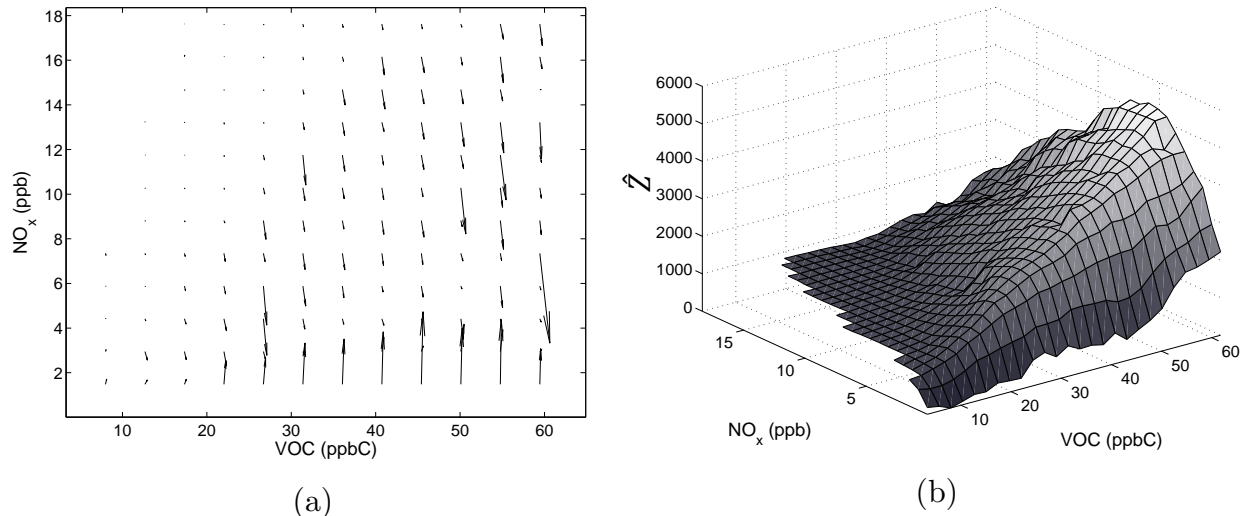
Figure 3-4: The ozone exposure response for emissions in the Los Angeles Metropolitan Statistical Area (MSA). Panel (a) shows the gradient vector field based on hourly adjoint sensitivities of population exposure to daily maximum ozone with respect to NO_x and VOC emissions. The adjoint sensitivities are taken from all model grid cells within the MSA and include a mapping between emissions and concentration of NO_x and VOCs (as described in Section 3.2.2). Note that only vectors from every third NO_x-VOC bin are plotted for clarity. Panel (b) shows the ozone exposure surface (with units of ppl·ppb) obtained by numerically integrating the gradient vector field in (a).

The ozone exposure isopleths at the three most populous urban centers in the US – New York, Los Angeles and Chicago MSAs – are shown in Figure 3-5. The isopleths represent the impact of NO_x and VOC emissions within the cities on integrated ozone exposure in the US. The VOC/NO_x ratios of the ridge lines are 7.9, 10.1 and 6.7 ppbC/ppb for the New York, Los Angeles and Chicago MSAs, respectively. This is within the range of previous estimates of ridge lines isopleth diagrams for local ozone concentrations in urban environments: Finlayson-Pitts and Pitts (1993) and Pereira and Amiridis (1995) both suggest a ridge line VOC/NO_x ratio of ~8; Kinosian (1982) notes that the ridge line varies between 5-20; Seinfeld and Pandis (2006) present an ozone isopleth diagram in Atlanta with a VOC/NO_2 ratio of 5.5, and note that variations may exist depending on the mix of VOCs; Tonnesen and Dennis (2000) find a VOC/NO_x ratio of 8 from ozone simulations over Atlanta. The variability in ridge line ratio estimates reflects the differences in meteorology as well as variability in reactivity of different VOC constituents across locations (Seinfeld and Pandis, 2006).
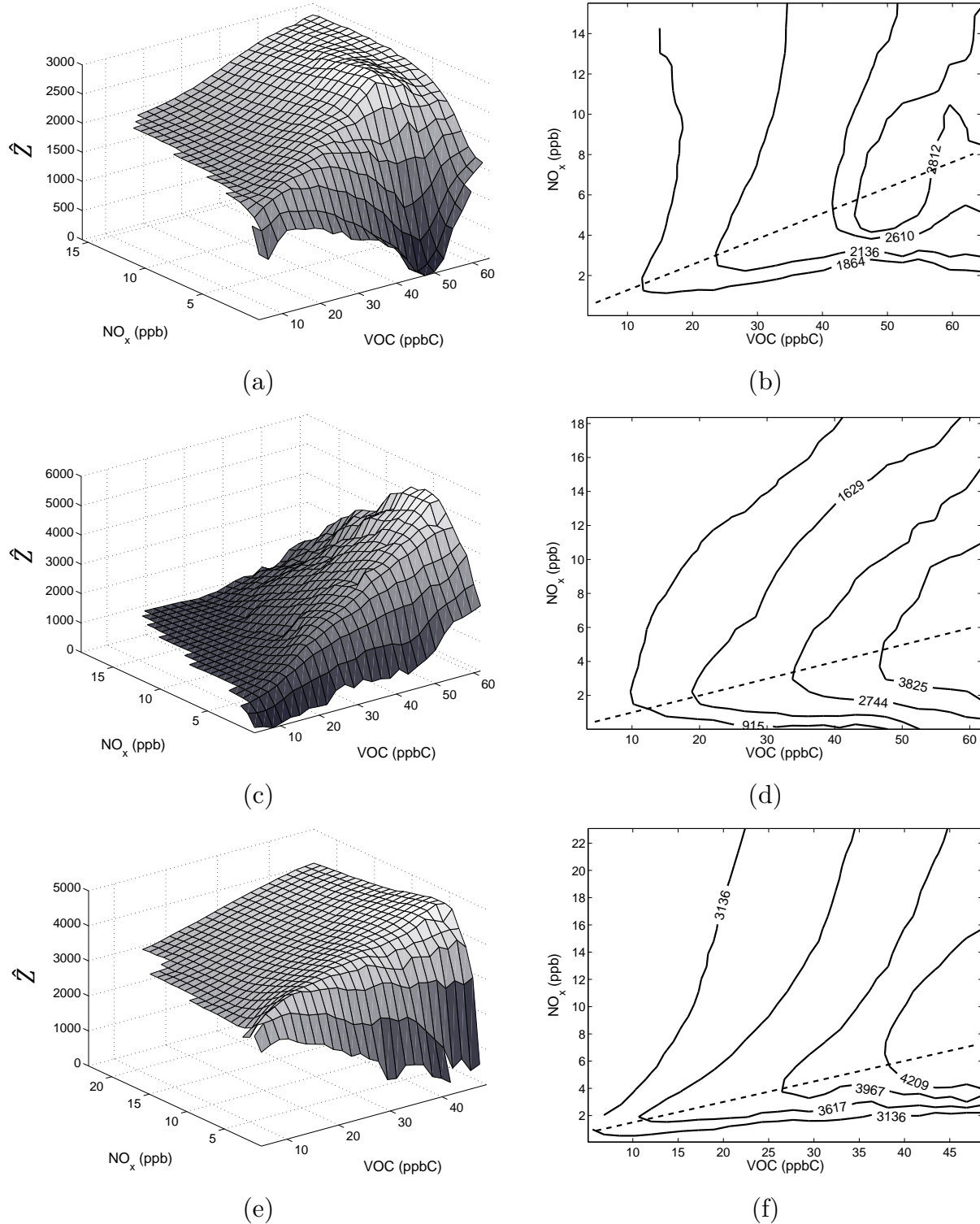
Figure 3-5: Ozone exposure surfaces and associated isopleths for the three MSAs of New York (a, b), Los Angeles (c, d) and Chicago (e, f). Exposure surfaces and contours (or isopleths) of the ozone exposure surface are obtained via numerical integration of the gradient vector field of adjoint sensitivities in each of the cities. Contours are labeled according to their population exposure values, with units of ppl·ppb. The dashed lines in plots (b), (d) and (f) represent the ridge of each ozone exposure isopleth.

The similarity between the local ozone ridge lines and exposure ridge lines of the three MSAs is likely a result of the population weighting used in the exposure calculations (e.g. Eq. 3-1). The weighting emphasizes local ozone formation given the relatively high population densities within the MSAs compared to surrounding areas. It must be noted, however, that the nationally-based ozone exposure metric does not explicitly quantify local-scale ozone exposure impacts. For instance, NO_x emissions often increase O_3 downwind while reducing local O_3 during VOC-limited conditions, and thus local O_3 disbenefits of NO_x controls could be under-estimated in cases where the population density was greater downwind than near the source. For regulatory analyses focused on local-scale impacts (e.g. State Implementation Plans), the adjoint function could be re-defined for selected urban domains of interest depending on the population distribution and prevailing wind patterns.

Using the ozone exposure ridge line and hourly modeled VOC and NO_x mixing ratios, the duration of VOC-limited exposure conditions is calculated to be 44%, 50% and 64% of the year for the three MSAs, respectively. VOC-limited exposure conditions occur more frequently in the winter months than the summer (68%, 66% and 88% of the time in December-February, and 20%, 35% and 37% in June-August for the three MSAs, respectively). The VOC-limited exposure duration may also be inferred from the sign of ozone sensitivity to NO_x, obtained from the adjoint simulation. If negative, it implies a VOC-limited atmosphere since ozone is reduced with NO_x emissions. The adjoint NO_x sensitivities are negative for 47%, 43% and 59% of the year for the three MSAs, respectively, and are within 3-7% of the VOC-limited durations predicted by the isopleth diagrams. Thus, the ridge line VOC/NO_x ratios, used together with modeled (or measured) NO_x and VOC concentrations, are useful in determining the ozone exposure regime.

The median and interquartile range of ozone exposure-neutral VOC/NO_x concentration ratios are 0.63 (0.09-1.31), 1.61 (0.87-2.81) and 0.72 (0.42-1.37) ppbC/ppb for the New York, Los Angeles and Chicago MSAs. The variability in exposure-neutral concentration ratios of each isopleth is a result of non-linear ozone response depending on different

ambient NO_x and VOC conditions. An emissions reduction during VOC-limited conditions that results in a VOC/NO_x concentration ratio lower than the ozone-neutral ratio leads to increased total ozone exposure. For instance, average VOC and NO_x emission factors for heavy-duty diesel trucks are 0.447 g/mile and 8.613 g/mile (US EPA, 2008a). The resulting VOC/NO_x concentration ratio (calculated using Eq. 3-7 and Eq. 3-8 and assuming the diesel exhaust VOC speciation) is ~0.067 ppbC/ppb. This is lower than the median and 25th percentile ozone-neutral ratios of all three cities. Under VOC-limited exposure conditions, therefore, reducing activity from heavy-duty diesel trucks in the three MSAs will likely increase national population exposure to ozone. The isopleths represent national exposure impacts arising from emissions at the specified location or MSA only, and may not be indicative of the integrated impact of regional or national emission controls. For instance in the case of regional NO_x emission reductions, ozone reductions in NO_x-limited environments upwind of the city could offset O_3 enhancements in VOC-limited conditions within urban areas due to ozone transport (Schichtel and Husar, 2001; Sillman, 1993).

3.4 Validation of ozone exposure isopleths

In this section, the ozone exposure isopleths are validated in two steps: first, the adjoint sensitivities are compared against the forward model; second, the changes in ozone exposure predicted by the isopleth diagrams are compared to those calculated by the adjoint sensitivities.

The adjoint sensitivities are validated against the forward GEOS-Chem model to establish their accuracy in predicting the ozone exposure response to an emission perturbation. Surface-layer NO_x emissions from the 2005 US NEI are perturbed by 10% in each of the four quadrants of the US during January and July. For each of the 8 cases, the integrated population exposure to daily maximum ozone from the forward model is compared to that calculated using the adjoint sensitivities. As shown in Figure 3-6, there is good agreement between the adjoint sensitivities and the forward model, with a slope of 1.03 and R^2 of ~1.0.
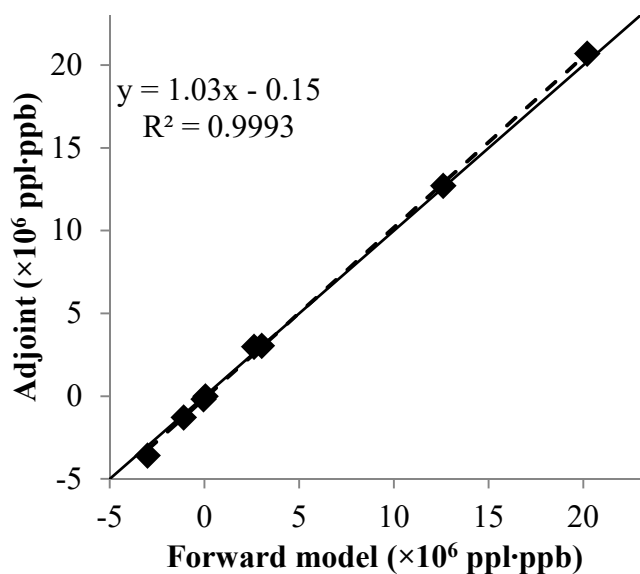
Figure 3-6: Comparison of the integrated population exposure to daily maximum ozone as calculated using the forward GEOS-Chem model and the adjoint sensitivities. Values computed using the forward GEOS-Chem model are plotted on the abscissa while values calculated using the adjoint sensitivities are shown on the ordinate. Exposures are calculated for a 10% perturbation to surface-level NO_x emissions in each of the four quadrants of the US during January and July. The dashed line represents the line of best fit, whose equation and coefficient of determination (R^2) are reported. The solid line denotes parity.

The ozone exposure response predicted by the isopleth is validated against the response calculated from the adjoint sensitivities. This quantifies the errors in the construction of the exposure surface (i.e. the averaging and integration steps). A NO_x concentration perturbation of 0.01 ppb is implemented for each VOC-NO_x bin on the isopleth and the ozone exposure response is quantified. The same NO_x perturbation is evaluated using the hourly adjoint sensitivities (where the concentration perturbation is mapped to equivalent emissions via Eq. 3-7). The adjoint-based exposures corresponding to the VOC and NO_x conditions of each bin are then averaged in order to compare against the isopleth-based exposure of that bin. This is done because the isopleth quantifies the average response to perturbations within each VOC-NO_x bin. The standard deviation of adjoint-based responses within each VOC-NO_x bin is calculated, which quantifies the variability in ozone response for a given VOC-NO_x condition.
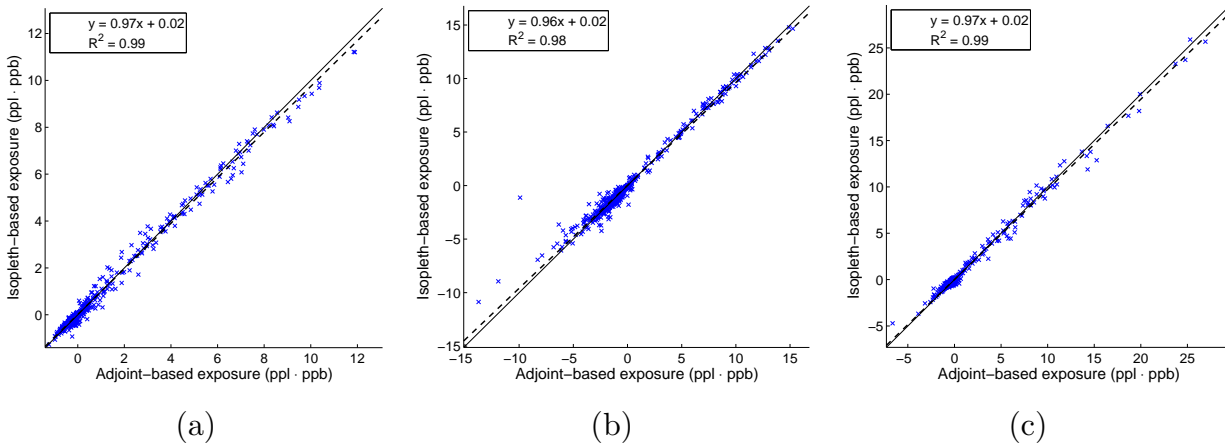
Figure 3-7: Comparison of isopleth-based and adjoint-based ozone exposures for a 0.01 ppb NO_x concentration perturbation. The concentration perturbation is mapped to an equivalent emission perturbation on an hourly basis via Eq. 3-7. Results are compared on the basis of each VOC-NO_x bin. Panel (a) shows the comparison for the New York isopleth, (b) for the Los Angeles isopleth and (c) for the Chicago isopleth. The coefficient of determination (R^2) and equation of the line of best fit (plotted as a dashed line) are reported in the inset of each figure.

Figure 3-7 shows the comparison between the isopleth-based and adjoint-based exposures for a 0.01 ppb NO_x perturbation for each VOC-NO_x bin (~600 bins in each isopleth diagram). In all three cases the isopleth-based results are well-correlated with the adjoint-based results ($R^2 \geq 0.98$), with slopes between 0.96 and 0.97. Figure 3-8 shows the mean and standard deviation of the hourly adjoint-based exposures in each VOC-NO_x bin for the New York, Los Angeles and Chicago exposure surfaces. The standard deviation varies from bin to bin, and the average normalized standard deviation for bins with at least ±1 ppl·ppb is ~237% for the Los Angeles isopleth, ~284% for the New York isopleth and ~225% for the Chicago isopleth. This variability is likely due to meteorology and other factors that vary hourly and are not explicitly represented by the exposure response surface.
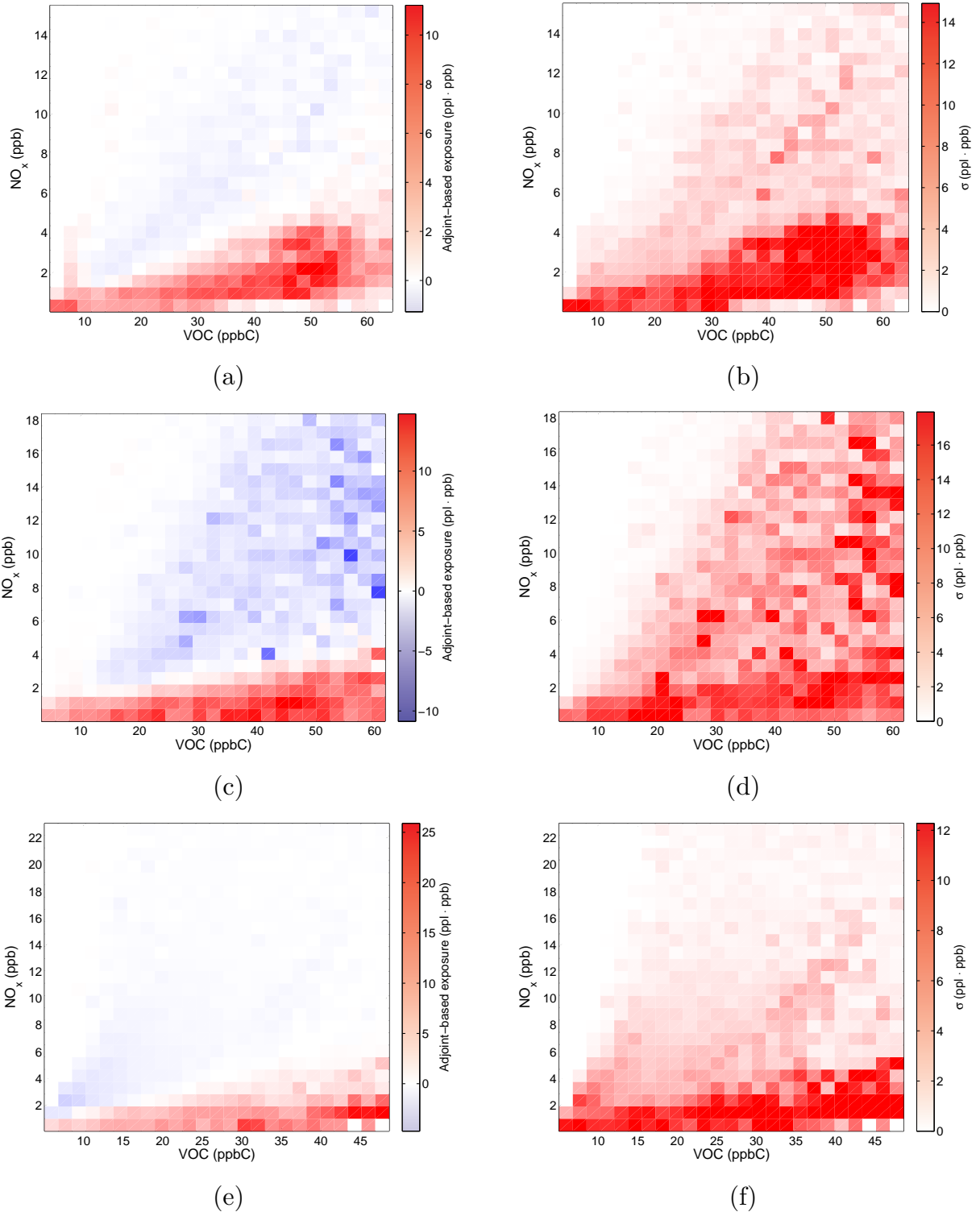
Figure 3-8: The mean and standard deviation of the hourly adjoint-based exposures within each VOC-NO_x bin from a 0.01 ppb NO_x concentration perturbation. Panels (a) and (b) show the mean and standard deviation for the New York exposure surface, (c) and (d) for the Los Angeles exposure surface and (e) and (f) for the Chicago exposure surface. The concentration perturbation is applied within each VOC-NO_x bin and mapped to an equivalent emission perturbation on an hourly basis via Eq. 3-7.

71

It is therefore observed that the isopleths successfully predict the average exposure response to concentration (or emission) perturbations for each VOC-NO$_x$ condition as well as trends in the ozone exposure regime (i.e. annual duration of VOC-limited exposure conditions as quantified in Section 3.3). However, a key limitation is that they do not capture variations in hourly ozone exposure responses for a given ambient VOC-NO$_x$ condition. The adjoint sensitivity data is hourly so isopleths for a specific subset of time can be computed in principle. It is noted that there may be a delay between the time of emissions and the resulting O$_3$ impacts (e.g. the impact of nighttime emissions on O$_3$ isn't felt until the daytime).

3.5 Ozone exposure isopleths across the US

3.5.1 Duration of VOC-limited exposure conditions

Figure 3-9 shows the duration of VOC-limited exposure conditions for each model grid cell in the US. The durations are computed based on the NO$_x$ and VOC concentrations modeled by GEOS-Chem for 2006 and the ridge line VOC/NO$_x$ ratio, shown in Figure 3-12(a). An empty grid cell means that VOC-limited conditions were not detected (71% of locations, explained further in the following section).
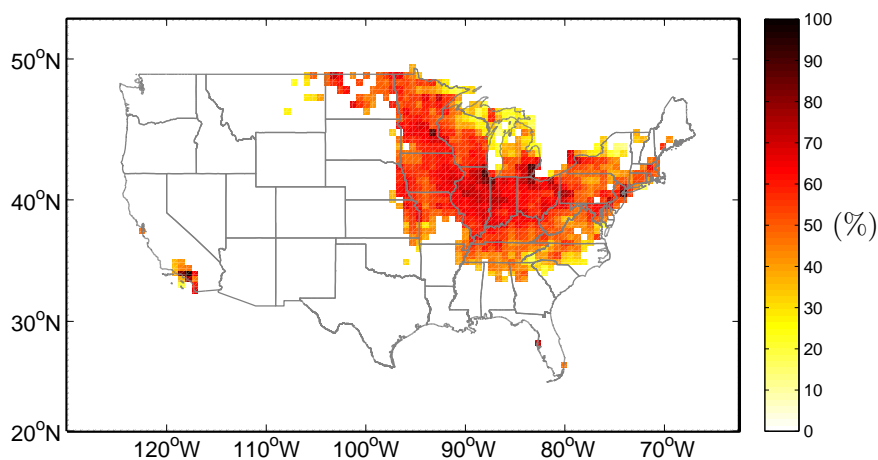
Figure 3-9: Duration of VOC-limited exposure conditions in each grid cell, expressed as a percentage of year. Blank grid cells mean VOC-limited conditions were not detected in that grid cell (71% of grid cells).

Figure 3-9 shows that VOC-limited exposure conditions occur in the Northeast and Midwestern US, around the Los Angeles area in California, as well as in grid cells

72

containing major cities. VOC-limited exposure conditions occur, on average, for 51% of the year at these locations (varying between 13% and 98% of the year). In comparison, the adjoint sensitivities with respect to NO_x emissions are negative for 44% of the year at these locations. These areas are typically polluted with NO_x emissions from industrial activities (e.g. the Midwest), power generation or road traffic in major cities (Caiazzo et al., 2013; Russell et al., 2012) and are therefore more likely to be NO_x-saturated (VOC-limited) with respect to local ozone concentrations as compared to other (relatively unpolluted) areas.

VOC-limited conditions are approximately evenly distributed diurnally, with 45% occurring during the daytime (defined as 6 a.m. to 6 p.m. local time) and 57% occurring at night (6 p.m. to 6 a.m.). VOC-limited conditions occur more frequently during the fall and winter months (67% of the time, on average) than in the spring and summer (37% on average) as seen in Figure 3-10.
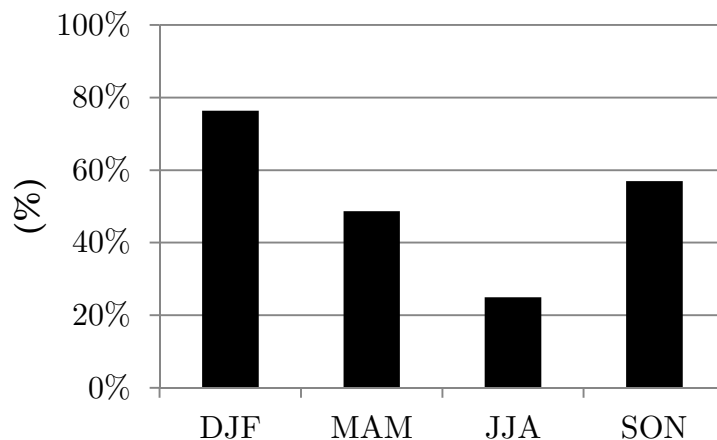
Figure 3-10: Duration of VOC-limited exposure conditions by season, expressed as a percentage of time. Values are averaged over all locations which experience VOC-limited conditions over the year. December, January and February (DJF) are defined as the Winter months, March, April and May (MAM) as Spring, June, July and August (JJA) as Summer and September, October and November (SON) as the Fall.

3.5.2 Isopleths without a VOC-limited exposure regime

Across the US, 71% of locations do not have a VOC-limited exposure regime. As an example, Figure 3-11 shows the ozone exposure isopleth for the Houston MSA. Here, ozone exposure predominantly increases with NO_x emissions and the isopleth does not

have an exposure ridge line (i.e. a local maximum in ozone exposure with respect to NO_x concentrations at each VOC level). Thus, ridge line and exposure-neutral VOC/NO_x ratios do not exist for these locations.
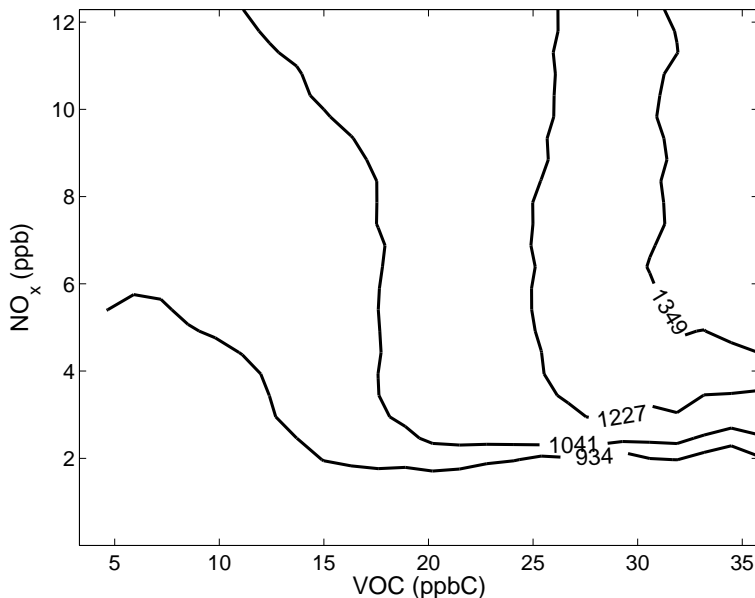
Figure 3-11: Ozone exposure isopleth for the Houston MSA. Contours (or isopleths) are labeled according to their population exposure values, with units of ppl·ppb. Note the absence of an ozone ridge line (and consequently, VOC-limited exposure conditions) since NO_x emissions predominantly increases ozone exposure.

3.5.3 Ridge line and ozone exposure-neutral ratio

The exposure ridge line VOC/NO_x ratios for grid cells that experience VOC-limited exposure conditions are plotted in Figure 3-12(a). The average ridge line ratio across these grid cells is 9.2 ppbC/ppb, varying between 3.1 and 24.0 ppbC/ppb across locations. The highest ridge line ratios (>~10 ppbC/ppb) occur along the Northern US boundary as well as areas surrounding Los Angeles. Grid cells in the eastern Midwestern states have an average ridge line ratio of ~7.6 ppbC/ppb.

The ridge line VOC/NO_x ratios are used to identify the ozone exposure regime at each location based on the atmospheric concentration of VOC and NO_x. For instance, a ridge line ratio of 1 ppbC/ppb suggests that increasing NO_x emissions locally (and therefore increasing ambient NO_x concentrations) will increase national ozone impacts as long as ambient NO_x concentrations are less than ambient VOC concentrations at that location.

74

A relatively higher ridge line ratio of 10 ppbC/ppb indicates that increased NO_x emissions will increase national ozone impacts as long as ambient NO_x concentrations are less than 10% of ambient VOC concentrations, and will reduce national ozone impacts if ambient NO_x concentrations are any higher.
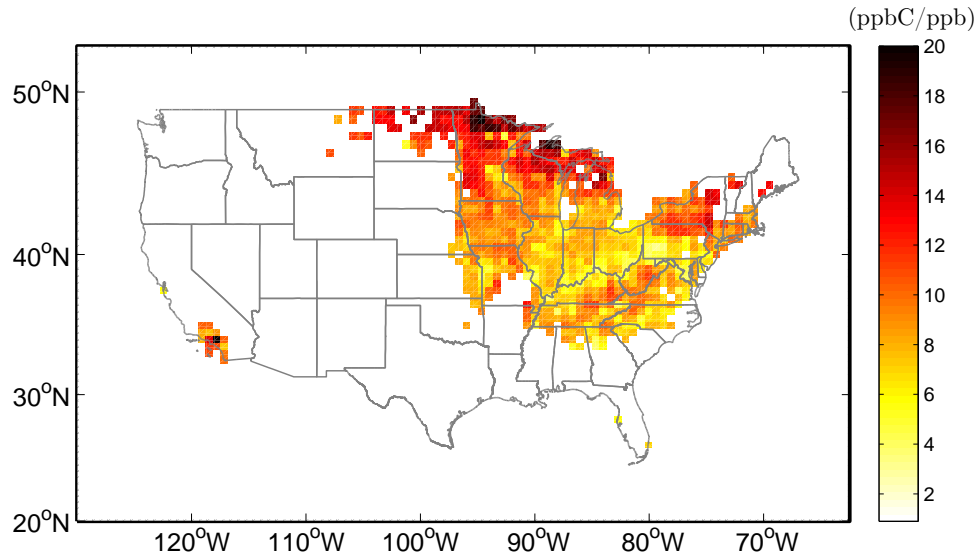
(a)
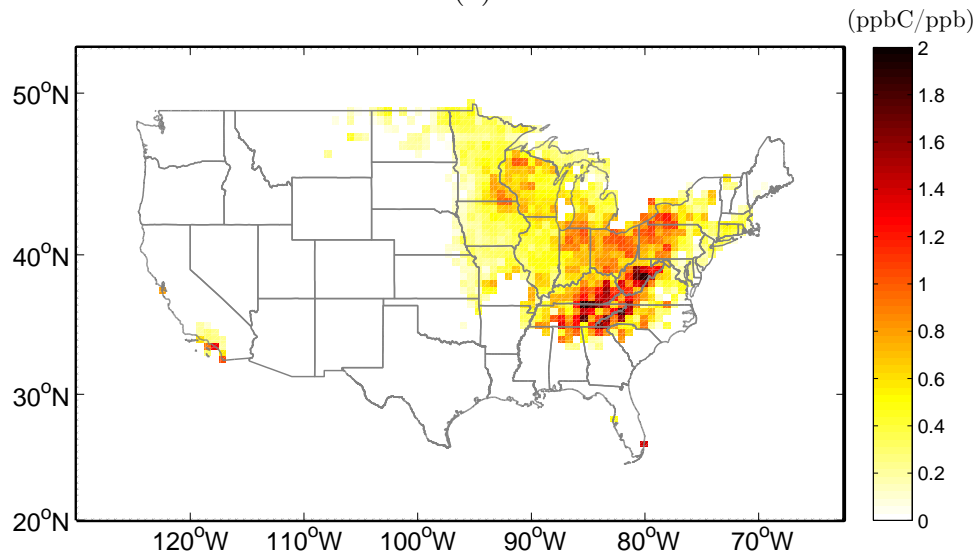
(b)

Figure 3-12: Ridge line VOC/NO_x ratio (a) and ozone exposure-neutral VOC/NO_x ratio (b) in each grid cell, in units of ppbC/ppb. Blank grid cells mean VOC-limited conditions were not detected (71% of grid cells).

Figure 3-12(b) shows the ozone exposure-neutral emissions ratio for grid cells in the US that experience VOC-limited exposure conditions, which range from ~0.01-1.91

ppbC/ppb across the grid cells. As a comparison, Table 3-1 lists the VOC and NO_x emission factors and resulting concentration ratios for several sources. As discussed in Section 3.3, local emissions reductions resulting in VOC/NO_x concentration ratios lower than the ozone neutral ratio at that location are likely to increase US population exposure to annual average daily maximum ozone. The range of spatial variation in the ozone-neutral emissions ratio plotted in Figure 3-12(b) therefore implies the need for site-specific analyses of emissions mitigation policies to minimize the inadvertent increase in ozone exposure.

Table 3-1: Emission factors and VOC/NO_x ratios for five emission sources. Emissions for gasoline cars are average annual emission factors reported in US EPA (2008b), those for heavy-duty diesel vehicles are average annual emission factors reported in US EPA (2008a), those for bituminous coal-fired boilers are U.S. average values reported in Cai et al. (2012) and those for aircraft taxi and takeoff operations for the CFM56-7B22 engine are taken from ICAO (2012). Source-specific VOC speciation profiles are used from the US EPA's SPECIATE database along with Eq. 3-7 and Eq. 3-8 to convert from mass units to concentration units.

	Gasoline car (g/mile)	Heavy-duty diesel (g/mile)	Coal-fired boiler (g/kWh)	Aircraft Taxi (g/kg-fuel)	Aircraft Takeoff (g/kg-fuel)
NO_x	0.69	8.61	1.46	4.50	23.10
VOC	1.03	0.45	0.01	2.88	0.12
VOC/NO_x ratio (ppbC/ppb)	1.822	0.067	0.005	0.771	0.006

Appendix C includes a worked example that shows the usage of the data from Figure 3-9 and Figure 3-12 (i.e. the ridge line VOC/NO_x ratio, ozone-neutral VOC/NO_x ratio and annual duration of VOC-limited exposure conditions) in determining the effect of a reduction in emissions at a particular location.

3.6 Magnitude of emission sensitivities

Figure 3-13 plots the sensitivity of ozone exposure to NO_x and VOC emissions (i.e. the adjoint sensitivities Z_N and Z_V) in each grid cell, and provides a spatial comparison of the impact on ozone exposure due to NO_x and VOC emissions at each location. The sensitivities are taken at 11am local time and are averaged over every day of the year. The hour was chosen to be when ozone exposure is most sensitive to NO_x emissions (the

diurnal pattern of NO_x and HC sensitivities is shown in Figure 3-14). The sensitivities vary diurnally, and in particular, the NO_x sensitivity could change its sign during other times of the day. Thus, VOC-limited conditions (i.e. when NO_x emissions reduce ozone exposure) could exist at certain locations even if they have positive NO_x sensitivity at the specific hour shown in Figure 3-13.

The sensitivity of ozone exposure to NO_x emissions is relatively lower in the Midwest and Mountain regions of the US compared to other areas. The magnitude of NO_x sensitivity peaks near major cities and population centers in the US, with positive values larger than 0.45 ppl·ppb·$(kg/hr/box)^{-1}$ in the areas surrounding New York, New Jersey and the West Coast of the US and negative values lower than -0.05 ppl·ppb·$(kg/hr/box)^{-1}$ within large cities such as New York, Chicago, Miami and Los Angeles. The NO_x sensitivity is less than 0.1 ppl·ppb·$(kg/hr/box)^{-1}$ at rural locations in the Midwest – i.e. from Ohio to Minnesota. The sensitivity of ozone exposure to VOC emissions is relatively higher in the Northeast and Midwest regions of the US as compared to the Southern and Mountain regions. VOC sensitivities peak near major population centers, similar to NO_x sensitivities, with values at or exceeding 0.1 ppl·ppb·$(kg/hr/box)^{-1}$.

The magnitude of emission sensitivities provide context to the ozone exposure isopleths and derived metrics discussed in the previous sections. While the VOC-limited exposure durations, exposure ridge line VOC/NO_x ratios and ozone exposure-neutral emissions ratios provide information on when and where emissions reductions increase national ozone exposure, they do not indicate how much ozone exposure would change if emissions are perturbed at each location. This may be inferred from Figure 3-13, which indicates that controlling emissions near major cities and populated areas (i.e. where the sensitivities are highest) would result in a larger change in ozone exposure relative to controlling emissions in other areas.
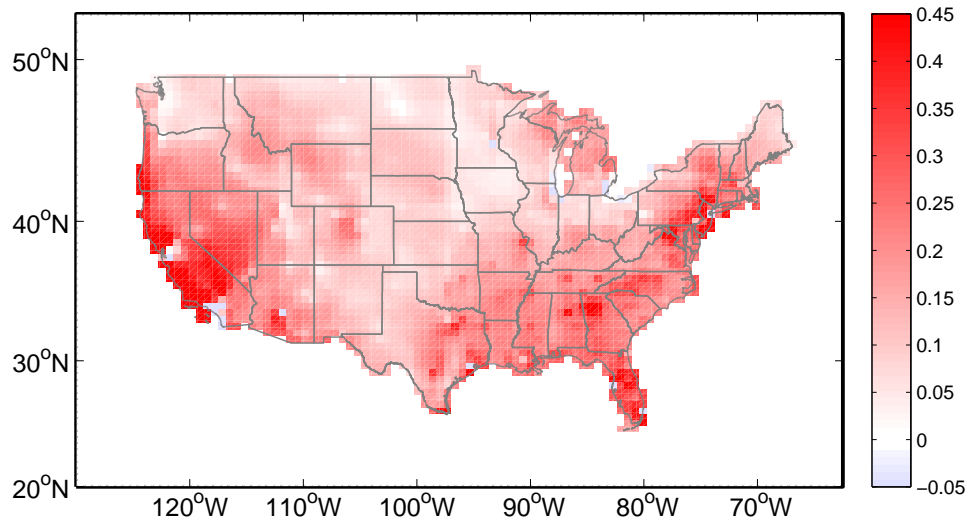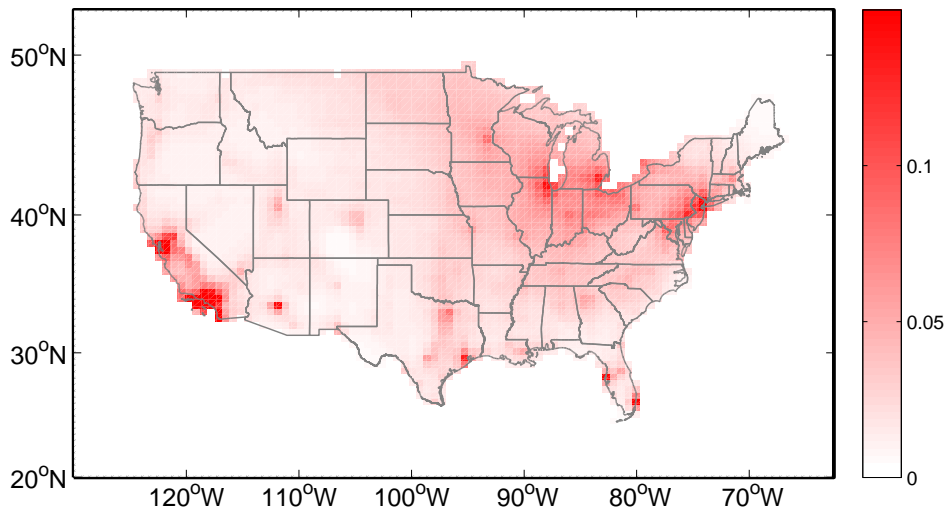
Figure 3-13: Sensitivity of one-hour daily maximum ozone exposure to (a) NO_x emissions and (b) VOC emissions at 11am local time in every grid cell in the US. Sensitivities are averaged over all days of the year and are in units of ppl·ppb·$(kg/hr/box)^{-1}$.
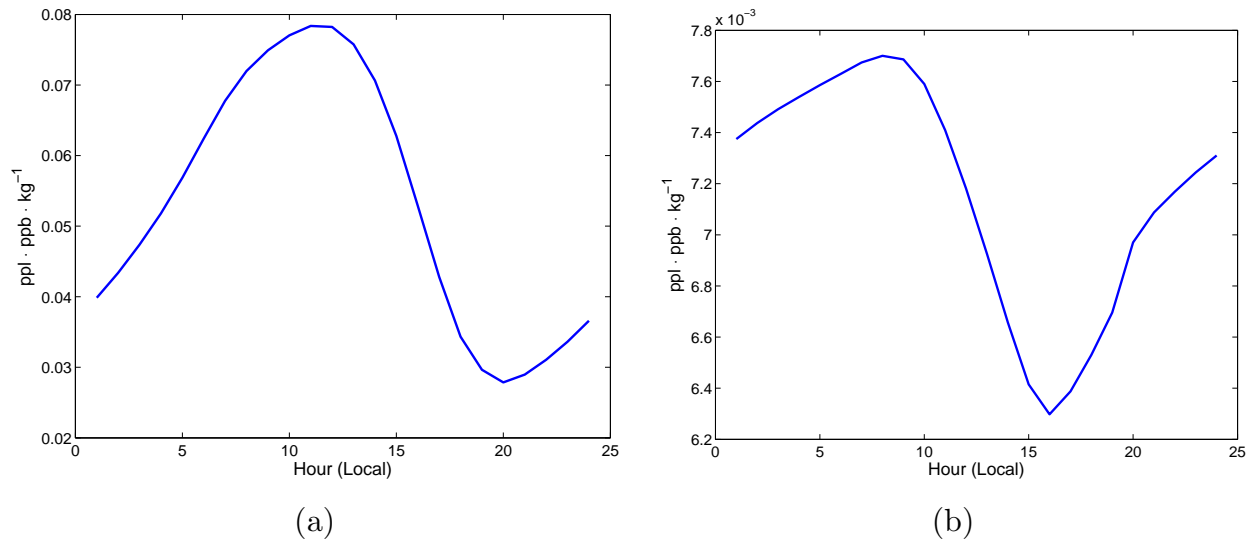
Figure 3-14: Diurnal variation of the sensitivity of population exposure to daily maximum ozone with respect to (a) NO_x emissions and (b) VOC emissions. Sensitivities are spatially averaged throughout the domain and annually averaged. All times are corrected to local solar time based on longitude of the grid cell.

3.7 Summary

Ozone exposure surfaces are created as a function of ambient NO_x and VOC concentrations for all locations in the contiguous US. The adjoint of the GEOS-Chem air quality model used to calculate sensitivities of population exposure to ozone with respect to NO_x and VOC emissions, which are numerically integrated to create the ozone exposure surfaces. Using isopleths derived from the ozone exposure surfaces, the following three metrics have been calculated that quantify the impact of emissions at every location in the US on ozone exposure. The duration of VOC-limited exposure conditions identifies times during the year when lowering NO_x emissions increases ozone exposure. The VOC/NO_x ratio of the exposure ridge line – a line on the ozone exposure isopleth that separates the NO_x-limited and VOC-limited exposure regimes – characterizes the exposure regime based on ambient VOC and NO_x concentrations. Finally, the ozone exposure-neutral emissions (concentration) ratio indicates a ratio of emissions that neither increases nor decreases ozone exposure when in a VOC-limited exposure regime. The main results of this work are listed below:

1) Across the US, 29% of locations experienced VOC-limited exposure conditions in 2006, with an average duration of 51% of the year.

79

2) VOC-limited conditions are approximately evenly distributed diurnally and occur more frequently during the fall and winter months (67% of the time) than in the spring and summer (37% of the time).

3) VOC-limited exposure conditions at the three most populous cities in the US – the New York, Los Angeles and Chicago Metropolitan Statistical Areas (MSAs) – were found to occur during 44%, 50% and 64% of the year.

4) The VOC/NO_x ratio of the exposure ridge line was 9.2 ppbC/ppb on average across individual grid cells in the US that experience VOC-limited exposure conditions.

5) The ridge line ratio was 7.9, 10.1 and 6.7 ppbC/ppb for the three cities, respectively, which is similar to estimates in current literature of 5-20 ppbC/ppb for local ozone maxima in urban areas.

6) Ozone exposure-neutral VOC/NO_x emission ratios were calculated to be 0.63, 1.61 and 0.72 ppbC/ppb in New York, Los Angeles and Chicago.

7) Ozone exposure-neutral emission ratios ranged from ~0.01-1.91 ppbC/ppb across the grid cells in the US, implying the need for site-specific analyses of emissions mitigation policies in order to minimize the inadvertent increase in ozone exposure.

8) Sensitivity of ozone exposure to VOC and NO_x emissions is found to be highest near densely-populated areas and major cities around the US.

It must be noted that the ozone exposure isopleths developed in this work predict the average exposure response of emissions (concentration) perturbations as well as trends in the ozone exposure regime, but they do not capture hourly variations in exposure response for a given VOC-NO_x condition. Local-scale exposure impacts, though included in the aggregate, may not be well-represented by the nationally-based exposure metric, which potentially affects regulatory studies. Future work should consider an adjoint cost function that quantifies ozone concentration exceedances above the US EPA's National Ambient Air Quality Standards (NAAQS). The adjoint emission sensitivities used in this study are based on air quality calculations performed with 2005 anthropogenic emissions, which have declined since. In particular, decreasing NO_x emissions (e.g. due

to reduction in coal usage for power generation or NO_x reduction technologies) will likely lead to greater ozone sensitivity to NO_x emissions, given that net ozone production is increased as a result of reduced titration of ozone at low NO_x concentrations (Seinfeld and Pandis, 2006). Further research is required to quantify the effect of changing anthropogenic emissions on the adjoint emission sensitivities (e.g. using second-order sensitivities or performing new adjoint calculations using an updated emissions inventory).

Nevertheless, this work overcomes the computational complexity of generating ozone exposure isopleths for multiple locations by employing emission sensitivities from the adjoint of an air quality model, thereby providing the information needed to compute ozone exposure isopleths at all locations simultaneously. This is useful in assessing (for all locations in the contiguous US) where NO_x and/or VOC reductions will be effective in reducing national ozone exposure, where they will be counterproductive, as well as the optimal NO_x/VOC reduction ratio.

The next chapter, Chapter 4, couples the hourly variations in atmospheric responses to aircraft emissions with temporal variations in aircraft activity at the DTW airport. Aircraft taxi and takeoff operations are controlled with the objective of minimizing $PM_{2.5}$ and O_3 impacts, accounting for tradeoffs between fuel burn and air quality identified in Chapter 2. This quantifies the improvements in air quality that can be achieved beyond minimizing fuel burn at airports.

Chapter 4

Reducing the air quality and CO_2 impacts of taxi and takeoff operations at airports

This chapter quantifies the air quality and CO_2 climate benefits of two emission mitigation strategies for taxi and takeoff operations at the Detroit Metropolitan Wayne County (DTW) airport in 2007, namely pushback control and de-rated takeoffs. The air quality, climate and fuel costs are monetized, and the minimum air quality, environmental and total fuel combustion-related impacts of ground and takeoff operations are calculated by optimizing pushback delay and takeoff thrust.

Section 4.1 presents the methods used to simulate aircraft operations on the ground and during takeoff. The calculation of fuel burn, emissions and air quality impacts and their valuation is also described. Section 4.2 presents the air quality and CO_2 impacts for one year of simulated taxi operations at DTW, as well as the benefits of pushback control. Section 4.3 performs a similar quantification for de-rated takeoffs. In sections 4.2 and 4.3, the minimum air quality impacts achievable via pushback control and de-rated thrust are shown, and the associated tradeoffs with fuel burn are quantified. The sensitivity of the results to fleet mix, traffic level, takeoff weight and climb profile are also calculated. Section 4.4 presents a summary of this chapter.

4.1 Methods

First, the models used to simulate aircraft movements on the ground and during takeoff are presented in sections 4.1.1 and 4.1.2. Next, the methods used to calculate fuel burn, emissions and air quality impacts as well as their monetized damages are described. Finally, section 4.1.6 describes the optimization of pushback delay and de-rated thrust strategies to minimize air quality and other objectives.

4.1.1 Airport model and gate hold policy

Aircraft taxi operations at the DTW airport are simulated using the integer programming model developed by Lee and Balakrishnan (2010). The model represents the airport taxiways as a set of nodes and links (Figure 4-1) and calculates arrival times at each node along an aircraft's taxi path to minimize total travel time. Constraints representative of those found at airports are implemented including taxi speed limits, minimum separation between aircraft, overtaking on taxiways, maximum gate occupancy time limits and collision avoidance (Lee and Balakrishnan, 2010).
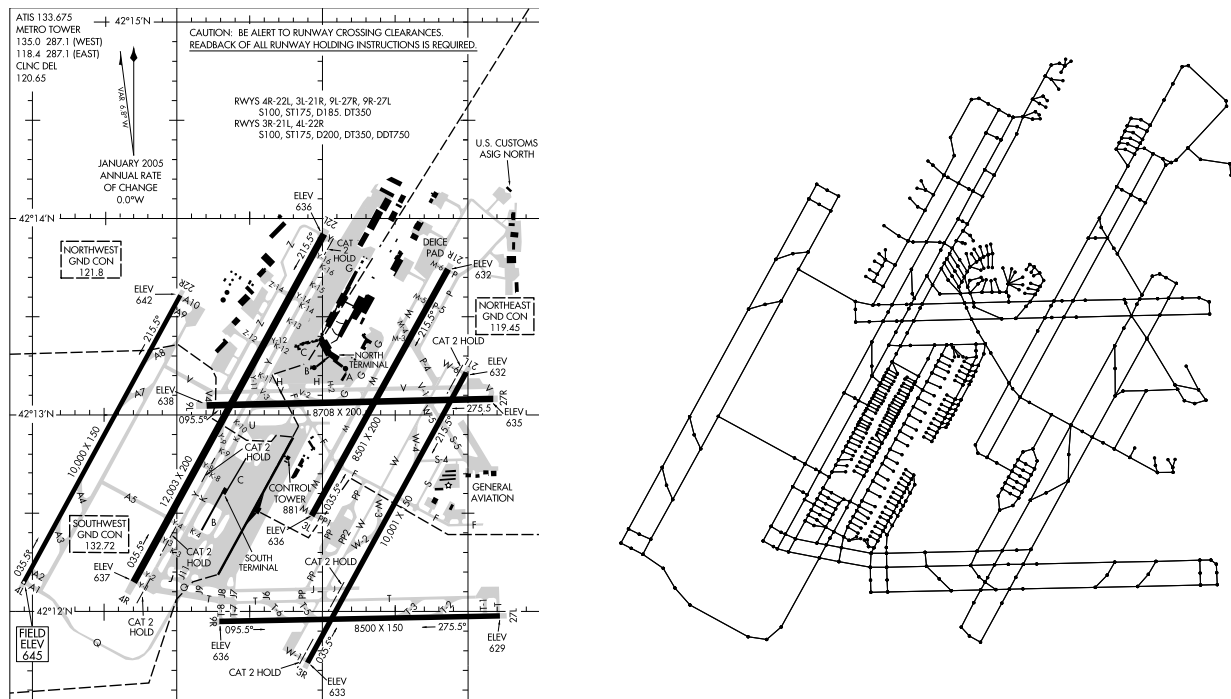
Figure 4-1: Airport layout and node-link representation of the airport surface for the Detroit Metropolitan Wayne County Airport (DTW) as of 2007. Figure is reproduced from Lee and Balakrishnan (2010).

The aircraft schedules for a typical day of operations at DTW are taken from hourly operation counts averaged over the year 2007 from the FAA's Aviation System Performance Metrics (ASPM) database (FAA, 2015). The hourly operation counts are plotted in Figure 4-2. The fleet composition is derived from the FAA's Traffic Flow Management System Counts (TFMSC) database (FAA, 2015). Traffic at DTW in 2007 was comprised of ~5% heavy aircraft (maximum takeoff weight larger than 300,000 lbs), ~10% Boeing 757 aircraft and ~85% large aircraft (takeoff weight between 41,000 lbs and 300,000 lbs). The fleet mix is modeled according to these weight categories since they form the basis of wake vortex separation requirements mandated by the FAA (De Neufville and Odoni, 2013) and therefore affect the runway and gate departure schedule. The Boeing 757 aircraft is categorized in a separate class as it has a relatively strong wake vortex compared to other aircraft in its weight category ("large"). A fourth category exists for aircraft lighter than 41,000 lbs (known as "small"), but activity from this category is not modeled in this thesis given that they comprise mainly general aviation aircraft and non-jet aircraft (De Neufville and Odoni, 2013). The top 5 aircraft types by number of operations are shown in Figure 4-3, and together these aircraft types represent 72% of all departure activity at DTW. Aircraft types are assigned randomly to flights based on their probability of occurrence (e.g. Figure 4-3). A commonly used airport configuration consisting of two departure runways (21R and 22L) and two arrival runways (21L and 22R) is assumed (Lee and Balakrishnan, 2010). Each flight is assigned a gate and runway at random, and a runway scheduler is used to schedule runway times for departing flights (Balakrishnan and Chandran, 2010).
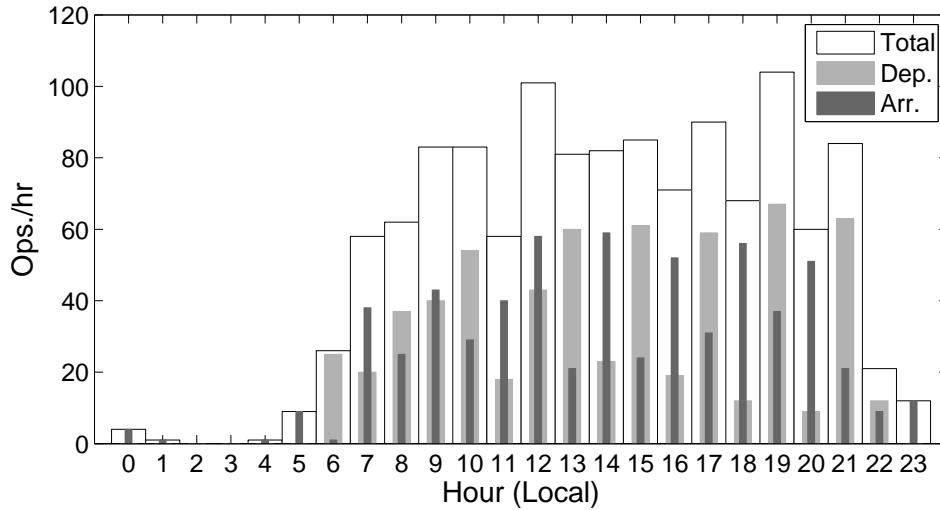
Figure 4-2: Annual average number of operations per hour at DTW in 2007, split by arrival and departure operations. Data is obtained from the FAA's Aviation System Performance Metrics (ASPM) database.
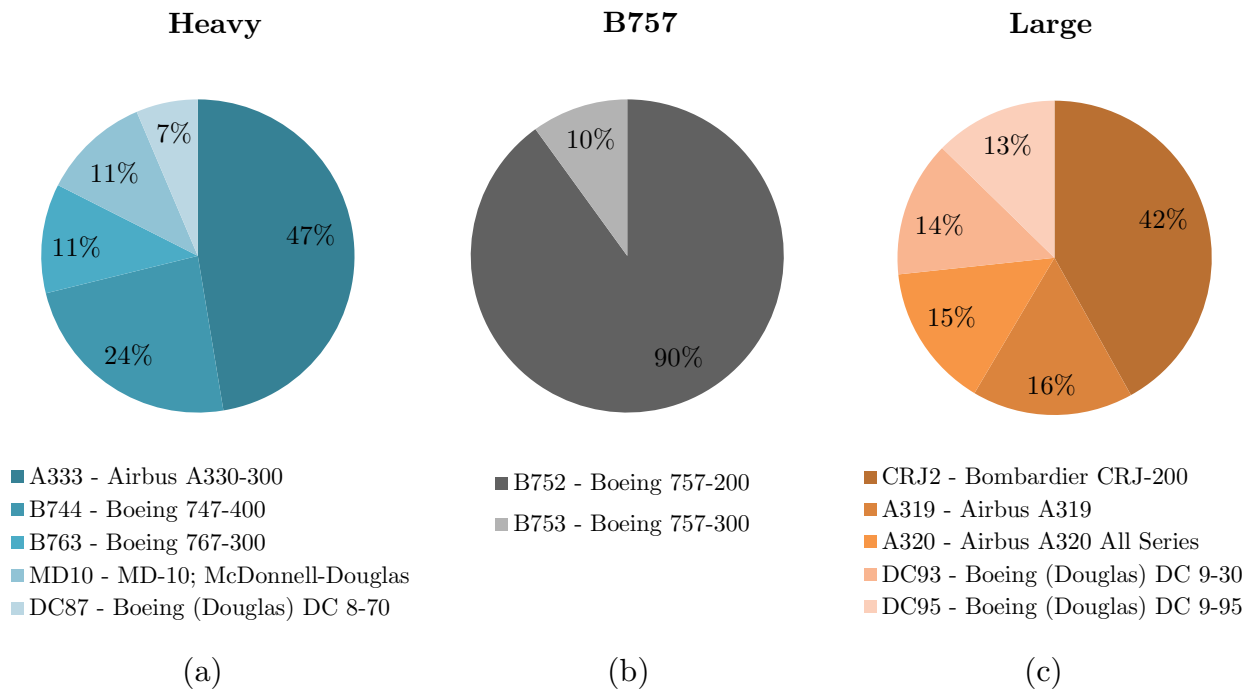
Figure 4-3: Fleet composition of operations at the DTW airport in 2007. The breakdown of (a) Heavy aircraft types, (b) B757 aircraft and (c) Large aircraft types are shown as percentages of the total number of aircraft within each category. Only the top 5 aircraft types by number of operations are shown in each category and are considered in this study.

The airport surface model is used to simulate aircraft taxi movements under a pushback control policy known as gate holding (Lee and Balakrishnan, 2010). Under this policy,

aircraft are held at their gates beginning at their scheduled departure time up to some maximum gate hold limit (e.g. 25 minutes in Lee and Balakrishnan (2010)) in order to reduce taxi-out times. Nine different gate hold limits ranging from no gate holds (i.e. immediate pushback) up to 25 minutes are modeled in this work. The air quality and climate impacts of two policy implementations are assessed: in the first case, the same gate hold limit is applied at all times of the year and for all flights; in the second, the gate hold limit is optimized for each flight based on hourly atmospheric conditions in order to minimize annual air quality, environmental and total impacts (see Section 4.1.6).

4.1.2 Aircraft takeoff performance model and de-rated takeoffs

The takeoff and climb performance of aircraft is modeled using the Base of Aircraft Data (BADA) and models developed therein (BADA, 2013). The BADA total energy model equates the rate of work done by forces acting on the aircraft to changes in potential and kinetic energy,

$$(T - D) \cdot V = mg \frac{\mathrm{d}h}{\mathrm{d}t} + mV \frac{\mathrm{d}V}{\mathrm{d}t} \qquad \text{Eq. 4-1}$$

where T is thrust (N), D is drag (N), V is the true air speed of the aircraft (ms^{-1}), m is the mass of the aircraft (kg), g is acceleration due to gravity (ms^{-2}) and h is altitude above ground (m). Eq. 4-1 is numerically integrated with respect to time given a set of initial conditions, thrust setting and aircraft weight to calculate altitude and speed. It is assumed that all takeoffs occur at 80% of their maximum takeoff weight based on an analysis of Flight Data Recorder (FDR) archives from King and Waitz (2005) and Khadilkar and Balakrishnan (2011a). The takeoff weight of an aircraft is affected by the stage length, passenger load factor and payload (Belobaba et al., 2009; Eyers et al., 2004), and thus the sensitivity of the results to takeoff weight is quantified.

Drag is calculated using the BADA drag model, while maximum takeoff thrust is obtained from the International Civil Aviation Organization (ICAO) engine emissions databank (ICAO, 2012). Fuel flow rates during takeoff are modeled using the thrust specific fuel consumption (TSFC) under takeoff conditions (ICAO, 2012), while those

during other phases of flight are modeled according to the BADA fuel consumption model. The takeoff performance modeling done in this thesis is validated against the PIANO-X aircraft performance model (Lissys, 2008) as well as a previous analysis using FDR data by King and Waitz (2005). Each aircraft is flown at its maximum takeoff weight with both 100% and 85% takeoff thrusts up to 3000 ft, and estimates for total takeoff fuel burn and change in fuel burn due to de-rated takeoffs are compared. Figure 4-4(a) shows that takeoff fuel burn is predicted to within 30% of those calculated from the PIANO-X aircraft performance model, while changes in fuel burn from de-rated takeoffs are estimated to within 2% (Figure 4-4(b)). Comparison with a previous analysis using FDR data for the B777-200ER aircraft by King and Waitz (2005) indicates that the BADA-ICAO model over-predicts fuel burn by ~20% (489kg c.f. 416kg from King and Waitz (2005)) but matches the change in fuel burn from de-rated takeoffs (12% c.f. 12.3% from King and Waitz (2005)).

De-rated takeoffs have been studied from the perspective of extending engine lifetime, reducing maintenance costs as well as mitigating noise impacts (FAA, 1988; Lee, 2005). De-rated takeoffs have been shown to reduce NO_x emissions within the LTO regime as a result of lower combustion temperatures in the aircraft engine (Hall et al., 2007; King and Waitz, 2005), and takeoff thrust reductions of up to 25% are observed in commercial aircraft operations (King and Waitz, 2005; Patterson et al., 2009). This study models reduced thrust takeoffs of 75-100% of maximum thrust using departure activity from the flight schedules developed in Section 4.1.1. Similar to gate holds, the air quality and climate impacts of two implementations of de-rated takeoffs are assessed: in the first case, all aircraft take off with the same thrust setting; in the second case, takeoff thrust is optimized hourly given varying atmospheric conditions for each aircraft in order to minimize annual air quality, environmental and total impacts (explained further in Section 4.1.6).

(a)

(b)
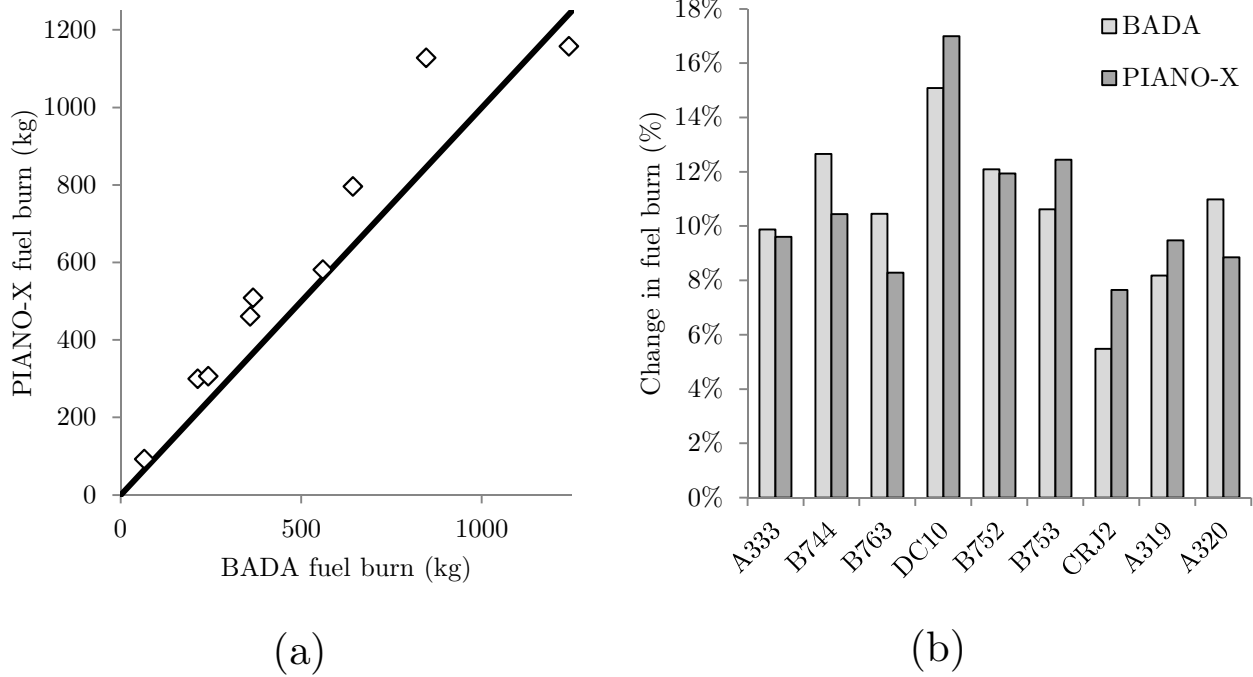
Figure 4-4: Model comparison between the BADA and PIANO-X aircraft performance models. Panel (a) shows fuel burn from climb up to 3000 ft with 100% thrust for nine aircraft types (shown in panel (b)) as predicted by the BADA model and the PIANO-X aircraft performance model. Panel (b) shows the percentage increase in fuel burn for de-rated takeoffs at 85% thrust relative to 100% thrust for nine aircraft types.

The takeoff trajectory is modeled as a series of speed or altitude changes in three segments up to 1000 ft: (a) ground roll acceleration from standstill to takeoff velocity; (b) climb at constant speed to the thrust reduction altitude of 1000 ft; (c) acceleration to the initial climb speed. The trajectory above 1000 ft is not modeled since de-rated takeoffs affect climb performance only up to the thrust reduction altitude. De-rated takeoffs have slower climb rates and travel further during climb than full-thrust takeoffs; an example of this is shown in Figure 4-5 for a Boeing B747-400 aircraft, which traverses an additional 1.2km at 75% thrust compared to 100% thrust. This implies that de-rated takeoffs have a shorter cruise distance and consequently lower cruise fuel burn and emissions relative to higher-thrust takeoffs (James and O'Dell, 2005). The additional fuel burn and emissions incurred at cruise by takeoffs with > 75% thrust is accounted for by calculating the additional cruise flight time required to equalize distance travelled (relative to takeoffs at 75% thrust). In this way, the results of this

study quantify changes in fuel burn, emissions and air quality impacts from de-rated takeoffs over the course of an entire flight.
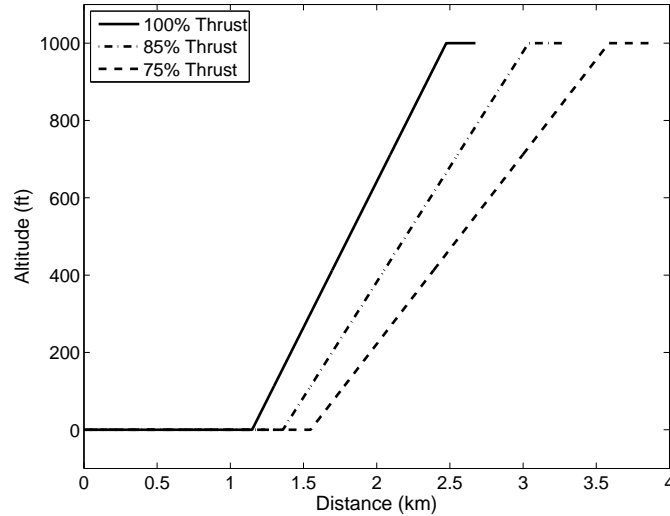
Figure 4-5: Altitude profiles for the Boeing B747-400 aircraft taking off at 80% of its maximum takeoff weight with 75%, 85% and 100% of takeoff thrust. The climb trajectories of aircraft are calculated up to the thrust reduction altitude of 1000ft, after which the climb profile is assumed to be the same regardless of takeoff de-rate. The takeoff trajectory is modeled as a series of speed or altitude changes in three segments (ground roll, climb at constant speed to 1000 ft and acceleration to the climb speed at 1000 ft).

4.1.3 Fuel burn and emissions calculations

Fuel burn and emissions for each aircraft movement are estimated in three steps. First, an engine type is assigned to each flight based on the fleet of aircraft operating in the US. The JP Airline Fleets database (JP Fleets, 2009) is used to determine the most common engine type in use for each fleet of aircraft operated by US airlines. Table 4-1 lists the aircraft-engine mappings used in this work.

Next, fuel burn is calculated based on the engine thrust setting and duration of operation. The engine thrust setting for taxi operations is estimated as a function of the surface trajectory. Two taxi modes are assumed: acceleration from stop (when the aircraft begins to taxi from a standstill) and constant-speed (non-acceleration) taxi. This approach is similar to that used in Jung et al. (2011), Nikoleris et al. (2011) and Stettler et al. (2011).

Table 4-1: The twelve aircraft types modeled in this study and their ICAO code, size category and engine assignments.

Aircraft Model		ICAO Code	Category	Engine
Canadair	RJ-200	CRJ2	Large	GE CF34-3B
Airbus	A-319	A319	Large	IAE V2524-A5
Airbus	A-320	A320	Large	IAE V2527-A5
McDonnell Douglas	DC-9-30	DC93	Large	PW JT8D-7
McDonnell Douglas	DC-9-50	DC95	Large	PW JT8D-17A
Boeing	757-200	B752	B757	PW2037
Boeing	757-300	B753	B757	PW2040
Airbus	A-330-300	A333	Heavy	PW4168A
Boeing	747-400	B744	Heavy	PW4056
Boeing	767-300	B763	Heavy	GE CF6-80C2B6
McDonnell Douglas	MD-10	MD10	Heavy	GE CF6-6D
McDonnell Douglas	DC-8-70	DC87	Heavy	CFM56-2C

The taxi thrust settings are estimated using data from Flight Data Recorder (FDR) archives (Khadilkar and Balakrishnan, 2011a). The FDR is a device onboard commercial aircraft that captures several aircraft parameters such as position, velocity and fuel flow rate. The FDR archive contains data from over 2300 flights from 2004 and 9 aircraft types, originating from the US, Europe, Asia and Africa (Khadilkar and Balakrishnan, 2011a). A Kalman filter approach similar to that of Khadilkar and Balakrishnan (2011b) is employed to identify accelerating and non-accelerating taxi modes from the FDR archives and calculate the taxi thrust that was applied during each mode.

Figure 4-6 shows the non-acceleration taxi and acceleration thrust values calculated from the FDR archives for the 9 aircraft types. Surface tracks from all flights of a particular aircraft type are pooled and the average thrust value for each taxi phase is calculated. For all aircraft except the ARJ-85 and Airbus A319, the non-accelerating taxi thrust is less than the ground/idle thrust assumption of 7% per the ICAO standard LTO cycle. A negative correlation is seen between the taxi thrust setting and the size of aircraft, with a slope of -0.006 thrust %/tonne, y-intercept of 7.32% and R^2 value of 0.73. During acceleration events, the thrust increases to 8% - 10% depending on aircraft type.
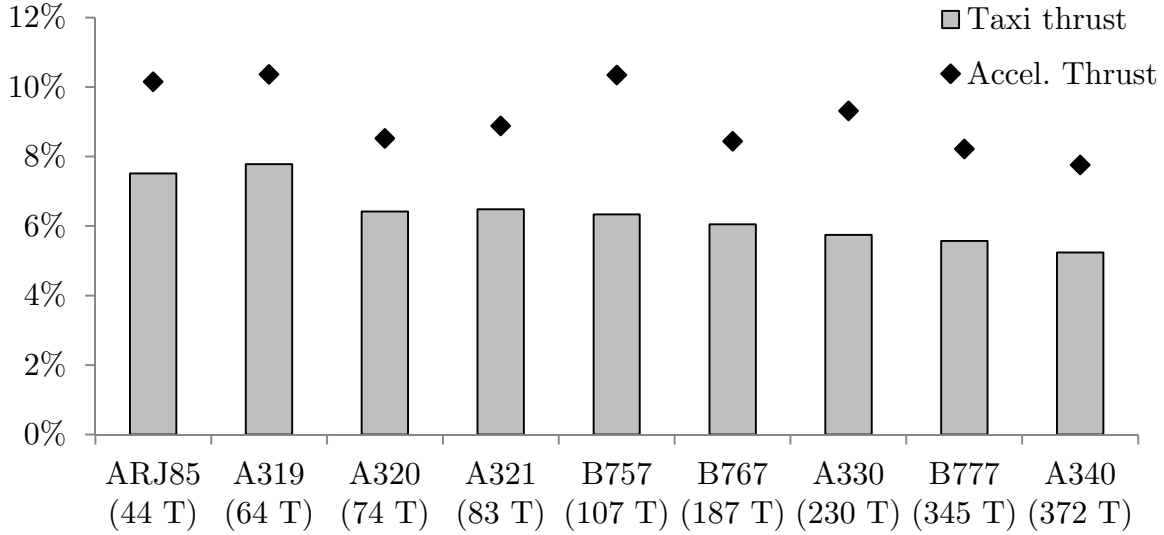
Figure 4-6: Taxi and acceleration thrust levels calculated from the FDR archives for each aircraft type. Taxi data from all flights are combined for each aircraft type. The maximum takeoff weight or each aircraft type is specified in the label in tonnes (T).

Aircraft types are matched exactly to those in the FDR database where possible. For aircraft types not represented in the FDR database, the non-accelerating taxi thrust is interpolated using the aircraft's maximum takeoff weight (MTOW) and acceleration thrusts are assumed to be 40% higher than taxi thrusts (this is the average thrust increment observed from the FDR dataset). Acceleration events are assumed to occur when the aircraft starts to taxi from a stop, and acceleration thrust is assumed to be applied for 5 seconds. Non-acceleration taxi thrust is assumed during all other times.

Fuel burn is calculated by multiplying the fuel flow rate and the duration of operation in each mode. It is noted that the fuel flow rate is approximately linearly proportional to the thrust setting (Wey et al., 2006). For taxi operations, $F = \dot{m}_{f,\text{taxi}} \cdot t_{\text{taxi}} + \dot{m}_{f,\text{accel}} \cdot t_{\text{accel.}}$, where F is the total fuel burn in kg, $\dot{m}_f$ is the fuel flow rate in kg/s and t is the time (in s) operating in the taxi and acceleration modes. Total fuel burn from takeoff operations consists of the fuel burned during takeoff and climb to 1000 ft, as well as the additional distance travelled during the cruise phase of flight (for takeoffs at > 75% thrust), $F = \dot{m}_{f,\text{takeoff}} \cdot t_{\text{takeoff}} + \dot{m}_{f,\text{cruise}} \cdot t_{\text{cruise}}$, where t_{takeoff} is the time (in s) to reach 1000 ft and t_{cruise} is the cruise duration required to equalize distance traveled relative to the 75% thrust takeoff.

Finally, the mass of emissions of species i, M_i, is calculated by multiplying total fuel burn with an emission index, $M_i = F \cdot EI_i(\dot{m}_f)$. Aircraft emissions of NO_x, SO_2, HC, CO, BC, OC and $SO_4^=$ are modeled using the Aviation Emissions Inventory Code (AEIC) v2.1 as described in section 2.1.1. BC emissions are calculated using the FOX method (Stettler et al., 2013), while CO_2 emissions are computed using an emission index of 3.159 kg/kg-fuel (Hileman et al., 2010). Uncertainty distributions are applied to account for variability in EIs from the measurements upon which emissions estimates are based (Baughcum et al., 1996; Herndon et al., 2012; Stettler et al., 2011) and a Monte Carlo approach is used to propagate uncertainties in the calculations.

4.1.4 Air quality impacts

The air quality impacts of aircraft emissions are calculated using the GEOS-Chem air quality model as described in section 2.1.2. Population exposure to one-hour daily maximum ozone and annual average $PM_{2.5}$ is considered here based on epidemiological evidence linking them to increased risk of premature mortality (Jerrett et al., 2009; Krewski et al., 2009). Whereas the analysis section 2.1.2 was limited to population exposure to secondary $PM_{2.5}$, in this chapter population exposure to both primary and secondary $PM_{2.5}$ are calculated. Premature mortality from O_3 exposure is estimated to be ~5% - ~15% of those from $PM_{2.5}$ exposure attributable to combustion emissions in the US including aviation (Caiazzo et al., 2013; Yim et al., 2015).

Only the US population is considered when calculating exposure to $PM_{2.5}$ and O_3, and therefore the population within grid cells outside the US is set to zero. Pollutant exposure of population above 30 years of age is calculated given that the epidemiological studies linking exposure to premature mortality are based on a cohort of participants aged 30 years or greater (Jerrett et al., 2009; Krewski et al., 2009). A constant age fraction of population above 30 years of age, obtained from the U.S. Census Bureau, 2009-2013 5-Year American Community Survey, is applied across the US.

Annual population exposure to emissions from aircraft operations at an airport is computed using the adjoint sensitivities by multiplying the sensitivities with the mass of emissions occurring during each hour of the year,

$$P = \sum_{T}^{N_{\text{hours}}} \sum_{i} S_i(T) \cdot M_i(T), \qquad \text{Eq. 4-2}$$

where T is the hour of emission, $N_{\text{hours}}=8760$ is the number of hours in a year, i indexes the emission species, and S_i is the adjoint sensitivity of $PM_{2.5}$ or O_3 exposure to emissions M_i. This couples hourly variations in atmospheric sensitivities to the temporally-varying aircraft activity profile shown in Figure 4-2. Since flight schedules are developed only for a typical day of operations at DTW (as discussed in Sections 4.1.1 and 4.1.2), the same daily schedule of operations is assumed for every day of the year when evaluating annual impacts. The main results of this work are calculated using emission sensitivities at the DTW airport grid cell, and variations with respect to atmospheric conditions at other airports are presented as a sensitivity study. Emissions occurring at cruise are multiplied by emissions sensitivities averaged within ~225 km of the airport at ~9.4 km (~31,000 ft) in altitude (this distance range was chosen assuming a conservative climb gradient of 2.4 degrees).

4.1.5 Mortality and valuation calculation

Population exposure to $PM_{2.5}$ and O_3 are translated into premature mortalities using concentration response functions (CRFs) developed in literature. Krewski et al. (2009) finds an enhanced risk of all-cause premature mortality of 6% (90% confidence interval (CI): 4-8%) per 10 μg/m^3 increase in $PM_{2.5}$ concentration. Jerrett et al. (2009) found an increased risk of mortality from respiratory disease of 4% (90% CI: 1-6.7%) per 10 ppb increase in one-hour daily maximum O_3 concentration. Baseline mortality incidence rates are obtained from the United States Centers for Disease Control and Prevention (CDC et al., 2015). Morbidity impacts from $PM_{2.5}$ and O_3 exposure are not calculated or monetized given that they are estimated to be < 10% of total health costs (Hubbell et al., 2005; Levy et al., 2001; USEPA, 2011).

Premature mortalities are monetized using the US EPA's value of statistical life (VSL) of 2006 USD 7.4 million and its distribution (US EPA, 2010) converted to 2007 USD via the Consumer Price Index (CPI). Climate damages from CO_2 emissions are monetized using the Interagency Working Group on Social Cost of Carbon estimate of \$31/ton

CO_2 at a 3% discount rate for 2010 and associated distribution (IAWG, 2015). Fuel consumption is monetized using the US Gulf Coast jet fuel spot price of \$0.70/kg in 2007 and a normalized standard deviation of 22% (US EIA, 2015). All values are specified in 2007 US dollars unless explicitly stated otherwise. Uncertainty is propagated through the calculations using a Monte Carlo approach with 1000-member ensemble drawn from a Sobol' set. The number of Monte Carlo draws is sufficient such that the running mean of the baseline costs (i.e. no gate holds and maximum-thrust takeoffs) are within 0.4% of the ensemble average value.

In addition to mortality, social cost of carbon and fuel costs, three additional aggregate metrics are calculated: air quality (defined to be the sum of $PM_{2.5}$ and O_3 costs), environmental (sum of air quality and climate costs) and total fuel combustion-related costs (sum of environmental and fuel costs). Other costs such as labor and equipment depreciation are not included in the present analysis.

4.1.6 Optimal gate hold and takeoff thrust reduction strategy

The first goal of this work is to assess the annual impacts of the gate holding and de-rated takeoff policies on fuel consumption, air quality and climate. This is accomplished by applying a given gate hold limit or reduced takeoff thrust for all flights throughout the year. The results are compared against a baseline scenario with no gate holds and full-thrust takeoffs (i.e. no takeoff de-rate).

A second goal of this work is to find the optimal gate hold and takeoff thrust setting that minimizes a chosen cost function. The objectives considered in this study are fuel burn, CO_2 emissions (which is directly proportional to fuel burn by a factor of 3.159 as discussed in section 4.1.3), $PM_{2.5}$, O_3, air quality, environmental and total fuel combustion-related costs as defined in Section 4.1.5. For every hour of the year and for each flight, the gate hold allowance and takeoff thrust that minimizes the chosen objective is selected. The optimization is performed for every hour because the adjoint sensitivities vary hourly.

The optimal choice of gate hold or takeoff thrust may differ based on the metric being minimized. For example, tradeoffs between CO_2 emissions and $PM_{2.5}$ or O_3 exposures have been quantified at US airports in Chapter 2. King and Waitz (2005) show that while de-rated takeoffs reduce LTO NO_x emissions by 0.7%, fuel burn (and therefore CO_2) is increased by 0.6% for every percent de-rate in thrust. The tradeoffs are graphically illustrated by creating Pareto fronts between fuel burn and $PM_{2.5}$ or O_3 optima using the scalarization technique (Stadler, 1979).

4.2 Environmental impacts of surface movements

In this section, the air quality and climate impacts of aircraft taxi operations at DTW in 2007 are quantified. Section 4.2.1 presents the annual monetized impacts of airport surface operations and the benefit of implementing gate holds. Section 4.2.2 presents the optimization of gate holds and associated tradeoffs with fuel burn. The sensitivity of the results to the airport traffic level, fleet mix and atmospheric conditions at other airports are summarized in Section 4.2.3, with further detailed results shown in Appendix D.

4.2.1 Baseline taxi operations at DTW and benefits of gate holding

The costs due to premature mortality from $PM_{2.5}$ and O_3 exposure, climate impacts of CO_2 emissions and fuel consumption from taxi operations without gate holds are listed in Table 4-2. The average taxi-out time per departing aircraft is 19.7 minutes, close to the taxi-out time of 20.1 minutes for actual operations in 2007 at DTW (FAA, 2015). Arriving aircraft have an average taxi-in time of ~9.7 minutes. Average fuel consumption of 197 kg, NO_x emissions of 0.7 kg and HC emissions of 1.0 kg per aircraft are estimated. Annual air quality costs are estimated to be \$7.1 M (90% CI: 0.9-17.4 M), of which ~85% is attributed to premature mortalities from $PM_{2.5}$ exposure. The climate damage from CO_2 emissions is calculated to be \$7.7 M (90% CI: 0.7-21.4 M), while fuel costs are a factor of ~4 larger than environmental costs.

Table 4-2: The estimated annual impacts of baseline taxi and takeoff operations at DTW in 2007. Monetary impacts from $PM_{2.5}$ and O_3-related mortalities, total air quality (AQ) costs, social cost of CO_2 emissions (SCC), cost of fuel consumption (FB), environmental (Env.) and total fuel combustion-related costs (Tot.) are shown. Monetary values are expressed in millions of 2007 US dollars. Also shown are taxi times for arrival and departure flights (surface operations only) and the mass of fuel burn and NO_x and HC emissions per flight. For takeoffs, the portion of cruise included in the results corresponds to the additional distance travelled relative to the 75%-thrust takeoff.

	Taxi (no gate holds)	Takeoffs (100% thrust, incl. cruise)	Takeoffs (100% thrust)
$PM_{2.5}$ (Million USD)	6.0 (0.8-14.5)	3.0 (0.5-7.1)	3.0 (0.5-7.1)
O_3 (Million USD)	1.2 (0.1-3.5)	-0.5 (-1.1--0.1)	-0.5 (-1.1--0.1)
AQ (Million USD)	7.1 (0.9-17.4)	2.6 (0.4-6.1)	2.6 (0.4-6.1)
SCC (Million USD)	7.7 (0.7-21.4)	1.5 (0.1-3.9)	1.4 (0.1-3.8)
Env. (Million USD)	14.8 (4.4-30.8)	4.0 (1.1-8.6)	4.0 (1.1-8.5)
FB (Million USD)	62.3 (39.1-85.1)	11.5 (7.2-15.8)	11.1 (7.0-15.2)
Tot. (Million USD)	77.1 (51.3-106.7)	15.5 (10.0-21.6)	15.1 (9.7-21.1)
Taxi–out time (min/flight)	19.7	-	-
Taxi–in time (min/flight)	9.7	-	-
FB (kg/flight)	197	72.7	70.2
NO_x (kg/flight)	0.7	1.61	1.59
HC (kg/flight)	1.0	0.011	0.010

Figure 4-7 illustrates the impact of gate holding on taxi-out times and annual fuel burn, emissions and air quality impacts. As seen in Figure 4-7(a), gate holding reduces taxi-out times by absorbing delays at the gate instead of on the taxiways, consistent with findings from previous studies (e.g. Lee and Balakrishnan (2010). At the gate hold allowance of 25 minutes, the average taxi-out time is lowered by ~52% relative to the baseline (no gate holds). Taxi-in times are affected by less than 0.02% since arrival traffic is given greater priority over departures (Lee and Balakrishnan, 2010).

Figure 4-7(a) shows that the average gate hold duration per aircraft increases approximately linearly with gate hold allowance up to ~8 minutes, after which it plateaus to its final value of 10.4 minutes. Similarly, ~75% of the reductions in taxi-out times are achieved with a gate hold allowance of ~8 minutes, with progressively smaller improvements for larger gate hold allowances. This suggests that the gate hold allowance could be lowered from 25 minutes if required – for example due to gate availability limitations – while still achieving significant improvements in taxi-out times and fuel burn.
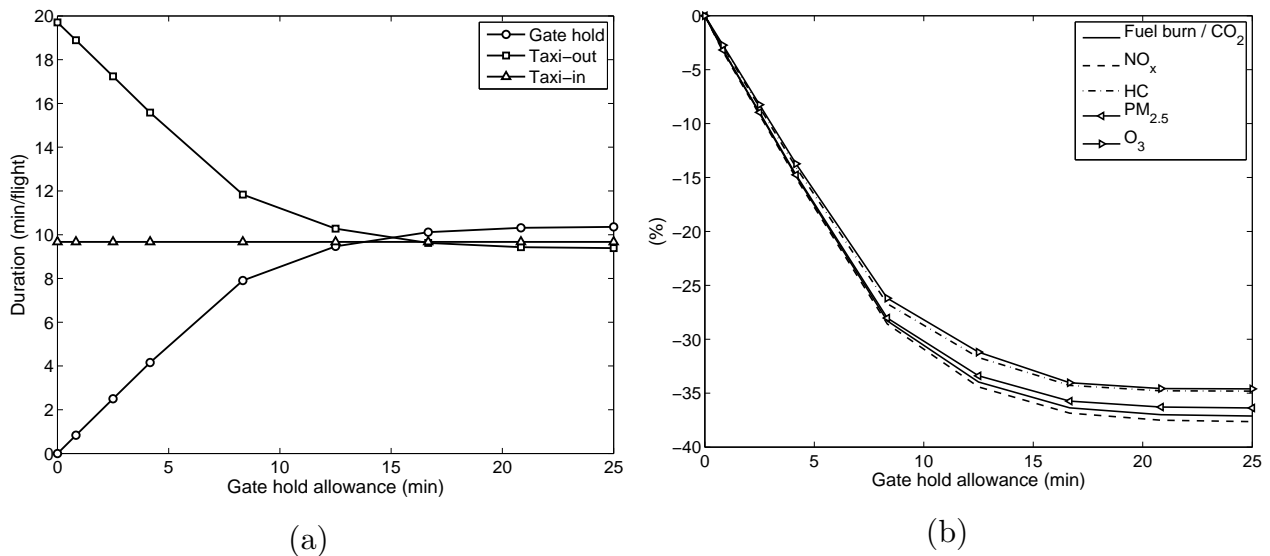
Figure 4-7: The effect of gate hold on impacts from surface taxi operations at DTW in 2007. Panel (a) shows the effect of increasing gate hold allowance on average taxi-in, taxi-out and gate hold times. Panel (b) shows the effect of increasing gate hold allowance on fuel burn, emissions and air quality impacts, as a percentage change relative to the no gate hold scenario.

Fuel consumption and CO_2 emissions are minimized with a gate hold allowance of 25 minutes and are 37% lower relative to the baseline, as shown in Figure 4-7(b). Fuel burn is reduced because delays are absorbed at the gates where engines are assumed to be switched off instead of during taxi. CO_2 climate impacts are also minimized with fuel burn since CO_2 emissions scales linearly with fuel burn (see Section 4.1.3). Applying 25-minute gate holds during all times of the year results in reductions in HC and NO_x emissions and annual $PM_{2.5}$ and O_3 mortalities of between 35-38% relative to the baseline scenario without gate holds.

4.2.2 Optimizing gate holds

The previous section showed that a 25-minute gate hold allowance minimizes fuel burn and CO_2 emissions, while reducing $PM_{2.5}$ and O_3 impacts by 36% and 35%, respectively, relative to the baseline scenario without gate holds. In this section, the optimal air quality, environmental and total costs achieved beyond fuel burn minimization are presented – that is, where gate holds are optimized hourly accounting for variations in atmospheric conditions. Figure 4-8 plots the annual fuel burn, $PM_{2.5}$ and O_3 costs that result from optimizing gate holds to minimize these objectives.
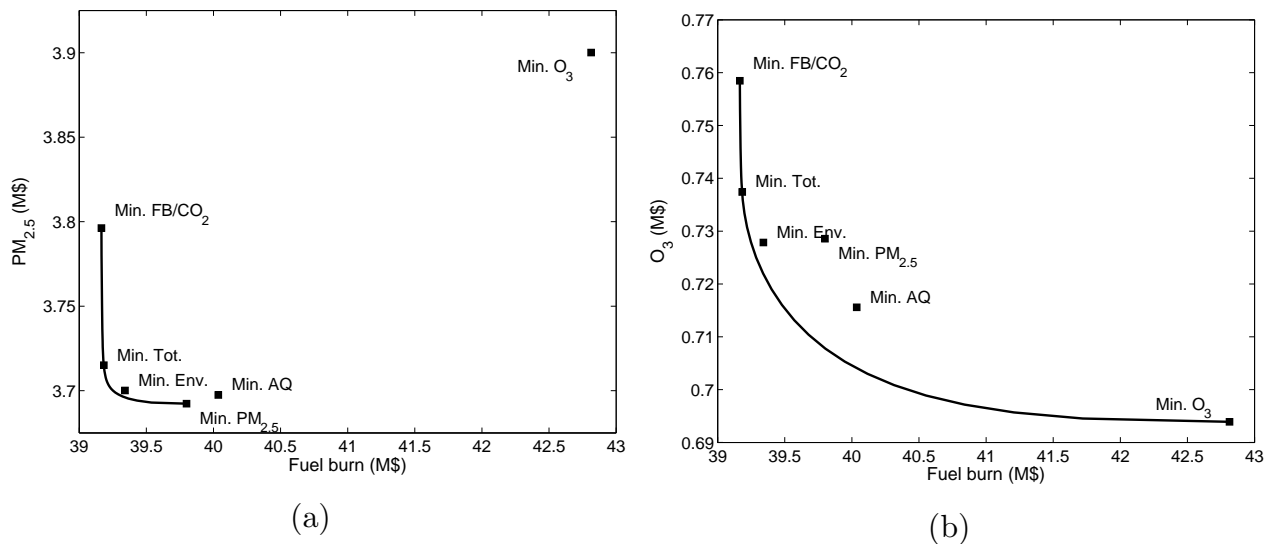
Figure 4-8: Annual fuel burn, $PM_{2.5}$ and O_3 costs resulting from optimizing gate holds to minimize fuel burn (FB), air quality (AQ), environmental (Env.) and total fuel combustion-related costs (Tot.) at DTW airport in 2007. The Pareto fronts between fuel burn and (a) $PM_{2.5}$ and (b) O_3 costs are plotted as the black line, representing the tradeoff between fuel burn and $PM_{2.5}$ or O_3 costs of surface taxi operations at DTW.

Optimizing gate holds for $PM_{2.5}$ impacts results in 2.7% lower PM-related mortality costs relative to the minimum fuel burn solution, while optimizing gate holds for O_3 impacts improves O_3-related mortality costs by 8.5%. These represent a ~38% and ~40% reduction in $PM_{2.5}$ and O_3 impacts, respectively, relative to baseline operations without gate holds. The improvements in $PM_{2.5}$ and O_3 impacts are achieved by optimizing gate holds accounting for tradeoffs between fuel burn and air quality, presented in Chapter 2. During these tradeoff conditions, reduction of fuel burn results in a net increase in $PM_{2.5}$ or O_3 exposures. For taxi operations at DTW, tradeoff conditions occur for 7% ($PM_{2.5}$) and 25% (O_3) of the year as seen in Appendix A. Thus, gate holds are implemented to

lower fuel burn (and emissions) only in the absence of tradeoff conditions, while during tradeoff conditions aircraft push back as scheduled. Consequently, the optimal gate hold for minimum $PM_{2.5}$ and O_3 is 2.7% and 15.7% lower than that for minimum fuel burn, as shown in Table 4-3. It should be noted that the gate hold decision is a binary one when optimizing for $PM_{2.5}$ or O_3 costs individually, given that changes in emissions are monotonic with respect to gate hold and that the adjoint emission sensitivities are linear (i.e. either the maximum gate hold limit is applied to all aircraft or no gate holds are applied depending on tradeoff conditions). Therefore the gate hold values reported in Table 4-3 should be interpreted as a measure of aggregate gate delay over the course of one year of operations. However, when optimizing gate holds for other objective functions (e.g. minimum air quality, environmental or total fuel combustion-related costs) the optimal gate hold limit could take on an intermediate value.

Table 4-3: Optimal gate hold duration for surface operations required to minimize fuel burn (FB), $PM_{2.5}$, O_3, air quality (AQ), environmental (Env.) and total fuel combustion-related (Tot.) costs. Values are averaged over all flights for one year of operations at DTW.

	Surface movements **Gate hold** **(min/flight)**
Min. FB	10.4
Min. $PM_{2.5}$	10.1
Min. O_3	8.7
Min. AQ	10.0
Min. Env.	10.3
Min. Tot.	10.3

Figure 4-8 also shows the Pareto fronts of $PM_{2.5}$ and O_3 impacts with respect to fuel burn, which indicate the tradeoffs between air quality impacts and fuel burn/CO_2. The optimal $PM_{2.5}$ and O_3 solutions increase fuel burn/CO_2 costs by 1.6% and 9.3%, respectively. The Pareto front between fuel burn and $PM_{2.5}$ (Figure 4-8(a)) indicates that most of the reductions in $PM_{2.5}$ impacts occur with relatively small increases in fuel burn and CO_2: for instance, optimizing surface operations for environmental costs results in 2.5% reduction in $PM_{2.5}$ impacts (out of a possible 2.7%) for a 0.4% increase in fuel burn and CO_2. The Pareto front between fuel burn and O_3 impacts (Figure 4-8(b))

shows that the tradeoff is more gradual than that of $PM_{2.5}$ impacts: at the environmental optimum (i.e. 0.4% increase in fuel burn), ozone impacts are lowered by 4.0% (out of a possible 8.5%). Minimizing total fuel combustion-related costs (i.e. costs from environmental impacts and fuel consumption) results in 0.04% increase in fuel burn and CO_2 but lowers $PM_{2.5}$ and O_3 impacts by 2.1% and 2.8%, respectively. This objective function places more importance on fuel burn compared to the environmental objective function, since fuel costs are ~4 times higher than environmental costs (Table 4-2).

4.2.3 Sensitivity of the environmental impacts of surface movements

Here, the sensitivity of the gate hold strategy to traffic level, fleet mix and atmospheric conditions at other airports is quantified. This is done through analysis of scenarios where the airport traffic level is lowered by up to 50% of the 2007 levels and the proportion of heavy aircraft (i.e. maximum takeoff weights > 300,000 lbs) is increased from the 2007 level of 5% to 25%. The resulting emission and air quality impacts are calculated using the methods described in section 4.1. Finally, sensitivity to atmospheric conditions at other airports is evaluated using adjoint emission sensitivities from other airport locations instead of the DTW location alone. The results are summarized in this section, and further details are provided in Appendix D.

Traffic level

The aircraft traffic level at the DTW airport is reduced by up to 50% of the 2007 levels. The average taxi-out time per aircraft (without gate holds) is lowered from 19.7 minutes to 17.5 minutes, and total fuel burn, emissions and air quality impacts scale approximately linearly with traffic levels. At this traffic level, implementing the gate holding strategy reduces fuel consumption, emissions and air quality impacts by 31-33%, with optimal $PM_{2.5}$ and O_3 costs 2.4% and 8.2% lower than those at the fuel burn minimum.

Proportion of heavy aircraft

The proportion of heavy aircraft (maximum takeoff weight larger than 300,000 lbs) in the fleet at DTW is increased from the 2007 level of 5% to 25%. Baseline fuel burn,

emissions and air quality impacts increase by 29-116% relative to the 2007 fleet given the growth in proportion of heavy aircraft. The gate holding strategy reduces air quality impacts by 37-38% relative to the baseline case without gate holds. Improvements in $PM_{2.5}$ and O_3 costs beyond fuel burn minimization are relatively smaller than those for the 2007 fleet (2.2% c.f. 2.7% for $PM_{2.5}$ impacts and 3.1% c.f. 8.5% for O_3 impacts).

Atmospheric conditions at other airports

The air quality impacts of the DTW surface activity are evaluated under the atmospheric conditions of the top 34 busiest airports (by passenger enplanements) in the US. Fuel burn and emissions do not change as aircraft activity is held constant across the airports, whereas baseline $PM_{2.5}$ and O_3 impacts vary between \$1.3M – \$25.9M and \$0.5M – \$4.7M, respectively, given the changing atmospheric conditions. Application of 25-minute gate holding reduces $PM_{2.5}$ by 36-37% and O_3 impacts by 16-37% across all airports. $PM_{2.5}$ costs are improved beyond fuel burn minimization by up to 3.3% and O_3 costs by up to 180% (~15% at the 75th percentile).

4.3 Environmental impacts of takeoff operations

The fuel burn, emissions and air quality impacts of de-rated takeoffs at DTW in 2007 are quantified in Section 4.3.1, while the optimization of takeoff thrust and associated tradeoffs with fuel burn are calculated in Section 4.3.2. The sensitivity of the results to aircraft takeoff weight and atmospheric conditions at other airports is summarized in Section 4.3.3, with detailed results presented in Appendix D.

4.3.1 Baseline takeoff operations and de-rated takeoffs

The air quality, CO_2 and fuel costs from baseline takeoff operations (i.e. 100% takeoff thrust) are listed in Table 4-2. For takeoffs up to 1000 ft, an average fuel consumption of 70.2 kg, NO_x emissions of 1.59 kg and HC emissions of ~0.01 kg are estimated per aircraft. Mean annual air quality costs are \$2.6 million, with $PM_{2.5}$ mortality-related costs estimated to be \$3.0 million. Ozone-related costs from full-thrust takeoffs at DTW are negative, implying that net ozone mortality is reduced due to emissions from takeoffs. This is attributed to VOC-limited atmospheric conditions at DTW during

which the rate of ozone production is slowed due to removal of oxidants via chemical reaction with NO_x (Seinfeld and Pandis, 2006). VOC-limited exposure conditions occur for 84% of the year at DTW in 2006, during which emissions resulting in a VOC/NO_x concentration ratio less than 0.76 ppbC/ppb reduces net O_3 exposure, as shown in Figure 3-9 and Figure 3-12. It is noted that annual ozone-related mortality costs may be either positive or negative at other airport locations (e.g. see Section 4.3.3). CO_2 climate damages are calculated to be \$1.4 M, while the mean estimate for fuel cost is a factor of ~3 larger than environmental costs.

The additional cruise fuel burn and emissions – resulting from additional cruise distance traveled by takeoffs with > 75% thrust in order to equalize ground track distance relative to the 75% thrust takeoff – increases the average per-flight fuel burn and CO_2 by ~3%, NO_x emissions by 1% and HC emissions by 6% relative to those from takeoffs up to 1000 ft. Air quality costs increase by < 0.3% relative to those from takeoffs up to 1000 ft, because the additional emissions that occur at cruise altitudes have relatively less impact on the population than emissions near ground (Koo et al., 2013).

Figure 4-9 shows the impact of reduced-thrust takeoffs on annual fuel burn, emissions and air quality impacts, including additional cruise fuel burn, emissions and air quality impacts required to equalize ground track distance relative to the 75% thrust takeoff. Fuel burn and CO_2 are minimized with full-thrust takeoffs, whereas reducing takeoff thrust to 75% lowers NO_x emissions by ~18% while increasing fuel burn/CO_2 by ~3%. The trends are similar to those reported in King and Waitz (2005), who find that LTO NO_x emissions are reduced by 0.7% for every percentage de-rate (c.f. 0.72% in this study) while fuel burn is increased by 0.6% per percent de-rate (c.f. 0.12% in this study). The King and Waitz (2005) study accounts for fuel burn from takeoff activity below 3000 ft only and not the additional fuel burn incurred during cruise by full-thrust takeoffs, thereby over-estimating the increase in fuel burn from de-rated takeoffs relative to full-thrust takeoffs. Increased fuel consumption at lower takeoff thrusts occurs due to slower climb rates relative to full-powered takeoffs (e.g. see Figure 4-5), while reduced NO_x emissions are a result of smaller NO_x EIs at lower thrust settings (Baughcum et al.,

1996) which offsets the increase in fuel burn. Applying 75% takeoff thrust during all times of the year reduces annual $PM_{2.5}$ mortality costs by ~18% but increases O_3 costs by 17% relative to full-powered takeoffs. However, total air quality costs (sum of $PM_{2.5}$ and O_3 costs) are lowered by 19% as $PM_{2.5}$ costs are ~6 times larger than the magnitude of O_3 costs.
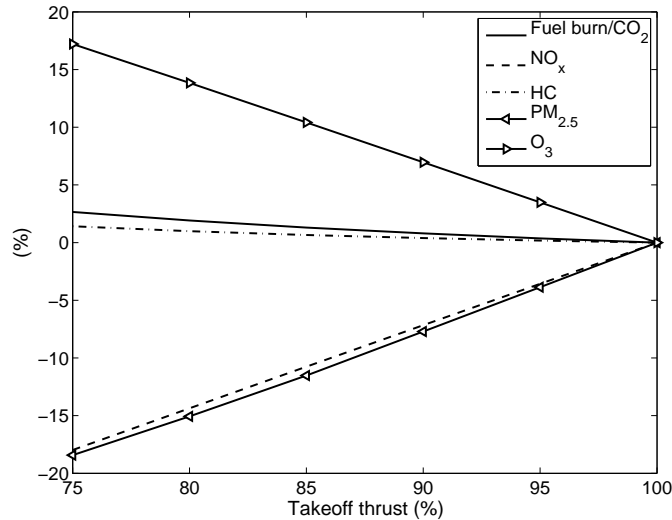
Figure 4-9: The effect of reduced-thrust takeoffs on fuel burn, emissions and air quality impacts from departure operations at DTW in 2007. Note that additional fuel burn, emissions and air quality impacts from the cruise phase are included, which accounts for the additional distance traveled at cruise by takeoffs at > 75% thrust in order to equalize ground track distance relative to the 75% thrust takeoff. Results are shown as a percentage change relative to baseline operations (100% thrust).

4.3.2 Optimizing takeoff thrust settings

Fuel burn and CO_2 is minimized with full-thrust takeoffs (i.e. the baseline scenario of operations) whereas NO_x emissions are minimized at 75% takeoff thrust, as shown in Section 4.3.1. This section presents the optimal air quality, environmental and total fuel combustion-related costs from takeoff activities. Takeoff thrust settings are optimized on an hourly basis accounting for tradeoffs between fuel burn and air quality impacts. Figure 4-10 plots the annual fuel burn, $PM_{2.5}$ and O_3 costs that result from optimizing takeoff thrusts to minimize these objectives, and Table 4-4 lists the optimal takeoff thrust setting – averaged annually and over all flights – for each objective function.

103

Table 4-4: Optimal thrust setting for takeoff operations required to minimize fuel burn (FB), $PM_{2.5}$, O_3, air quality (AQ), environmental (Env.) and total fuel combustion-related (Tot.) costs. Values are averaged over all flights for one year of operations at DTW.

	<u>Takeoffs</u> Thrust setting (% of max. thrust)
Min. FB	100%
Min. PM$_{2.5}$	78%
Min. O$_3$	92%
Min. AQ	80%
Min. Env.	81%
Min. Tot.	89%

The optimal $PM_{2.5}$ cost is 21.6% lower than that at the fuel burn minimum, achieved with an average takeoff thrust setting of 78% (shown in Table 4-4). This indicates that de-rated takeoffs are employed to reduce NO_x emissions using during all times of the year except during tradeoffs between fuel burn and $PM_{2.5}$ (when NO_x emissions reductions increase $PM_{2.5}$ exposure). The optimal O_3 cost is 11.8% lower than that at minimum fuel burn, achieved with an average optimal takeoff thrust setting of 92% (Table 4-4). Contrary to minimizing $PM_{2.5}$ impacts, the optimal strategy in this case is to perform full-thrust takeoffs as long as VOC-limited exposure conditions prevail (i.e. for 84% of the year at DTW), with reduced-thrust takeoffs implemented at other times. It is noted that this is not always the case across varying atmospheric conditions at other airports (see section 4.3.3). Total air quality costs, which are the sum of $PM_{2.5}$ and ozone costs, are minimized at an average takeoff thrust of 80%. It is noted that the decision of takeoff thrust setting is a binary one (i.e. maximum thrust or 75%-thrust depending on tradeoff conditions) when minimizing $PM_{2.5}$ or O_3 costs individually, given that changes in emissions are monotonic with respect to thrust setting and that the adjoint emission sensitivities are linear. However, when optimizing takeoff thrusts for other objective functions (e.g. minimum air quality, environmental or total fuel combustion-related costs) the optimal thrust setting could take on intermediate values.
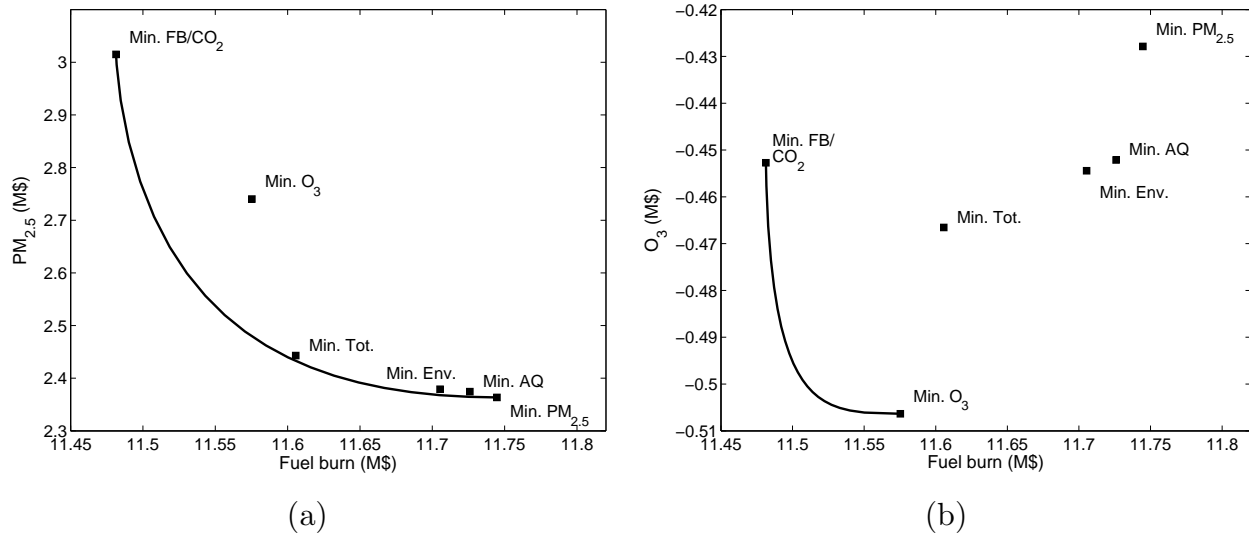
Figure 4-10: Annual fuel burn, $PM_{2.5}$ and O_3 costs resulting from optimizing takeoff thrust setting to minimize fuel burn (FB), air quality (AQ), environmental (Env.) and total fuel combustion-related (Tot.) costs at DTW airport in 2007. The Pareto fronts between fuel burn and (a) $PM_{2.5}$ and (b) O_3 costs are plotted as the black line, representing the tradeoff between fuel burn and $PM_{2.5}$ or O_3 costs of takeoff operations at DTW.

Tradeoffs between fuel burn and $PM_{2.5}$ or O_3 impacts of takeoff operations are depicted by the Pareto fronts plotted in Figure 4-10(a) and (b). Minimizing $PM_{2.5}$ impacts results in an increase in fuel burn of 2.3% relative to the minimum fuel burn solution, while minimizing O_3 costs leads to 0.8% increased fuel burn. Optimizing thrust setting for minimum air quality, environmental and total fuel combustion-related costs lowers $PM_{2.5}$ and O_3 costs relative to fuel burn minimization while increasing fuel burn and CO_2 climate costs by varying degrees. In particular, environmental costs are minimized at an average thrust setting of 81% (as tabulated in Table 4-4), where $PM_{2.5}$ costs are lowered by 21.1% and O_3 costs are lowered by 0.4% while fuel burn is increased by 2.0% relative to minimum fuel burn. Minimizing total fuel combustion-related costs yields about 90% of the improvements in $PM_{2.5}$ costs and ~1/4 of the improvements in O_3 costs and a 1.1% increase in fuel costs, with an average thrust setting of 89%.

4.3.3 Sensitivity of the environmental impacts of de-rated takeoffs

The sensitivity of the de-rated takeoff thrust strategy to takeoff weight and atmospheric conditions at other airports is assessed. The takeoff weight of aircraft is varied from the baseline assumption of 80% MTOW to between 70% and 100% MTOW and the resulting emission and air quality impacts are calculated using the methods described in

section 4.1. The sensitivity to atmospheric conditions at other airports is evaluated using adjoint emission sensitivities from other airport locations instead of the DTW location alone. The results are summarized in this section, and further details are provided in Appendix D.

Takeoff weight

The nominal takeoff weight of 80% Maximum Take-Off Weight (MTOW) is varied between 70% and 100% MTOW for all aircraft, and the takeoff trajectory is re-calculated for the modified aircraft weights. Baseline fuel burn and emissions increase as takeoff weight increases. Higher takeoff weights lead to larger fuel burn increments and smaller improvements in $PM_{2.5}$ impacts due to de-rated takeoffs relative to full-thrust takeoffs. For example, the optimal $PM_{2.5}$ costs are 16.3% lower than the fuel burn optimum at 100% MTOW (c.f. 21.6% at 80% MTOW). The optimal thrust settings that minimize $PM_{2.5}$ and environmental impacts change by $< 3\%$ with takeoff weight.

Atmospheric conditions at other airports

The air quality impacts of takeoff operations are evaluated under the atmospheric conditions of the top 34 busiest airports (by passenger enplanements) in the US in addition to those at DTW. $PM_{2.5}$ impacts from full-powered takeoffs vary between \$0.7M – \$16.6M, while O_3 impacts span positive and negative values between \$-6.5M – \$2.5M indicating that annual atmospheric conditions are VOC-limited at some airports while not at others. Across all airports, $PM_{2.5}$ costs are reduced by 14.1-21.6% for takeoffs at 75% thrust relative to the full-thrust takeoffs, and up to 27.4% for optimized thrust settings (which range from 75-83% depending on airport location). De-rated takeoffs at 75% thrust increase or decrease O_3 impacts relative to full-thrust takeoffs depending on airport location (ranging from a 19.1% reduction to a 31.6% increase). Optimizing takeoff thrust for O_3 impacts reduces O_3 costs up to a factor of 8 beyond fuel burn minimization (~37% at the 75th percentile across all airports). Environmental impacts are minimized with thrust settings between 77-85% depending on the airport.

4.3.4 Maintenance cost savings from de-rated takeoffs

De-rated takeoffs reduce engine maintenance costs by reducing the amount of time the engines are operated at high temperatures (Lee, 2005). In this section, the material maintenance cost savings from de-rated takeoffs are estimated and the tradeoff with fuel costs is assessed.

The impact of takeoff thrust setting on maintenance costs is quantified using operational severity curves, which is a normalized measure of the relative stress placed on the engine's components (Ackert, 2011). Severity curves compiled by Seemann et al. (2010) for a short-haul and a medium- to long-haul engine are used in this study, assuming nominal average block times (i.e. gate-to-gate flight times) of 1.9 hours and 6.0 hours respectively. Engine maintenance costs are calculated per flight cycle by aircraft type using the Bureau of Transportation Statistics (BTS) Form 41 financial and traffic data spanning 2004-2014 (BTS, 2016b), corrected to 2007 USD using historical Producer Price Index (PPI) and Employment Cost Index (ECI) data. It is assumed that 62% of the reported costs are material costs, of which 19% is attributable to life-limited parts which are replaced on schedule and therefore not affected by takeoff de-rate (AeroStrategy, 2009). The reported engine maintenance costs are also assumed to be for an average de-rate of 10% (Ackert, 2011; Seemann et al., 2010).

Figure 4-11 plots the tradeoff between material maintenance cost and fuel cost from takeoffs with varying levels of de-rate. The costs are aggregated for one year of takeoff operations of the DTW fleet and with takeoff weights at 80% MTOW. De-rated takeoffs at 75% thrust reduce material maintenance costs by ~18% but increase fuel costs (over the full flight accounting for additional cruise distance traveled) by 3%. The material maintenance cost savings due to de-rated takeoffs is two orders of magnitude larger than the increase in fuel cost (e.g. $21.2M c.f. $0.3M as seen from Figure 4-11). Maintenance cost savings therefore incentivize airlines to perform de-rated takeoffs in spite of increased fuel costs (at 2007 prices for fuel and maintenance materials). This is largely aligned with the minimization of air quality impacts (e.g. Table 4-3).
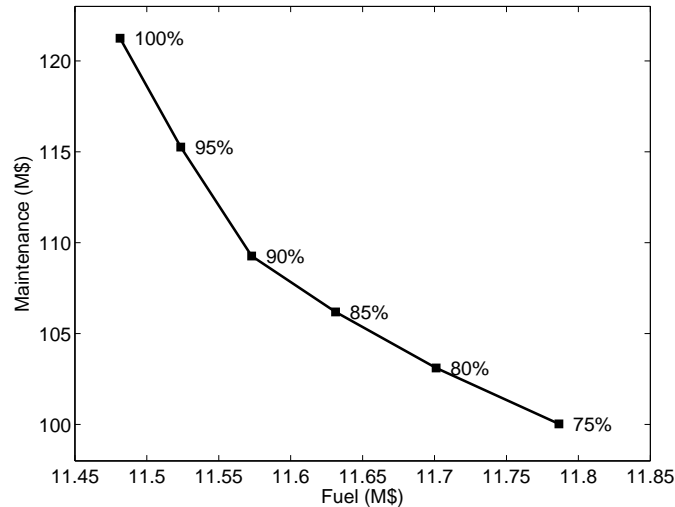
Figure 4-11: Tradeoff between material maintenance costs and fuel costs as a function of takeoff de-rate (labeled on the plot), for annual takeoff operations at DTW in 2007 at 80% MTOW.

4.4 Summary

This work has quantified the air quality and climate benefits of two emission mitigation strategies – pushback control and reduced-thrust takeoffs – for simulated aircraft operations at the Metropolitan Wayne County airport (DTW) in 2007. The minimum air quality costs, environmental costs (including air quality and CO_2 climate damages) and total fuel combustion-related costs (including environmental costs and fuel costs) have been calculated by optimizing pushback delay and takeoff thrust. The main findings from the study are summarized below:

1) The application of a 25-minute gate hold allowance – that is, delaying aircraft pushback by up to 25 minutes – minimizes fuel burn/CO_2 while reducing $PM_{2.5}$ and O_3 air quality impacts by 36% and 35%, respectively, relative to the baseline.

2) Minimizing $PM_{2.5}$ and O_3 costs by optimizing gate holds (accounting for time-varying atmospheric conditions) lowers these costs by an additional 2.7% and 8.5%, respectively, beyond fuel burn minimization (these are ~38% and ~40% lower than the baseline costs, respectively).

3) Improvements to the O_3 impacts of taxi operations are most sensitive to varying atmospheric conditions across airport locations, with 25-minute gate holds reducing O_3 impacts by 16-37% relative to a baseline without gate holds and

optimal O_3 costs lowered beyond fuel burn minimization by up to ~15% (at the 75th percentile across airports).

4) De-rated takeoffs at 75% thrust increase fuel burn/CO_2 by 3% relative to full-thrust takeoffs (considering takeoffs up to 1000 ft as well as additional cruise segments flown) while reducing NO_x emissions and total air quality costs (sum of $PM_{2.5}$ and O_3 costs) by 19%.

5) Minimizing environmental costs balances the opposing trends in air quality and CO_2 climate costs, achieving ~98% of the improvements in $PM_{2.5}$ with an average optimal takeoff thrust setting of 81%.

6) Optimizing takeoff thrusts to minimize O_3 impacts result in lowering these costs beyond fuel burn minimization by up to ~37% (at the 75th percentile over all airports).

7) The effect of de-rated takeoffs is sensitive to airport location: de-rated takeoffs at 75% thrust lower $PM_{2.5}$ impacts by 14.1-21.6% and change O_3 costs by -19.1% to 31.6% relative to full thrust takeoffs, while environmental costs are minimized with average optimal thrust settings of 77-85% depending on the airport.

8) Material maintenance cost savings from de-rated takeoffs are estimated to be two orders of magnitude larger than the increase in fuel cost.

The results suggest that the pushback control strategy is effective in mitigating the environmental impacts of taxi operations at airports, given that the air quality minima are largely aligned with fuel burn/CO_2 minimization.

For takeoff operations, fuel burn/CO_2 is minimized at full-thrust whereas de-rated takeoffs up to 75% thrust reduce NO_x emissions and $PM_{2.5}$ health impacts. The opposing trends in air quality and CO_2 impacts are balanced by minimizing environmental costs, which results in an average optimal takeoff thrust setting of 81% thrust. Furthermore, the estimated savings in maintenance costs further incentivizes de-rated takeoffs in spite of increase in fuel costs.

The O_3 optimum is potentially relevant if specific improvements in O_3 are targeted (e.g. non-compliance with regulatory standards), with reductions beyond fuel burn

minimization of up to ~15% for taxi operations and ~37% for takeoff operations (at the 75th percentile across all airport locations). For example, 27 out of the 34 airports studied are in O_3 non-attainment areas and fall under the FAA's Voluntary Airport Low Emissions Program (FAA, 2010) as of March 2016. It must be noted that these improvements are achieved with an increase in fuel burn relative to the fuel burn minimum. Optimizing gate holds for O_3 costs increases $PM_{2.5}$ costs relative to the minimum fuel burn solution at all airports studied, but optimizing takeoff thrust setting for O_3 costs produces $PM_{2.5}$ co-benefits at all airports studied.

The findings are relevant to airline and airport operators as they quantify the fuel consumption and combustion-related costs of aircraft operations at airports. They are also relevant from an aviation policy perspective as they quantify improvements in environmental impacts achievable using operations-based strategies which are complementary to technology-based efforts (e.g. NO_x stringencies).

Limitations of the current study are acknowledged here and opportunities for future work are highlighted. Operational constraints beyond those considered in this study may exist that could lower the potential improvements in air quality (e.g. runway constraints for de-rated takeoffs, or gate availability limitations for gate holds). A detailed quantification of total climate impacts, such as such those from O_3 and NO_x, are beyond the scope of this work and thus not captured in the results. At present only material maintenance cost savings are quantified, and further work is required to quantify other aspects of the maintenance program likely to be affected by takeoff de-rate (e.g. labor cost savings due to reduced shop visit frequency) in order to formally include maintenance costs in the optimization. Finally, the air quality calculations herein are based 2005 anthropogenic emissions which have declined since; in particular, decreasing SO_2 emissions will likely lead to greater impact of aircraft NO_x emissions on ammonium nitrate $PM_{2.5}$ due to increased availability of free ammonia (Woody et al., 2011), and decreasing NO_x emissions will likely lead to greater ozone sensitivity to NO_x emissions, as net ozone production is increased as a result of reduced titration of ozone at low NO_x concentrations (Seinfeld and Pandis, 2006).

Chapter 5

Conclusion

The overarching aim of this thesis is to enable the reduction of the air quality impacts of aircraft operations at airports. The research presented in Chapter 2 and Chapter 3 addresses this objective by advancing the understanding of the relationship between aircraft activity and its air quality impacts, while the research presented in Chapter 4 does so by evaluating the air quality benefits achievable via controlling aircraft operations at airports. Key findings from each chapter are synthesized in section 5.1 and opportunities for future work are summarized in section 5.2.

5.1 Key findings

This thesis identifies tradeoffs between CO_2 emissions and population exposure to $PM_{2.5}$ and O_3 – i.e. where decreasing fuel burn (which is directly proportional to CO_2 emissions) results in increased exposure. The thesis has quantified the duration of time and magnitude of these tradeoffs as a function of engine and thrust setting. Airports with relatively high exposure reduction potentials (relatively high magnitude and duration of tradeoffs) are also identified, which have the greatest scope for reducing air quality impacts beyond minimizing fuel burn. This improves the current understanding of the air quality impacts of aircraft emissions by showing that, at the airports and for the engines studied, there are times during the year where population exposure to both $PM_{2.5}$ and O_3 can be improved with an increase in fuel burn.

The thesis then characterizes the atmospheric conditions during which tradeoffs between emissions and ozone exposure occur. The ozone exposure response to NO_x and VOC emissions is characterized as a function of ambient VOC and NO_x concentrations using ozone exposure isopleths. For every location in the US, the thesis quantifies the duration of VOC-limited exposure conditions where lowering NO_x emissions increases ozone exposure, calculates the VOC/NO_x ratio of the exposure ridge line that separates the NO_x-limited and VOC-limited exposure regimes and computes an ozone exposure-neutral emissions ratio at which ozone exposure is neither increased nor decreased. The above-mentioned metrics enhance the understanding of the O_3 impacts of emissions, as they quantify whether NO_x and/or VOC reductions will be effective or counter-productive in reducing national ozone exposure based on ambient NO_x and VOC conditions. This is especially relevant given that significant tradeoffs were found between fuel burn and O_3 exposure (occurring up to 60% of the year with exposure reductions during tradeoff conditions up to 10 times the annual average exposure per unit fuel burn).

Finally, the thesis evaluates the air quality and climate benefits achievable by controlling taxi and takeoff operations using the pushback control (gate holding) and de-rated takeoff strategies. The minimum air quality and environmental impacts beyond fuel burn minimization are also quantified, accounting for tradeoff conditions between fuel burn and $PM_{2.5}$ or O_3 exposure. The findings show that the pushback control strategy is effective in reducing the environmental impacts of taxi operations at airports, with a 35-40% reduction in CO_2 and air quality impacts at DTW relative to a baseline without gate holds. De-rated takeoffs are found to be effective in reducing the air quality impacts of takeoff operations: takeoffs at 75% thrust reduce combined air quality costs ($PM_{2.5}$ + O_3 costs) by 19% relative to full-thrust takeoffs at DTW but increase fuel burn by 3%. Minimizing environmental costs balances the opposing trends in air quality and CO_2 climate costs with an average optimal thrust setting of 81%. Material maintenance cost savings from de-rated takeoffs are calculated to be two orders of magnitude larger than the increase in fuel costs, further incentivizing takeoffs with lower thrust settings. Optimizing taxi and takeoff operations for O_3 costs lowers O_3-related

premature mortality impacts significantly beyond fuel burn minimization (e.g. up to 15% and 37%, respectively, at the 75th percentile across all airports), which could potentially be relevant for targeted reductions in O_3 such as non-compliance with regulatory standards.

The tools developed in this thesis are applicable to other emission sectors beyond aviation. For example, the replacement of current methods of energy generation using renewable sources could be implemented at locations where NO_x emissions reductions decrease ozone exposure during all times of the year (i.e. locations in the US where VOC-limited conditions do not occur). An analysis of the diurnal or seasonal variations in ambient VOC and NO_x concentrations could be used in conjunction with the isopleth ridge line VOC/NO_x ratio at a given location of interest in the US (for example, in major cities) to determine temporal patterns in the occurrence of VOC-limited exposure conditions. This could be used to develop temporally-varying emission reduction policies (e.g. regulating diesel vehicle activity only during spring and summer when NO_x-limited conditions are prevalent). Furthermore, the ozone-neutral VOC/NO_x emissions ratio can be used to develop effective ozone mitigation policies targeted at sources from which emission reductions almost always result in reduced ozone exposure (e.g. gasoline cars).

5.2 Limitations and future work

There are a number of areas of further research that can be undertaken to improve the results of this thesis and broaden the scope of analysis, and these are outlined below.

Changing anthropogenic (background) emissions: The air quality calculations performed in this thesis are based on 2005 anthropogenic emissions, which have declined since. In particular, decreasing SO_2 emissions will likely lead to greater ammonium nitrate $PM_{2.5}$ formation from aircraft NO_x emissions due to increased availability of free ammonia (Woody et al., 2011). Decreasing NO_x emissions will likely lead to greater ozone sensitivity to NO_x emissions, given that net ozone production is increased as a result of reduced titration of ozone at low NO_x concentrations (Seinfeld and Pandis, 2006). Uncertainty in ammonia emissions is likely to influence the formation of secondary $PM_{2.5}$. For example, Park et al. (2004) found that $PM_{2.5}$ in the US is over-

predicted by 30% in the fall due to excessive ammonia emissions assumed in the GEOS-Chem model. Henze et al. (2009) found an excess of ammonia emissions in the US averaging 25% (varying spatially and temporally) through inverse modeling based on surface measurements of nitrate and sulfate aerosols. Future research could address these issues by updating the emission inventories to account for changes in emissions over time and/or calculating second-order sensitivities that quantify the effects of changing background conditions on the adjoint emission sensitivities.

Population exposure metric: The thesis uses a nationally-based population exposure metric to quantify the impacts of emissions on $PM_{2.5}$ and O_3 exposure, whereas regulatory analyses are often focused on impacts on a city or state level (e.g. US EPA State Implementation Plans). Furthermore, the ozone exposure isopleths developed in Chapter 3 predict the average exposure response of emissions perturbations but they do not capture hourly variations in exposure response. Future work aimed at addressing regulatory questions should consider population exposures on more localized domains and time periods of interest. This could include, for example, re-defining the model domain to focus on non-attainment areas where pollutant levels exceed the US National Ambient Air Quality Standards (NAAQS) and refining the model grid resolution to capture local-scale impacts (explained below).

Model grid scale uncertainty: Outputs of grid-based regional air quality models are inherently uncertain due to the fact that these models do not capture local effects such as chemically reactive plumes and high pollutant concentrations near point sources (Gillani and Pleim, 1996; Seinfeld, 1988). For example, Liang and Jacobson (2000) found up to 60% over-estimation of ozone production efficiency due to coarse grid resolution. Kumar and Russell (1996) found that localized O_3 concentrations from large NO_x point sources in the Eastern US decreased by up to 90 ppb when using a sub-grid scale plume chemistry model, but found $< 2\%$ change in region-wide maximum ozone concentrations. Arunachalam et al. (2011) found that increasing grid resolution from 36 km to 12 km more than doubled peak $PM_{2.5}$ concentrations attributable to aircraft emissions at three US airports, but changed the integrated mortality risks (evaluated at

the regional scale) by $< 2\%$. Further research is required to capture these local-scale effects, especially for localized model domains such as over a city or state. Potential approaches include performing adjoint calculations on higher-resolution domains (e.g. 20-30 km as recommended by Gillani and Pleim (1996)) or incorporating sub-grid scale plume models.

Detailed climate impacts: Besides CO_2 emissions, climate impacts are also associated with other emission species such as soot and sulfate aerosols, water vapor, and NO_x both directly and indirectly (Lee et al., 2010). For example, the mean global warming potential (GWP) for NO_x emissions in North America (considering a time horizon of 100 years) is -8.2 (Myhre et al., 2013). This means that the NO_x emission from an RB-211 engine at takeoff thrust (for example) results in a (negative) CO_2-equivalent emission that is ~14% of the warming related from CO_2. Further numerical simulations are required to quantify the total climate impacts and the associated tradeoffs. In addition, large uncertainties associated with current estimates (e.g. the GWP value for NO_x emissions used above has an uncertainty bound of ± 10.3 (Myhre et al., 2013)) mean that more work is required in obtaining a better understanding of the climate impacts of emissions.

Evaluation of other emission reduction measures: This thesis has quantified the air quality and environmental benefits of two emission reduction measures, namely pushback control and de-rated takeoffs. It is anticipated that future research will be done to quantify the environmental benefits and especially the associated tradeoffs of other strategies at airports. Three examples are highlighted below:

1. Operational tow-outs involve towing the aircraft to the runway with its engines switched off until five minutes before takeoff. Deonandan and Balakrishnan (2010) estimate that operational tow-outs using diesel tugs reduce fuel burn and CO_2 emissions by ~60-75% but increase total NO_x emissions by up to ~125% at US airports. The implications of this tradeoff on air quality and environmental damages need to be quantified.

2. Continuous descent approaches (CDA) have been studied from the perspective of reducing noise and emissions during approach by delaying deceleration and descent so as to avoid intermediate level phases of flight (Clarke et al., 2004; Reynolds et al., 2005). From analysis of FDR data, Lee (2005) finds that CDAs reduce fuel burn and NO_x emissions by 30-50%, but increase CO and HC emissions by 20-70%. Furthermore, Cao et al. (2013) find that CDAs could result in airborne delays due to increased spacing between aircraft, partially offsetting fuel burn savings. A study of the air quality impacts of CDAs is necessary given varying traffic levels (and therefore, airborne delays) incurred at different airports as well as the non-uniform effect of CDAs on emission species and location.

3. The potential for mitigation of the air quality impacts of airports extends beyond control of aircraft operations. Further research could be done to assess the electrification of ground support vehicles and avoidance of APU usage (Yim et al., 2013) as well as alternative methods of airport access and mobility (Miyoshi and Mason, 2013).

Appendices

Appendix A Magnitude and duration of CO_2 – air quality tradeoffs at airports

The magnitude and duration of $PM_{2.5}$ and O_3 tradeoffs with fuel burn are tabulated in Table A-1 and Table A-2 for the operation of the CFM56 engine at each airport. Four engine operation scenarios are considered: increased fuel burn at constant 7% and 100% thrust settings, as well as thrust increments over the taxi and takeoff thrust regimes. In each table, the first four columns list the average tradeoff between fuel burn and $PM_{2.5}$ or O_3 exposure (in units of $ppl \cdot ngm^{-3} \cdot kg^{-1}$ or $ppl \cdot ppt \cdot kg^{-1}$ respectively) per unit fuel burn at constant thrust or per unit fuel burn increased via thrust increments. The last four columns list the duration for which the respective tradeoff conditions occur, as a fraction of year.

Table A-1: Average PM$_{2.5}$ exposure tradeoffs (in ppl·ngm^{-3}·kg^{-1}) at each airport for operation of the CFM56 engine. The magnitude of tradeoff is averaged over the duration of tradeoff at each airport. Airports are identified by their IATA airport code.

| | Magnitude of tradeoff [ppl ngm^{-3} kg^{-1}] | | | | Duration of tradeoff [% of year] | | | |
| | Fuel burn at constant thrust | | Thrust increments | | Fuel burn at constant thrust | | Thrust increments | |
Airport	7%	100%	Taxi	Takeoff	7%	100%	Taxi	Takeoff
ATL	0.03	0.21	0.15	0.38	3%	15%	15%	15%
BOS	0.02	0.11	0.07	0.23	5%	10%	8%	8%
BWI	0.05	0.30	0.17	0.53	9%	23%	22%	22%
CLE	0.04	0.27	0.20	0.48	5%	16%	15%	15%
CLT	0.05	0.23	0.14	0.41	2%	10%	10%	10%
CVG	0.11	0.46	0.27	0.79	8%	30%	30%	30%
DCA	0.07	0.34	0.22	0.59	7%	21%	20%	20%
DEN	0.04	0.14	0.08	0.36	1%	2%	1%	1%
DFW	0.04	0.16	0.09	0.35	1%	4%	3%	3%
DTW	0.09	0.44	0.22	0.80	7%	20%	19%	19%
EWR	0.03	0.26	0.11	0.48	9%	22%	19%	19%
FLL	0.03	0.32	0.11	0.75	9%	35%	24%	24%
IAD	0.07	0.34	0.22	0.59	7%	21%	20%	20%
IAH	0.04	0.18	0.09	0.37	4%	14%	12%	12%
JFK	0.03	0.26	0.11	0.48	9%	22%	19%	19%
LAS	N. A.	0.05	0.04	0.14	0%	3%	2%	2%
LAX	1.58	3.56	1.60	6.76	3%	9%	8%	8%
LGA	0.03	0.31	0.15	0.58	9%	19%	17%	17%
MCO	0.04	0.10	0.05	0.23	1%	7%	5%	5%
MDW	0.12	0.43	0.20	0.77	6%	16%	15%	15%
MEM	0.08	0.13	0.09	0.25	1%	9%	8%	8%
MIA	0.03	0.32	0.11	0.75	9%	35%	24%	24%
MSP	0.14	0.56	0.30	1.05	4%	10%	9%	9%
ORD	0.12	0.43	0.20	0.77	6%	16%	15%	15%
PHL	0.14	0.68	0.31	1.21	13%	25%	23%	23%
PDX	0.15	0.52	0.30	1.23	3%	8%	5%	5%
PHX	0.07	0.23	0.13	0.55	1%	4%	3%	3%
PIT	0.04	0.36	0.24	0.65	11%	35%	34%	34%
SAN	0.07	0.48	0.19	0.99	8%	31%	25%	25%
SEA	0.42	1.93	0.89	3.69	3%	6%	5%	5%
SFO	0.04	0.28	0.10	0.53	1%	4%	3%	3%
SLC	0.01	0.05	0.03	0.09	0%	0%	0%	0%
STL	0.04	0.18	0.14	0.34	2%	12%	12%	12%
TPA	0.03	0.31	0.12	0.62	16%	40%	34%	34%

Table A-2: Average O_3 exposure tradeoffs (in ppl·ppt·kg^{-1}) at each airport for operation of the CFM56 engine. The magnitude of tradeoff is averaged over the duration of tradeoff at each airport. Airports are identified by their IATA airport code.

| Airport | Magnitude of tradeoff [ppl·ppt·kg^{-1}] | | | | Duration of tradeoff [% of year] | | | |
| | Fuel burn at constant thrust | | Thrust increments | | Fuel burn at constant thrust | | Thrust increments | |
	7%	100%	Taxi	Takeoff	7%	100%	Taxi	Takeoff
ATL	0.33	2.85	1.67	4.71	24%	50%	50%	50%
BOS	0.82	4.90	2.23	8.07	48%	76%	77%	77%
BWI	0.84	4.58	2.46	7.54	31%	63%	63%	63%
CLE	0.27	3.35	2.17	5.53	28%	73%	73%	73%
CLT	0.44	3.74	1.98	6.17	32%	56%	56%	56%
CVG	0.42	2.96	2.07	4.89	19%	67%	67%	67%
DCA	0.93	4.88	2.58	8.04	32%	64%	64%	64%
DEN	0.11	0.95	0.76	1.57	8%	34%	34%	34%
DFW	0.21	2.19	1.37	3.61	19%	45%	45%	45%
DTW	0.34	3.24	2.16	5.34	25%	76%	77%	77%
EWR	1.32	7.20	3.39	11.86	42%	76%	76%	76%
FLL	0.40	3.58	1.67	5.90	38%	52%	52%	52%
IAD	0.93	4.88	2.58	8.04	32%	64%	64%	64%
IAH	0.27	2.17	1.30	3.58	16%	37%	37%	37%
JFK	1.32	7.20	3.39	11.86	42%	76%	76%	76%
LAS	0.30	2.68	1.55	4.42	17%	31%	31%	31%
LAX	1.97	17.09	8.36	28.17	53%	83%	83%	83%
LGA	1.21	6.99	3.52	11.50	38%	71%	71%	71%
MCO	0.59	3.46	1.37	5.68	32%	42%	42%	42%
MDW	0.56	3.99	2.54	6.59	28%	82%	82%	82%
MEM	0.21	2.45	1.62	4.04	16%	47%	47%	47%
MIA	0.40	3.58	1.67	5.90	38%	52%	52%	52%
MSP	0.23	2.96	2.28	4.89	13%	67%	67%	67%
ORD	0.56	3.99	2.54	6.59	28%	82%	82%	82%
PHL	0.99	5.08	2.75	8.37	30%	67%	67%	67%
PDX	0.30	1.90	1.21	3.14	16%	48%	48%	48%
PHX	0.66	3.67	1.73	6.04	29%	54%	54%	54%
PIT	0.28	2.20	1.69	3.63	19%	66%	67%	67%
SAN	0.52	4.70	2.44	7.75	38%	65%	65%	65%
SEA	0.44	3.02	1.70	4.98	27%	62%	62%	62%
SFO	0.41	4.52	2.83	7.45	21%	48%	48%	48%
SLC	0.11	1.45	1.20	2.39	5%	33%	33%	33%
STL	0.17	2.70	1.97	4.46	13%	55%	55%	55%
TPA	0.32	2.52	1.23	4.15	36%	57%	57%	57%

Appendix B Calculating VOC speciation factors

In a regional air quality model, numerically calculating reactions involving each hydrocarbon species distinctly is infeasible due to the computational complexity and lack of knowledge about emissions or reaction rates of each of the species (Zaveri and Peters, 1999). The standard chemical mechanism in GEOS-Chem therefore lumps organic compounds into a smaller number of tracer species listed in Table B-1.

VOCs are a combination of several hydrocarbon compounds and an average speciation profile – i.e. the amount of each species emitted per unit of VOC – from the US EPA's SPECIATE database (US EPA, 2014b) is assumed for emissions within all grid cells in this study. The speciation profile is used in conjunction with mappings between hydrocarbon compounds and modeled tracer species in GEOS-Chem. The speciation profile is shown in Table B-1 according to the tracer species modeled in GEOS-Chem.

Table B-1: VOC tracer species in GEOS-Chem and VOC emission speciation profile used in this study.

VOC Tracer name	Units	US Average VOC emissions
ALK4	kgC/kgVOC	0.222
ACET	kgC/kgVOC	0.011
ALD2	kgC/kgVOC	0.006
C2H6	kgC/kgVOC	0.020
C3H8	kgC/kgVOC	0.050
CH2O	kg/kgVOC	0.018
PRPE	kgC/kgVOC	0.042
MACR	kg/kgVOC	0.011
RCHO	kg/kgVOC	0.013
ISOP	kgC/kgVOC	0.004
MEK	kgC/kgVOC	0.009
MVK	kg/kgVOC	0.000

Three steps are taken in creating these profiles: first, emissions of organic hydrocarbon compounds are identified for each source; second, the hydrocarbon compounds are

lumped into the GEOS-Chem tracer species on a molar basis; and finally, a unit conversion is performed to convert the molar basis into a mass basis.

Speciation of organic hydrocarbon emissions

The US EPA's SPECIATE database v4.2 (US EPA, 2014b) contains VOC speciation profiles – that is, emissions of hydrocarbon compounds per unit VOC emissions – based on the source of emissions. Profile number 0000, representing an average emissions profile, is used in the creation of ozone exposure isopleths.

Lumping of hydrocarbon compounds into GEOS-Chem tracers

Organic hydrocarbon compounds are mapped to GEOS-Chem tracers on a molar basis – that is, the number of moles of each GEOS-Chem tracer per mole of each hydrocarbon compound. A two-part method is used involving an intermediate chemical mechanism to perform this assignment, since a direct mapping from hydrocarbon compounds to GEOs-Chem tracer does not exist. First, the work of Carter (2000) is used to map hydrocarbon compounds to the SAPRC-99 chemical mechanism. Then, the work of Lam and Fu (2009) is used to relate the SAPRC-99 species to those used in the GEOS-Chem standard chemical mechanism.

Conversion from molar to mass-based units

The first two steps yield the number of moles of GEOS-Chem tracer per gram VOC emissions. A final step is required to convert molar units into mass units, since the adjoint method calculates sensitivities with respect to mass of emissions of each tracer. Molar masses as specified in the GEOS-Chem standard mechanism are used (Yantosca et al., 2012).

Calculation of sensitivity to VOC

The adjoint of GEOS-Chem calculates the sensitivity of ozone exposure with respect to emissions of each tracer species. Since VOC emissions are a combination of hydrocarbon species, the sensitivity of ozone to a unit of VOC emissions is calculated by weighting

individual tracer sensitivities by the VOC speciation profile according to the source type,

$$\partial Z/\partial V(K,T) = \sum_i \omega_i \cdot \partial Z/\partial E_i(K,T),$$

where the index i refers to the modeled hydrocarbon tracer species, ω_i refers to the VOC emissions speciation profile (with units of kg/kg VOC or kgC/kg VOC depending on the tracer) and $\partial Z/\partial E_i$ refers to the sensitivity of ozone exposure to emissions of tracer species i calculated by the adjoint method (with units of ppl·ppb·(kg/hr/box)[-1] or ppl·ppb·(kgC/hr/box)[-1] depending on the VOC tracer).

Appendix C Ozone exposure isopleth ridge line and ozone exposure-neutral ratios

This section provides an example of how to use the information presented in Chapter 3 – specifically data from Figure 3-9 and Figure 3-12 representing the duration of VOC-limited exposure conditions, isopleth ridge line VOC/NO$_x$ ratio and the ozone-neutral ratio – to determine the effectiveness of emission reductions at locations across the US. The goal is to evaluate whether or not a reduction in NO$_x$ and VOC emissions from a particular source will lead to increased national ozone exposure. The calculation method is as follows:

1) Convert the units of emissions from mass to mixing ratio units (for use with the ozone exposure isopleths)
2) Determine the exposure regime into which VOC and NO$_x$ are emitted
3) If a VOC-limited exposure regime exists: Compare the VOC/NO$_x$ ratio of emissions reduction with the ozone-neutral emissions ratio

The calculations assume that VOC and NO$_x$ emissions (in kg) from the source in consideration are known. Ambient NO$_x$ and VOC mixing ratios may or may not be known for a particular location and time, and both situations are considered in the example below.

1) Calculating the emissions ratio

The mass of VOC and NO$_x$ emissions are converted into mixing ratios assuming ISA conditions in a one-box model. NO$_x$ emissions in mass units (g) are converted to molar units based on its molecular weight (46 g/mol), while VOC emissions are converted according to speciation factors for each source from the US EPA's SPEICATE database. The average molecular weights of VOC based on five VOC emission profiles (including the US average profile) are listed in Table C-1. These are used to calculate the VOC/NO$_x$ emissions ratio for various emission sources, such as coal-fired boiler, heavy-duty diesel truck, taxi and takeoff operations of a Boeing B737 aircraft (CFM56-7B22 engine) and a light-duty gasoline vehicle listed in Table 3-1.

Table C-1: Average VOC molecular weight, to be used in the conversion between mass and molar units. VOC speciation profiles are obtained from the US EPA's SPECIATE database.

Source (SPECIATE profile)	MW VOC (g VOC / molC)
US average (0)	30.9
Coal-fired boiler (1178)	70.1
Diesel (4674)	35.8
Gasoline (8750)	37.7
Aviation (5565)	38.1

2) Determining the exposure regime

Known ambient NO_x and VOC mixing ratios

If ambient NO_x and VOC concentrations are known, the ozone exposure regime is determined by comparing the ambient VOC/NO_x ratio with that of the isopleth ridge line at that location. If the ambient VOC/NO_x ratio is higher than the ridge line ratio, a NO_x-limited exposure regime exists and a reduction in both NO_x and VOC emissions will reduce ozone exposure. If the ambient VOC/NO_x ratio is lower than the ridge line ratio, a VOC-limited exposure regime exists and emissions reductions could increase ozone exposure depending on the VOC/NO_x ratio of emissions.

A sample calculation is performed here for Wayne County, Michigan at 12:00pm on 1 July 2006. The ozone exposure isopleth ridge line VOC/NO_x ratio for this location is calculated to be 5.9 ppbC/ppb (Figure 3-12(a)). Ambient NO_x and VOC mixing ratios – obtained from the US EPA's Air Quality System (AQS) (US EPA, 2015) – are 10 ppb and 6.17 ppbC, respectively at this location and time. This evaluates to an ambient VOC/NO_x ratio of 0.617 ppbC/ppb, which is lower than the ridge line ratio. Therefore, a VOC-limited exposure regime exists and emissions reductions could increase ozone impacts depending on their VOC/NO_x ratios.

Ambient NO_x and VOC mixing ratios for the same location at 11:00am on 30 May 2006 are 14 ppb and 264 ppbC respectively according to the AQS (US EPA, 2015), resulting in a VOC/NO_x ratio of 18.9 ppbC/ppb. Here the exposure regime is NO_x-limited, meaning that VOC and NO_x emissions reductions will decrease ozone exposure.

<u>Unknown ambient NO_x and VOC mixing ratios</u>

If ambient NO_x and VOC mixing ratios are not known, the exposure regime occurring at the particular time of emissions cannot be identified. It is possible, however, to quantify the annual duration of VOC-limited exposure conditions expected to occur at that location using Figure 3-9 of the main paper. This figure shows the annual duration of VOC-limited conditions that occurred in 2006, calculated using ambient NO_x and VOC mixing ratios modeled by GEOS-Chem for 2006. In the example for Wayne County, Michigan, VOC-limited conditions occurred for 84% of the year in 2006.

3) Comparison with ozone exposure-neutral emissions ratio

If a VOC-limited exposure regime exists, the next step is to determine if ozone exposure is increased due to emissions reductions depending on its VOC/NO_x ratio. This is done by comparing the VOC/NO_x concentration ratio with the ozone exposure-neutral emissions ratio at that location. If the emissions ratio is higher than the ozone-neutral ratio, reducing emissions from this source will decrease ozone exposure. If, however, the emissions ratio is lower than the ozone-neutral ratio, emissions reductions will increase ozone exposure.

As an example, consider the effect of reducing emissions from diesel trucks, gasoline vehicles and aircraft taxi operations at the sample location and time (Wayne County, Michigan at 12:00pm on 1 July 2006; it is assumed that the same conditions exist at the Detroit Metropolitan Airport for the case of aircraft operations). The ozone-neutral emissions ratio at this location is calculated from the ozone exposure isopleth to be 0.76 ppbC/ppb (Figure 3-9 (b)). As shown in Table 3-1, the emission ratios for a diesel truck, taxiing aircraft and gasoline vehicles are 0.067, 0.771 and 1.822 ppbC/ppb respectively. The emissions ratio for diesel trucks and taxiing aircraft are lower than the ozone exposure-neutral emissions ratio while that of gasoline vehicles is higher than the exposure-neutral emissions ratio. Thus, reducing emissions from diesel trucks and taxiing aircraft is expected to increase ozone impacts while reducing gasoline vehicle activity is expected to decrease population exposure to ozone.

Appendix D Sensitivity analysis of taxi and takeoff operations

D.1   Taxi operations

This section presents the sensitivity of the air quality impacts of taxi operations to varying traffic level, fleet composition and annual atmospheric conditions at other airports in the US.

Traffic level

Table D-1 lists the baseline costs (i.e. operations without gate holds) for the mid- and low-traffic scenarios (with 75% and 50% of airport traffic relative to 2007 levels, respectively). The costs scale approximately linearly with traffic level, with the average taxi-out time reduced from 19.7 minutes/aircraft to 17.5 minutes/aircraft and average fuel burn reduced from 197 kg/aircraft to 186 kg/aircraft.

Table D-1: Baseline (no gate hold) costs of $PM_{2.5}$, O_3, air quality (AQ), CO_2 climate (SCC), environmental impacts (Env.), fuel burn (FB) and total fuel combustion-related costs (Tot.) from airport surface taxi operations with the nominal (2007), 75% (mid) and 50% (low) traffic levels. Also shown are the average taxi times, mass of fuel burn and emissions of NO_x and HC. Results for the mid and low traffic levels are presented as a percentage change from the nominal costs.

	Nominal	Mid	Low
$PM_{2.5}$ (Million USD)	6.0	-27%	-53%
O_3 (Million USD)	1.2	-26%	-56%
AQ (Million USD)	7.1	-27%	-53%
SCC (Million USD	7.7	-27%	-52%
Env. (Million USD)	14.8	-27%	-53%
FB (Million USD)	62.3	-27%	-52%
Tot. (Million USD)	77.1	-27%	-52%
Taxi-out time (min/aircraft)	19.7	18.9	17.5
Taxi-in time (min/aircraft)	9.7	9.7	9.9
Fuel burn (kg/aircraft)	197.2	193.8	185.7
NO_x (kg/aircraft)	0.7	0.7	0.7
HC (kg/aircraft)	1.0	1.0	0.9

Figure D-1 shows the trend in taxi-out time with respect to gate hold allowance. Taxi-out times are reduced with lower surface traffic and decrease approximately linearly until a gate hold allowance of ~ 8 minutes.

Figure D-2 shows that implementing gate holds reduces fuel burn, emissions and air quality impacts at all three traffic levels relative to their respective baseline cases without gate holds. Reductions of 34-36% are observed in the mid traffic level and reductions of 31-33% are seen at the low traffic level.
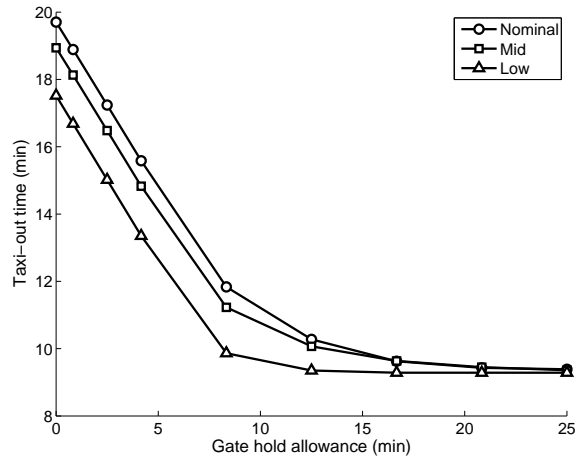

Figure D-1: Average taxi-out time per departing aircraft as a function of gate hold allowance for the nominal (2007), mid and low traffic levels at DTW.
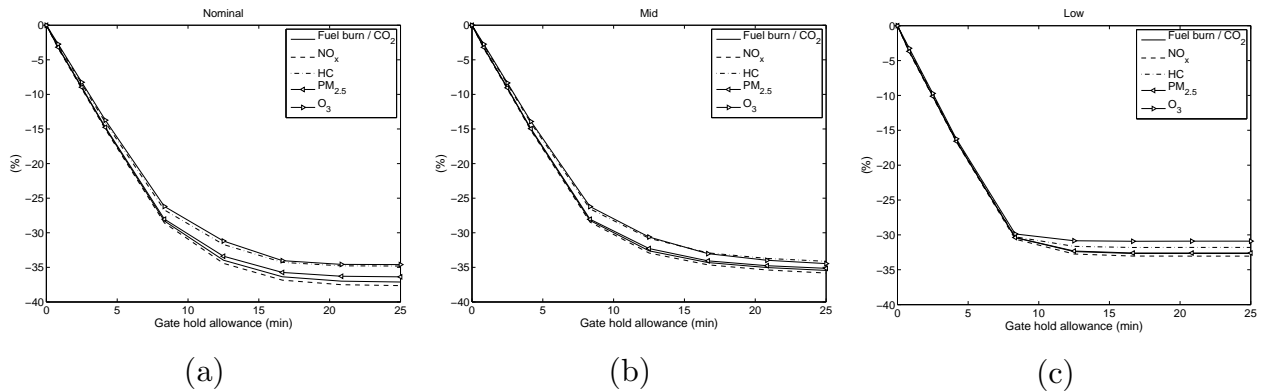

Figure D-2: The effect of increasing gate hold allowance on fuel burn, emissions and air quality impacts, as a percentage change relative to the no gate hold scenario. Panel (a) shows the results for the nominal level of traffic, (b) shows the results for the mid-level of traffic and panel (c) shows the results for the low level of traffic.

Figure D-3 shows the fuel burn, $PM_{2.5}$ and O_3 costs when gate holds are optimized beyond fuel burn minimization. The costs are shown as percentage changes with respect to the minimum fuel burn solution at each traffic level. At the low traffic level, optimizing gate holds for $PM_{2.5}$ (O_3) impacts reduces ozone costs by 2.4% (8.2%) beyond

127

fuel burn minimization, with 1.4% (7.9%) increase in fuel burn. At the mid traffic level, optimizing gate holds for $PM_{2.5}$ (O_3) impacts reduces ozone costs by 2.6% (8.4%) beyond fuel burn minimization, with 1.6% (9.1%) increase in fuel burn.
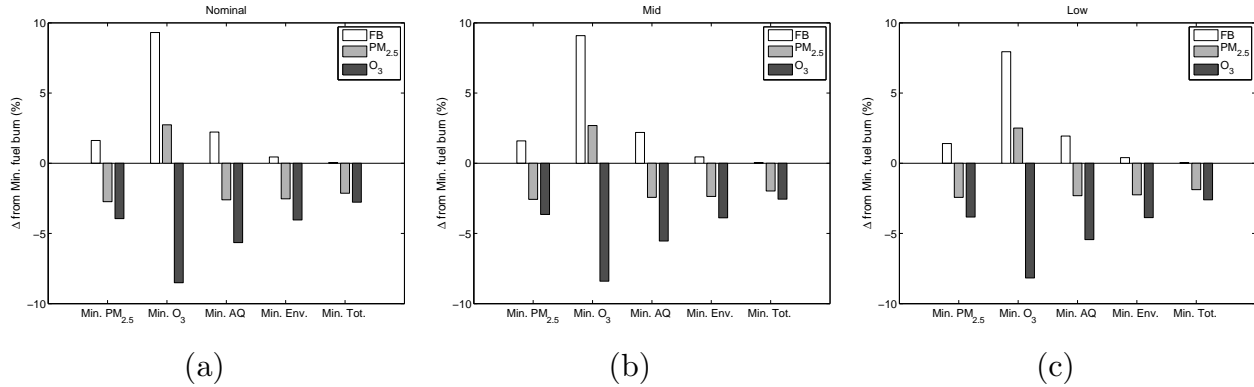

Figure D-3: Fuel burn (FB), $PM_{2.5}$ and O_3 costs from optimizing gate holds for minimum $PM_{2.5}$, O_3, air quality (AQ), environmental impacts (Env.) and total fuel combustion-related costs (Tot.). Panel (a) shows the results for the nominal level of traffic, (b) shows the results for the mid-level of traffic and panel (c) shows the results for the low level of traffic. Costs are expressed as a percentage change from the minimum fuel burn solution.

Fleet mix

Table D-2 shows the baseline (no gate hold) costs for operations with increasing proportion of Heavy aircraft from the nominal level of 5% (indicative of operations at DTW in 2007) up to 25%. Fuel burn, NO_x and HC emissions are increased by 29%, 27% and 97% relative to the 2007 fleet, respectively. $PM_{2.5}$ and O_3 costs increase by 47% and 116%, respectively. Figure D-4 shows that implementing gate holds reduces fuel burn, emissions and air quality impacts by 37-38% for the 25%-Heavy fleet mix.

Table D-2: Baseline (no gate hold) costs of $PM_{2.5}$, O_3, air quality (AQ), CO_2 climate (SCC), environmental impacts (Env.), fuel burn (FB) and total fuel combustion-related costs (Tot.) from airport surface taxi operations with the nominal (5% Heavy) and 25% Heavy fleet mix. Also shown are the average taxi times, mass of fuel burn and emissions of NO_x and HC. Results for the 25% case are presented as a percentage change from the nominal costs.

	Nominal (5% Heavy)	25% Heavy
$PM_{2.5}$ (Million USD)	6.0	47%
O_3 (Million USD)	0.9	116%
AQ (Million USD	6.8	58%
SCC (Million USD)	7.7	29%
Env. (Million USD)	14.5	43%
FB (Million USD)	62.3	29%
Tot. (Million USD)	76.8	32%
Taxi-out time (min/aircraft)	19.7	3%
Taxi-in time (min/aircraft)	9.7	0%
Fuel burn (kg/aircraft)	197.2	29%
NO_x (kg/aircraft)	0.7	27%
HC (kg/aircraft)	1.0	97%

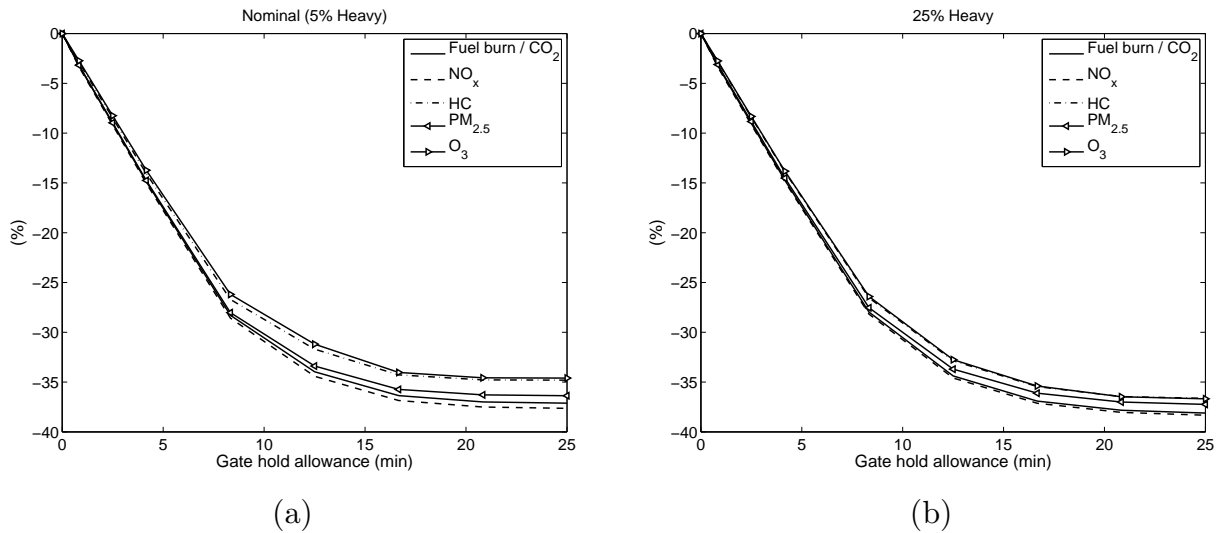(a)   (b)

Figure D-4: The effect of increasing gate hold allowance on fuel burn, emissions and air quality impacts, as a percentage change relative to the no gate hold scenario. Panel (a) shows the results for the nominal fleet mix (5% Heavy aircraft) and (b) shows the results for the 25% Heavy fleet mix.

Figure D-5 shows the improvements in air quality impacts beyond fuel burn minimization for increasing proportion of heavy aircraft in the fleet. The improvements in $PM_{2.5}$ costs become smaller with increased heavy aircraft (e.g. $PM_{2.5}$ impacts are reduced from 2.7% to 2.2%). The associated fuel burn tradeoffs also decrease from 1.6%

to 1.5%. Similarly, the improvements in ozone impacts become smaller from 8.5% to 3.1% for larger proportion of heavy aircraft. The associated fuel burn tradeoffs decrease from 9.3% to 4.5%.

This trend is explained by changes in emission profiles due to changing fleet composition. A negative correlation exists between aircraft size and taxi thrust setting is observed from FDR archives. Thus, heavy aircraft taxi at lower thrust settings and consequently emit relatively more HC emissions and less NO_x emissions per kilogram fuel than other aircraft. Therefore, as the proportion of heavy aircraft increases from 5% to 25%, the fleet-averaged NO_x emissions grow by ~27% whereas the fleet-averaged HC emissions grow by 97% (Table D-2). The emphasis on HC emissions relative to NO_x emissions means fewer tradeoffs between fuel burn and air quality, since the atmospheric sensitivity of $PM_{2.5}$ and O_3 to HC emissions is negative less frequently than the sensitivity to NO_x emissions as explained in Chapter 2.
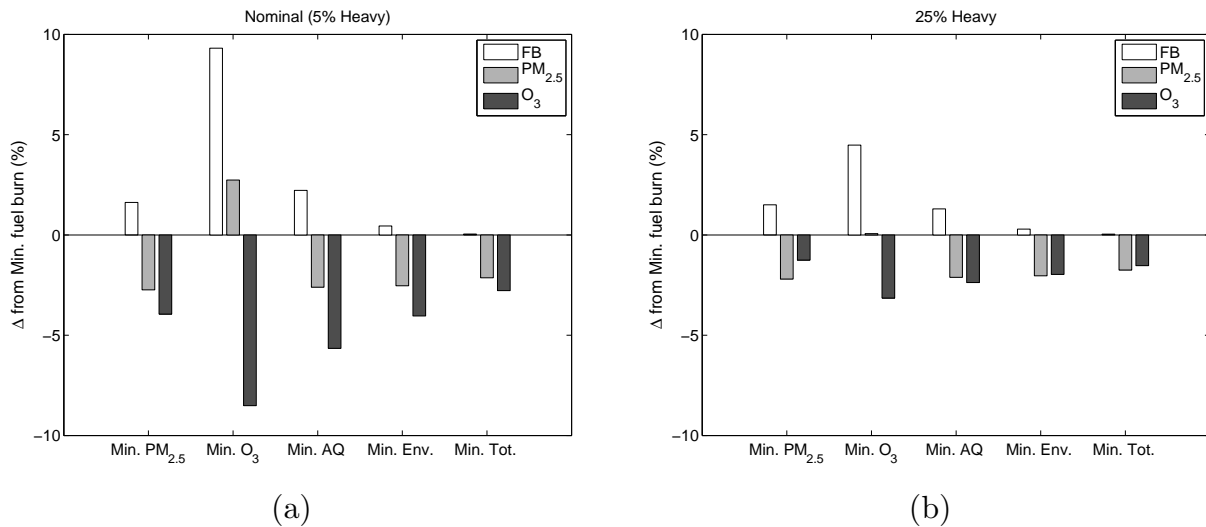
Figure D-5: Fuel burn, $PM_{2.5}$ and O_3 costs from optimizing gate holds for minimum $PM_{2.5}$, O_3, air quality (AQ), environmental impacts (Env.) and total fuel combustion-related costs (Tot.). Panel (a) shows the results for the nominal fleet mix and (b) shows the results for the 25% Heavy fleet mix. Costs are expressed as a percentage change from the minimum fuel burn solution.

Atmospheric conditions at other US airports

The variation in baseline (no gate hold) air quality, environmental and total fuel combustion-related costs with atmospheric conditions at the top 34 busiest airports in

the US is shown in Figure D-6 (a). Fuel burn and CO_2 climate costs do not change across airport locations, since the activity set is held constant while only the atmospheric conditions are varied. Baseline $PM_{2.5}$ and O_3 impacts vary between \$1.3M – \$25.9M and \$0.5M – \$4.7M.

Figure D-6 (b) shows that the application of 25-minute gate holding reduces $PM_{2.5}$ impacts by 36-37% across all airports, while the effect on O_3 impacts is more variable with reductions of 16-37%.

(a)   (b)
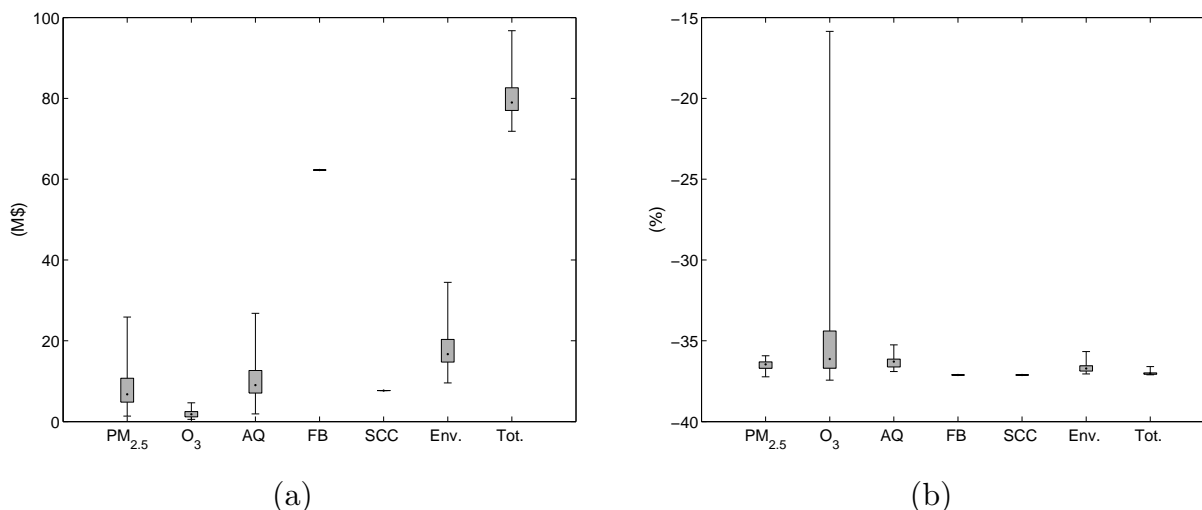
Figure D-6: Baseline (no gate hold) costs (a) and percent change from baseline due to the application of 25-minute gate holds (b) for $PM_{2.5}$, O_3, air quality (AQ), fuel burn (FB), CO_2 climate (SCC), environmental impacts (Env.) and total fuel combustion-related costs (Tot.). Bars depict the range of results across all 34 airports studied, with the whiskers showing the minimum and maximum values, the bar extends showing the 25th and 75th percentile bounds and the black dot representing the median value across all airports. Fuel burn and CO_2 climate costs do not vary across airports since aircraft activity is held fixed.

Gate holds are optimized for air quality and other objectives assuming atmospheric conditions at the top 34 busiest airports in the US. The change in fuel burn, $PM_{2.5}$ and O_3 impacts, relative to minimum fuel burn, resulting from optimizing operations for each objective function is shown in Figure D-7. The boxplots show the distribution of the changes across the 34 airports modeled. The biggest tradeoff occurs between fuel burn and ozone impacts, where ozone is reduced by up to 180% (~15% at the 75th percentile) relative to the minimum fuel burn solution with up to 18% increased fuel burn. $PM_{2.5}$ impacts are improved by up to 3.3% beyond fuel burn minimization with up to 4.3% increase in fuel burn.

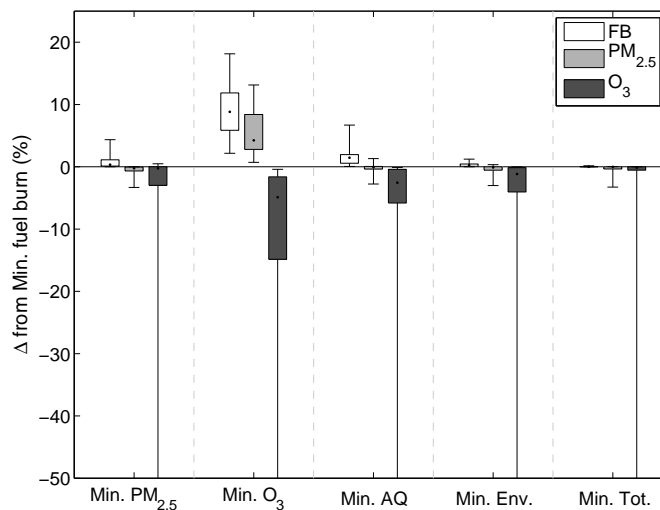Figure D-7: Percentage change in fuel burn, $PM_{2.5}$ and O_3 costs when gate holds are optimized for minimum $PM_{2.5}$, O_3, air quality (AQ), environmental impacts (Env.) and total fuel combustion-related costs (Tot.). Costs are expressed as a percentage change from the minimum fuel burn solution. Bars depict the range of results across all 34 airports studied, with the whiskers showing the minimum and maximum values, the bar extends showing the 25th and 75th percentile bounds and the black dot representing the median value across all airports. Note that the y-axis is truncated at -50%, whereas the whiskers extend up to -180%.

D.2 Takeoff operations

The sensitivity of the air quality impacts of takeoff operations to varying aircraft weight and annual atmospheric conditions at other airports in the US is shown in this section.

Takeoff weight

The sensitivity of the results to takeoff weight is assessed by calculating aircraft performance assuming a range of takeoff weights from 100% Maximum Takeoff Weight (MTOW) to 70% MTOW. Table D-3 lists the baseline costs at DTW (i.e. takeoffs at 100% thrust) for takeoff weights between 100% MTOW and 70% MTOW. As takeoff weight increases, all costs become larger except ozone impacts (given the prevalence of VOC-limited exposure conditions at DTW in 2007). Figure D-8 illustrates the trends in fuel burn and NO_x emissions as a function of takeoff de-rate. Fuel burn is observed to increase with reduced thrust, while NO_x emissions reduce with thrust reduction for all takeoff weights.

Table D-3: Annual costs of $PM_{2.5}$, O_3, air quality (AQ), CO_2 climate (SCC), environmental impacts (Env.), fuel burn (FB) and total fuel combustion-related costs (Tot.) from baseline takeoff operations (100% takeoff thrust) for full-thrust takeoffs between 70% and 100% Maximum Take-Off Weight (MTOW). Also shown are the average mass of fuel burn and emissions of NO_x and HC per flight. Results for the 100%, 90% and 70% MTOW cases are presented as a percentage change from the 80% MTOW case.

	100% MTOW	90% MTOW	80% MTOW	70% MTOW
$PM_{2.5}$ (Million USD)	34%	16%	3.0	-15%
O_3 (Million USD)	-35%	-16%	-0.5	15%
AQ (Million USD)	34%	16%	2.6	-15%
SCC (Million USD)	37%	17%	1.5	-15%
Env. (Million USD)	35%	16%	4.0	-15%
FB (Million USD)	37%	17%	11.5	-15%
Tot. (Million USD)	37%	17%	15.5	-15%
Fuel burn (kg/aircraft)	37%	17%	72.7	-15%
NO_x (kg/aircraft)	36%	17%	1.6	-15%
HC (kg/aircraft)	40%	18%	0.0	-16%
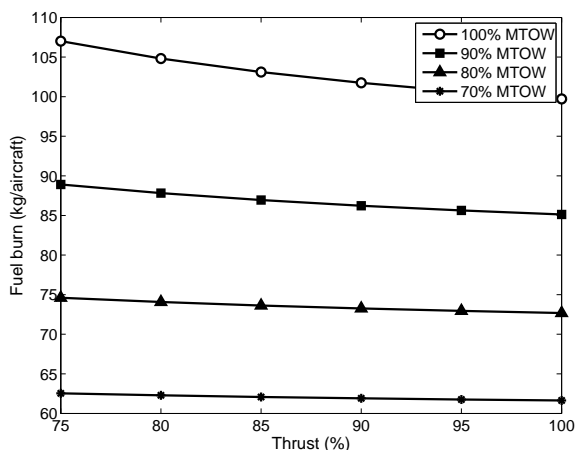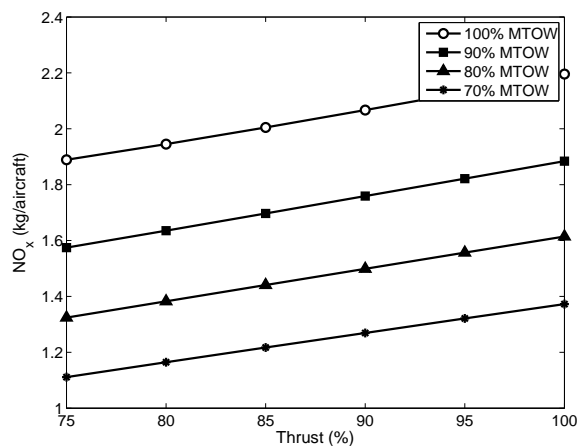
(a)   (b)

Figure D-8: Fuel burn (a) and NO_x emissions (b) as a function of takeoff thrust and aircraft weight. Values are averaged over the fleet of aircraft operating at DTW in 2007.

Figure D-9 shows the effect of takeoff de-rate on fuel burn, emissions and air quality impacts as the aircraft takeoff weight varies. As the aircraft become heavier, the additional fuel burn due to de-rated takeoffs grows disproportionately; for example, while de-rated takeoffs at 80% MTOW require 3% more fuel burn compared to full-thrust takeoffs, de-rated takeoffs at 100% MTOW require 7% additional fuel. This is because de-rated takeoffs result in 29% longer time-to-climb for aircraft at 80% MTOW

but result in 34% longer time-to-climb for aircraft at 100% MTOW. Consequently, smaller reductions in $PM_{2.5}$ impacts occur as a result of de-rated takeoffs at 100% MTOW than at 80% MTOW (-14% c.f. -18%).
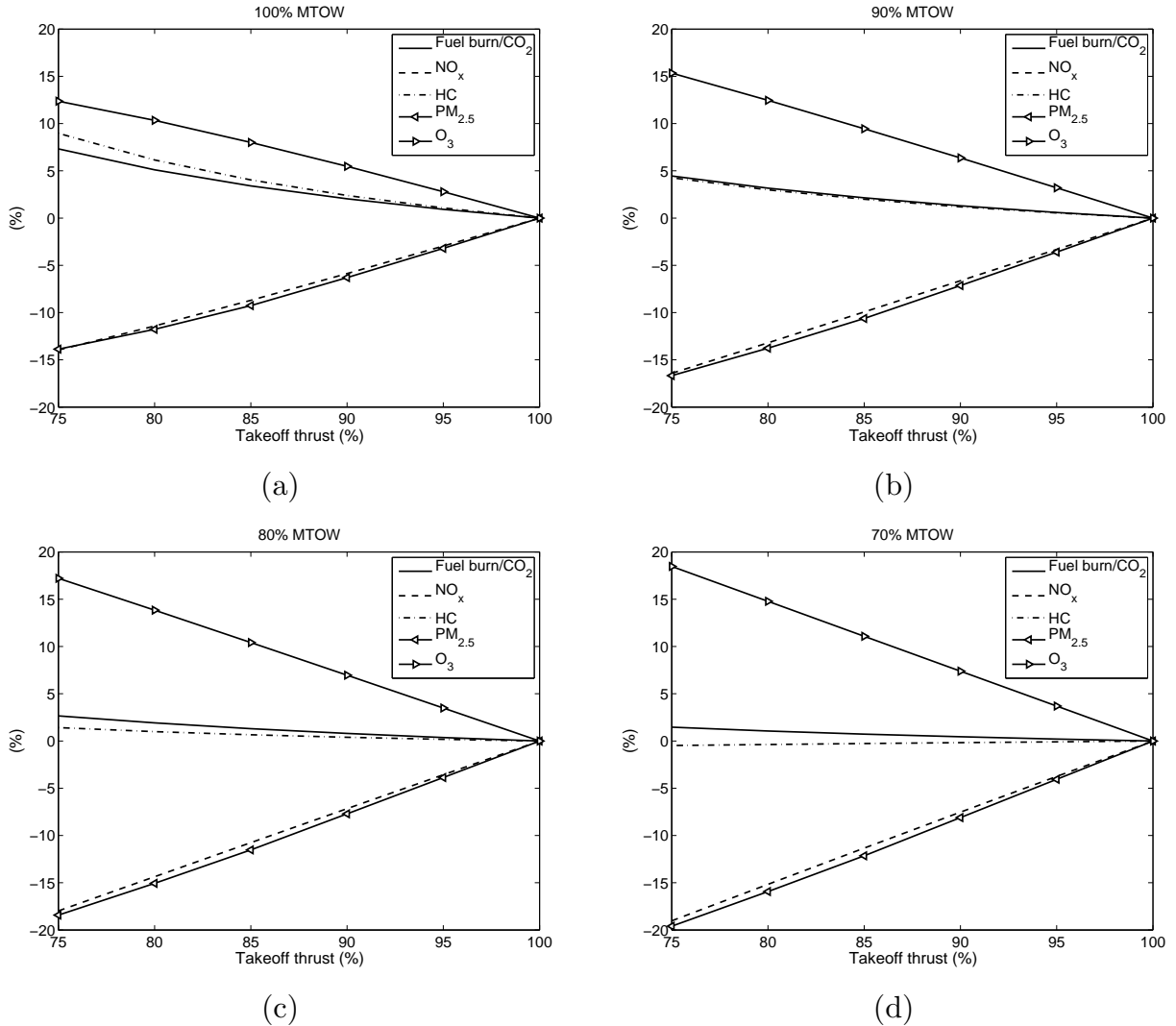
Figure D-9: The effect of reduced-thrust takeoffs on fuel burn, emissions and air quality impacts from departure operations at DTW in 2007. Results are shown as a percentage change relative to baseline operations (100% thrust) for takeoffs at 100% MTOW (a), 90% MTOW (b), 80% MTOW (c) and 70% MTOW (d).

Figure D-10 plots the changes in fuel burn, $PM_{2.5}$ and O_3 costs beyond fuel burn minimization when takeoff thrusts are optimized for minimum $PM_{2.5}$, O_3, air quality (AQ), environmental costs (Env.) and total fuel combustion-related costs (Tot.). The improvements to $PM_{2.5}$ costs beyond fuel burn minimization reduce as takeoff weight is increased (e.g. 21.6% at 80% MTOW c.f. 16.3% at 100% MTOW). Improvements to O_3

impacts also become smaller from 11.8% at 100% MTOW to 8.6% at 100% MTOW. The average optimal thrust settings that minimize $PM_{2.5}$ and O_3 change by <1% with takeoff weight, as shown in Table D-4. However, the solution for minimizing total fuel combustion-related impacts changes from 95% thrust at 100% MTOW to 86% thrust at 70% MTOW.
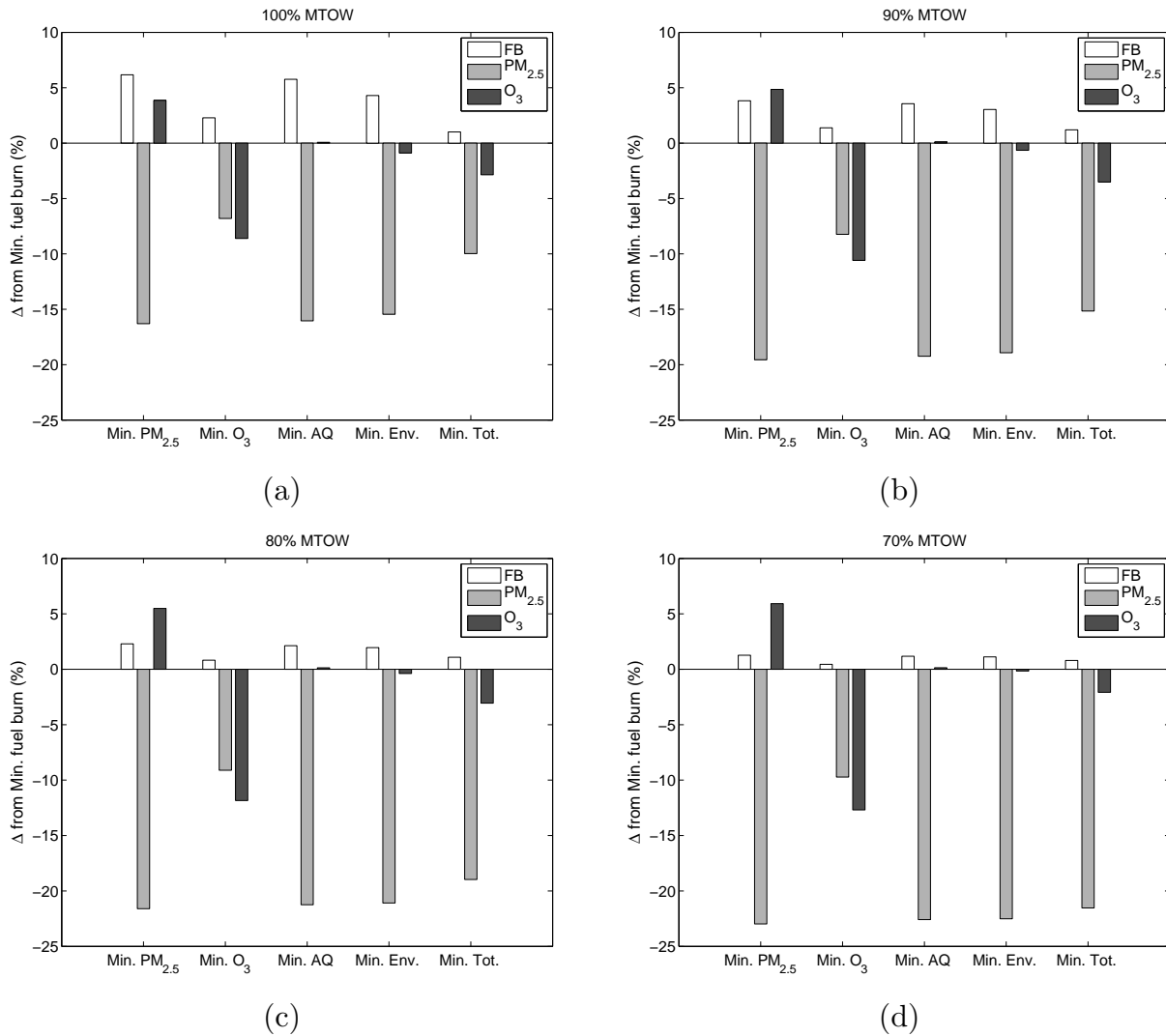
Figure D-10: Fuel burn, $PM_{2.5}$ and O_3 costs from optimizing takeoff thrust for minimum $PM_{2.5}$, O_3, air quality (AQ), environmental impacts (Env.) and total fuel combustion-related costs (Tot.). Panel (a) shows the results for takeoffs at 100% MTOW, (b) shows the results for 90% MTOW, (c) shows results for 80% MTOW and (d) shows results for takeoffs with 70% MTOW. Costs are expressed as a percentage change from the minimum fuel burn solution.

Table D-4: Fleet-averaged takeoff thrust (expressed as a percentage of maximum takeoff thrust) from optimizing takeoff operations over one year for minimum fuel burn (FB), PM$_{2.5}$, O$_3$, air quality (AQ), environmental impacts (Env.) and total fuel combustion-related costs (Tot.).

	100% MTOW	90% MTOW	80% MTOW	70% MTOW
Min. FB	100%	100%	100%	100%
Min. PM$_{2.5}$	79%	78%	78%	78%
Min. O$_3$	92%	92%	92%	92%
Min. AQ	80%	80%	80%	80%
Min. Env.	84%	82%	81%	80%
Min. Tot.	95%	92%	89%	86%

Atmospheric conditions at other US airports

Figure D-11 (a) shows the variation in baseline (100% takeoff thrust) air quality, environmental and total fuel combustion-related costs with atmospheric conditions at the top 34 busiest airports in the US. Fuel burn and CO$_2$ climate costs do not change across airport locations, since the activity set is held constant while only the atmospheric conditions are varied. Baseline PM$_{2.5}$ and O$_3$ impacts vary between \$0.7M – \$16.6M and \$-6.5M – \$2.5M. The range of ozone impacts spans both positive and negative values, which indicates that annual average atmospheric conditions are VOC-limited at some airports while not at others.

Figure D-11 (b) plots the change in air quality, environmental and total fuel combustion-related costs due to takeoffs at 75% thrust relative to takeoffs at 100% thrust. De-rated takeoffs reduce PM$_{2.5}$ impacts by 14.1-21.6% across all airports. O$_3$ impacts are either lowered or increased across airports (ranging from a 19.1% reduction to a 31.6% increase) as a result of de-rated takeoffs relative to full-thrust takeoffs. Total air quality costs are always lowered (2.3-21.6%) as a result of de-rated takeoffs at the 34 airports studied.
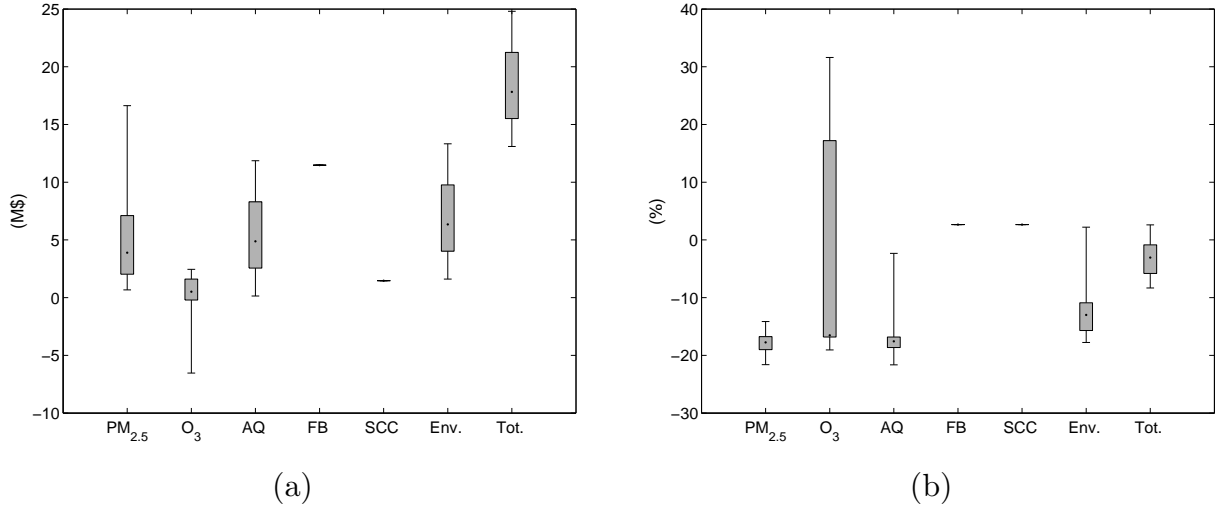
(a)   (b)

Figure D-11: Baseline costs from full-thrust takeoffs (a), the percent change from baseline due to de-rated takeoffs (75% thrust) for $PM_{2.5}$, O_3, air quality (AQ), fuel burn (FB), CO_2 climate (SCC), environmental impacts (Env.) and total fuel combustion-related costs (Tot.). Bars depict the range of results across all 34 airports studied, with the whiskers showing the minimum and maximum values, the bar extends showing the 25th and 75th percentile bounds and the black dot representing the median value across all airports. Fuel burn and CO_2 climate costs do not vary across airports since aircraft activity is held fixed.
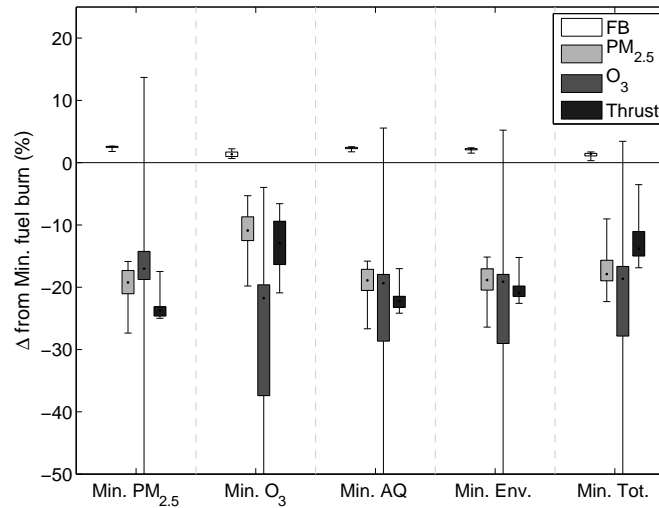
Figure D-12: Percentage change in fuel burn, $PM_{2.5}$ and O_3 costs and average takeoff thrust setting when takeoff thrust is optimized for minimum $PM_{2.5}$, O_3, air quality (AQ), environmental impacts (Env.) and total fuel combustion-related costs (Tot.). Costs are expressed as a percentage change from the minimum fuel burn solution. Bars depict the range of results across all 34 airports studied, with the whiskers showing the minimum and maximum values, the bar extends showing the 25th and 75th percentile bounds and the black dot representing the median value across all airports. Note that the y-axis is truncated at -50%, whereas the whiskers extend up to -846%.

137

Takeoff thrusts are optimized for air quality and other objectives assuming atmospheric conditions at the top 34 busiest airports in the US. The change in fuel burn, $PM_{2.5}$ and O_3 impacts, relative to minimum fuel burn, resulting from optimizing operations for each objective function is shown in Figure D-12. Optimizing takeoff thrusts for $PM_{2.5}$ impacts reduces $PM_{2.5}$ costs by up to 27.4% relative to the minimum fuel burn solution. Optimizing for O_3 impacts reduces O_3 costs up to a factor of 8 beyond fuel burn minimization (~37% at the 75th percentile). The average takeoff thrust setting varies between 75-83% across airports when optimized for $PM_{2.5}$ costs, while they vary between 79-93% when optimized for O_3 costs.

References

Aardenne, J.V., Dentener, F., Dingenen, R.V., Marmer, E., Vignati, E., Russ, P., Szabo, L., 2009. Global climate policy scenarios: The benefits and trade-offs for air pollution. IOP Conference Series: Earth and Environmental Science 6, 282001. doi:10.1088/1755-1307/6/8/282001

Ackert, S., 2011. Engine maintenance concepts for financiers: Elements of Turbofan Shop Maintenance Costs, Aircraft Monitor. Macquarie AirFinance.

Adamkiewicz, G., Hsu, H.-H., Vallarino, J., Melly, S.J., Spengler, J.D., Levy, J.I., 2010. Nitrogen dioxide concentrations in neighborhoods adjacent to a commercial airport: a land use regression modeling study. Environmental Health 9, 73. doi:10.1186/1476-069X-9-73

AeroStrategy, 2009. Global MRO Market Economic Assessment. Aerostrategy Management Consulting, Ann Arbor, Michigan.

Ainslie, B., Steyn, D.G., 2006. A scaling analysis of ozone photochemistry. Atmospheric Chemistry and Physics 6, 4067–4077. doi:10.5194/acp-6-4067-2006

Arunachalam, S., Wang, B., Davis, N., Baek, B.H., Levy, J.I., 2011. Effect of chemistry-transport model scale and resolution on population exposure to PM2.5 from aircraft emissions during landing and takeoff. Atmospheric Environment 45, 3294–3300. doi:10.1016/j.atmosenv.2011.03.029

Ashok, A., 2011. The air quality impact of aviation in future-year emissions scenarios. Massachusetts Institute of Technology.

Ashok, A., Lee, I.H., Arunachalam, S., Waitz, I.A., Yim, S.H.L., Barrett, S.R.H., 2013. Development of a response surface model of aviation's air quality impacts in the United States. Atmospheric Environment 77, 445–452. doi:10.1016/j.atmosenv.2013.05.023

BADA, 2013. User manual for the Base of Aircraft Data (BADA) revision 3.11 (No. 13/04/16-01). Eurocontrol Experimental Centre.

Bailis, R., 2005. Mortality and Greenhouse Gas Impacts of Biomass and Petroleum Energy Futures in Africa. Science 308, 98–103. doi:10.1126/science.1106881

Baker, A.K., Beyersdorf, A.J., Doezema, L.A., Katzenstein, A., Meinardi, S., Simpson, I.J., Blake, D.R., Sherwood Rowland, F., 2008. Measurements of nonmethane hydrocarbons in 28 United States cities. Atmospheric Environment 42, 170–182. doi:10.1016/j.atmosenv.2007.09.007

Balakrishnan, H., Chandran, B.G., 2010. Algorithms for Scheduling Runway Operations Under Constrained Position Shifting. Operations Research 58, 1650–1665. doi:10.1287/opre.1100.0869

Balakrishnan, H., Jung, Y., 2007. A framework for coordinated surface operations planning at Dallas-Fort Worth International Airport, in: AIAA Guidance, Navigation, and Control Conference, Hilton Head, SC.

Balk, D.L., Deichmann, U., Yetman, G., Pozzi, F., Hay, S.I., Nelson, A., 2006. Determining Global Population Distribution: Methods, Applications and Data, in: Advances in Parasitology. Elsevier, pp. 119–156.

Barrett, S., Yim, S., Gilmore, C., Murray, L.T., Kuhn, S., Tai, A., Yantosca, R., Byun, D., Ngan, F., Li, X., Levy, J., Ashok, A., Koo, J., Wong, H.M., Dessens, O., Balasubramanian, S., Fleming, G., Pearlson, M., Wollersheim, C., Malina, R., Arunachalam, S., Binkowski, F., Leibensperger, E., Jacob, D.J., Hileman, J., Waitz, I., 2012. Public Health, Climate and Economic Impacts of Desulfurizing Jet Fuel. Environmental Science & Technology 120301095418005. doi:10.1021/es203325a

Barrett, S.R.H., Britter, R.E., 2008. Development of algorithms and approximations for rapid operational air quality modelling. Atmospheric Environment 42, 8105–8111. doi:10.1016/j.atmosenv.2008.06.020

Barrett, S.R.H., Britter, R.E., Waitz, I.A., 2013. Impact of aircraft plume dynamics on airport local air quality. Atmospheric Environment 74, 247–258. doi:10.1016/j.atmosenv.2013.03.061

Barrett, S.R.H., Britter, R.E., Waitz, I.A., 2010. Global Mortality Attributable to Aircraft Cruise Emissions. Environmental Science & Technology 44, 7736–7742. doi:10.1021/es101325r

Baughcum, S.L., Tritz, T.G., Herndon, S.C., Pickett, D.C., 1996. Scheduled Civil Aircraft Emission Inventories for 1992: Database Development and Analysis (No. 4700). NASA.

Bell, M.L., 2004. Ozone and Short-term Mortality in 95 US Urban Communities, 1987-2000. Journal of the American Medical Association 292, 2372. doi:10.1001/jama.292.19.2372

Belobaba, P., Odoni, A.R., Barnhart, C. (Eds.), 2009. The global airline industry. Wiley, Chichester, West Sussex, U.K.

Bey, I., Jacob, D.J., Yantosca, R.M., Logan, J.A., Field, B.D., Fiore, A.M., Li, Q., Liu, H.Y., Mickley, L.J., Schultz, M.G., 2001. Global modeling of tropospheric chemistry with assimilated meteorology: Model description and evaluation. Journal of Geophysical Research 106, 23073–23095. doi:10.1029/2001JD000807

Brunelle-Yeung, E., Masek, T., Rojo, J.J., Levy, J.I., Arunachalam, S., Miller, S.M., Barrett, S.R.H., Kuhn, S.R., Waitz, I.A., 2014. Assessing the impact of aviation environmental policies on public health. Transport Policy 34, 21–28. doi:10.1016/j.tranpol.2014.02.015

BTS, 2016a. U.S. Air Carrier Traffic Statistics: System Passenger - Passenger Enplanements (December 2014 - January 2016) [WWW Document]. URL http://www.rita.dot.gov/bts/acts/customized/table?adfy=2014&adfm=12&adty=2016&adtm=1&aos=0&artd&arti&arts=3&asts&astns&astt=3&ascc&ascp=1 (accessed 2.19.16).

BTS, 2016b. Air Carrier Financial Reports (Form 41 Financial Data): Schedule P-5.2 [WWW Document]. URL http://www.transtats.bts.gov/Fields.asp?Table_ID=297 (accessed 3.17.16).

Burgain, P., Feron, E., Clarke, J.P., 2008. Collaborative virtual queue: Fair management of congested departure operations and benefit analysis. Arxiv preprint arXiv:0807.0661.

Cai, H., Wang, M., Elgowainy, A., Han, J., 2012. Updated greenhouse gas and criteria air pollutant emission factors and their probability distribution functions for electricity

generating units (No. ANL/ESD/12-2). Argonne National Laboratory (ANL), Argonne, IL.

Caiazzo, F., Ashok, A., Waitz, I.A., Yim, S.H.L., Barrett, S.R.H., 2013. Air pollution and early deaths in the United States. Part I: Quantifying the impact of major sectors in 2005. Atmospheric Environment 79, 198–208. doi:10.1016/j.atmosenv.2013.05.081

Cao, Y., DeLaurentis, D., Sun, D., 2013. Benefit and Trade-Off Analysis of Continuous Descent Approach in Normal Traffic Conditions. Transportation Research Record: Journal of the Transportation Research Board 2325, 22–33. doi:10.3141/2325-03

Carr, F., Evans, A., Clarke, J.-P., Feron, E., 2002. Modeling and control of airport queueing dynamics under severe flow restrictions, in: Proceedings of the 2002 American Control Conference. IEEE, pp. 1314–1319.

Carruthers, D., McHugh, C., Jackson, M., Johnson, K., 2011. Developments in ADMS-Airport to take account of near field dispersion and applications to Heathrow Airport. International Journal of Environment and Pollution 44, 332. doi:10.1504/IJEP.2011.038434

Carslaw, D., Beevers, S., Ropkins, K., Bell, M., 2006. Detecting and quantifying aircraft and other on-airport contributions to ambient nitrogen oxides in the vicinity of a large international airport. Atmospheric Environment 40, 5424–5434. doi:10.1016/j.atmosenv.2006.04.062

Carter, W.P., 2000. Development and Evaluation of an Updated Detailed Chemical Mechanism for VOC Reactivity Assessment, in: Proceedings of the A&WMA 93rd Annual Conference and Exhibition.

CDC, NCHS, US DHHS, 2015. Underlying Cause of Death, 1999-2013 on CDC WONDER Online Database, released 2015.

Chai, T., Carmichael, G.R., Tang, Y., Sandu, A., Heckel, A., Richter, A., Burrows, J.P., 2009. Regional NOx emission inversion through a four-dimensional variational approach using SCIAMACHY tropospheric NO2 column observations. Atmospheric Environment 43, 5046–5055. doi:10.1016/j.atmosenv.2009.06.052

Chameides, W.L., Fehsenfeld, F., Rodgers, M.O., Cardelino, C., Martinez, J., Parrish, D., Lonneman, W., Lawson, D.R., Rasmussen, R.A., Zimmerman, P., Greenberg, J., Mlddleton, P., Wang, T., 1992. Ozone precursor relationships in the ambient atmosphere. J. Geophys. Res. 97, 6037–6055. doi:10.1029/91JD03014

Chang, T.Y., Rudy, S.J., 1993. Ozone-precursor relationships: a modeling study of semiempirical relationships. Environmental Science & Technology 27, 2213–2219. doi:10.1021/es00047a031

Clarke, J.-P.B., Ho, N.T., Ren, L., Brown, J.A., Elmer, K.R., Zou, K., Hunting, C., McGregor, D.L., Shivashankara, B.N., Tong, K.-O., Warren, A.W., Wat, J.K., 2004. Continuous Descent Approach: Design and Flight Test for Louisville International Airport. Journal of Aircraft 41, 1054–1066. doi:10.2514/1.5572

Clegg, S.L., Brimblecombe, P., Wexler, A.S., 1998. Thermodynamic Model of the System H+−NH4+−SO42-−NO3-−H2O at Tropospheric Temperatures. J. Phys. Chem. A 102, 2137–2154. doi:10.1021/jp973042r

Cleveland, W.S., Graedel, T.E., Kleiner, B., Warner, J.L., 1974. Sunday and Workday Variations in Photochemical Air Pollutants in New Jersey and New York. Science 186, 1037–1038. doi:10.1126/science.186.4168.1037

Cleveland, W.S., McRae, J.E., 1978. Weekday-weekend ozone concentrations in the northeast United States. Environmental Science & Technology 12, 558–563. doi:10.1021/es60141a010

Cohan, D.S., Hakami, A., Hu, Y., Russell, A.G., 2005. Nonlinear Response of Ozone to Emissions: Source Apportionment and Sensitivity Analysis. Environ. Sci. Technol. 39, 6739–6748. doi:10.1021/es048664m

Cohan, D.S., Tian, D., Hu, Y., Russell, A.G., 2006. Control Strategy Optimization for Attainment and Exposure Mitigation: Case Study for Ozone in Macon, Georgia. Environmental Management 38, 451–462. doi:10.1007/s00267-005-0226-y

De Neufville, R., Odoni, A.R. (Eds.), 2013. Airport systems: planning, design, and management, 2nd ed. McGraw-Hill, New York.

Decker, M., Brunke, M.A., Wang, Z., Sakaguchi, K., Zeng, X., Bosilovich, M.G., 2011. Evaluation of the Reanalysis Products from GSFC, NCEP, and ECMWF Using Flux Tower Observations. J. Climate 25, 1916–1944. doi:10.1175/JCLI-D-11-00004.1

Dedoussi, I.C., Barrett, S.R.H., 2014. Air pollution and early deaths in the United States. Part II: Attribution of PM2.5 exposure to emissions species, time, location and sector. Atmospheric Environment 99, 610–617.

Deonandan, I., Balakrishnan, H., 2010. Evaluation of strategies for reducing taxi-out emissions at airports, in: Proceedings of the AIAA Aviation Technology, Integration, and Operations Conference (ATIO). Fort Worth, TX, pp. 1–14.

Diez, D.M., Dominici, F., Zarubiak, D., Levy, J.I., 2012. Statistical Approaches for Identifying Air Pollutant Mixtures Associated with Aircraft Departures at Los Angeles International Airport. Environmental Science & Technology 46, 8229–8235. doi:10.1021/es3007172

Dockery, D.W., Pope, C.A., Xu, X., Spengler, J.D., Ware, J.H., Fay, M.E., Ferris, B.G., Speizer, F.E., 1993. An Association between Air Pollution and Mortality in Six U.S. Cities. New England Journal of Medicine 329, 1753–1759. doi:10.1056/NEJM199312093292401

Dodson, R.E., Andres Houseman, E., Morin, B., Levy, J.I., 2009. An analysis of continuous black carbon concentrations in proximity to an airport and major roadways. Atmospheric Environment 43, 3764–3773. doi:10.1016/j.atmosenv.2009.04.014

Dorbian, C.S., Wolfe, P.J., Waitz, I.A., 2011. Estimating the climate and air quality benefits of aviation fuel and emissions reductions. Atmospheric Environment 45, 2750–2759. doi:10.1016/j.atmosenv.2011.02.025

EDR Group, Gillen, D., ICF SH&E, Kramer aerotek, Inc., Mead & Hunt, 2015. The Role of U.S. Airports in the National Economy (No. 132), Airport Cooperative Research Program. Transportation Research Board.

Eyers, C.J., Norman, P., Middel, J., Plohr, M., Michot, S., Atkinson, K., 2004. AERO2k Global Aviation Emissions Inventories for 2002 and 2025 (No. QINETIQ/04/01113). QinetiQ Ltd, Farnborough, Hampshire.

FAA, 2015. Federal Aviation Administration Aviation System Performance Metrics [WWW Document]. URL https://aspm.faa.gov/ (accessed 10.30.15).

FAA, 2012. Destination 2025. Federal Aviation Authority.

FAA, 2011. FAA Terminal Area Forecast. Federal Aviation Authority.

FAA, 2010. Voluntary Airport Low Emission Program: Technical Report (No. DOT/FAA/AR-04/37). Office of Airports, Airport Planning and Programming.

FAA, 1988. Reduced and derated takeoff thrust procedures - Advisory Circular (No. AC 25-13). Federal Aviation Authority.

Fann, N., Lamson, A.D., Anenberg, S.C., Wesson, K., Risley, D., Hubbell, B.J., 2012. Estimating the National Public Health Burden Associated with Exposure to Ambient PM2.5 and Ozone. Risk Analysis 32, 81–95. doi:10.1111/j.1539-6924.2011.01630.x

Finlayson-Pitts, B.J., Pitts, J.N., 1993. Atmospheric Chemistry of Tropospheric Ozone Formation: Scientific and Regulatory Implications. Air & Waste 43, 1091–1100. doi:10.1080/1073161X.1993.10467187

Fiore, A.M., Jacob, D.J., Bey, I., Yantosca, R.M., Field, B.D., Fusco, A.C., Wilkinson, J.G., 2002. Background ozone over the United States in summer: Origin, trend, and contribution to pollution episodes. J.-Geophys.-Res. 107, ACH 11-1. doi:10.1029/2001JD000982

Fiore, A.M., Oberman, J.T., Lin, M.Y., Zhang, L., Clifton, O.E., Jacob, D.J., Naik, V., Horowitz, L.W., Pinto, J.P., Milly, G.P., 2014. Estimating North American background ozone in U.S. surface air with two independent global models: Variability, uncertainties, and recommendations. Atmospheric Environment 96, 284–300. doi:10.1016/j.atmosenv.2014.07.045

Freeman, O.E., Zerriffi, H., 2012. Carbon credits for cookstoves: Trade-offs in climate and health benefits. The Forestry Chronicle 88, 600–608. doi:10.5558/tfc2012-112

Gillani, N.V., Pleim, J.E., 1996. Sub-grid-scale features of anthropogenic emissions of NOx and VOC in the context of regional eulerian models. Atmospheric Environment, A

WMA International Specialty Conference on Regional Photochemical Measurements and Modeling 30, 2043–2059. doi:10.1016/1352-2310(95)00201-4

Gilmore, C.K., Barrett, S.R.H., Koo, J., Wang, Q., 2013. Temporal and spatial variability in the aviation NO$_x$ -related O$_3$ impact. Environmental Research Letters 8, 34027. doi:10.1088/1748-9326/8/3/034027

Grieshop, A.P., Marshall, J.D., Kandlikar, M., 2011. Health and climate benefits of cookstove replacement options. Energy Policy 39, 7530–7542. doi:10.1016/j.enpol.2011.03.024

Hakami, A., Odman, M.T., Russell, A.G., 2004. Nonlinearity in atmospheric response: A direct sensitivity analysis approach. Journal of Geophysical Research 109. doi:10.1029/2003JD004502

Hakami, A., Seinfeld, J.H., Chai, T., Tang, Y., Carmichael, G.R., Sandu, A., 2006. Adjoint Sensitivity Analysis of Ozone Nonattainment over the Continental United States. Environmental Science & Technology 40, 3855–3864. doi:10.1021/es052135g

Hall, C.T., Mondoloni, S.L., Thrasher, T.G., 2007. Estimating the Impact of Reduced Thrust Takeoff on Annual NOX Emissions at Airports (No. 69800). CSSI, Inc., Washington, DC.

Harker, M., O'Leary, P., 2008. Least squares surface reconstruction from measured gradient fields. IEEE, pp. 1–7. doi:10.1109/CVPR.2008.4587414

Hayes, S.R., Rosenbaum, A.S., Richmond, H.M., 1991. Ozone Risk Assessment Implementation: Transferring Risk Analysis Technology to Ozone Nonattainment Planning, in: Garrick, B.J., Gekler, W.C. (Eds.), The Analysis, Communication, and Perception of Risk, Advances in Risk Analysis. Springer US, pp. 567–583.

Henze, D.K., Hakami, A., Seinfeld, J.H., 2007. Development of the adjoint of GEOS-Chem. Atmospheric Chemistry and Physics 7, 2413–2433. doi:10.5194/acp-7-2413-2007

Henze, D.K., Seinfeld, J.H., Shindell, D.T., 2009. Inverse modeling and mapping US air quality influences of inorganic PM2.5 precursor emissions using the adjoint of GEOS-Chem. Atmos. Chem. Phys. 9, 5877–5903. doi:10.5194/acp-9-5877-2009

Herndon, S.C., Wood, E.C., Franklin, J., Miake-Lye, R., Knighton, W.B., Babb, M., Nakahara, A., Reynolds, T., Balakrishnan, H., 2012. Measurement of Gaseous HAP Emissions from Idling Aircraft as a Function of Engine and Ambient Conditions (No. ACRP Report 63), ACRP. Transportation Research Board.

Heuss, J.M., Kahlbaum, D.F., Wolff, G.T., 2003. Weekday/Weekend Ozone Differences: What Can We Learn from Them? Journal of the Air & Waste Management Association 53, 772–788. doi:10.1080/10473289.2003.10466227

Hileman, J.I., Stratton, R.W., Donohoo, P.E., 2010. Energy Content and Alternative Jet Fuel Viability. Journal of Propulsion and Power 26, 1184–1195. doi:10.2514/1.46232

Horn, B.K., 1990. Height and gradient from shading. International journal of computer vision 5, 37–75.

Hsu, H.-H., Adamkiewicz, G., Andres Houseman, E., Vallarino, J., Melly, S.J., Wayson, R.L., Spengler, J.D., Levy, J.I., 2012. The relationship between aviation activities and ultrafine particulate matter concentrations near a mid-sized airport. Atmospheric Environment 50, 328–337. doi:10.1016/j.atmosenv.2011.12.002

Hsu, H.-H., Adamkiewicz, G., Houseman, E.A., Zarubiak, D., Spengler, J.D., Levy, J.I., 2013. Contributions of aircraft arrivals and departures to ultrafine particle counts near Los Angeles International Airport. Science of The Total Environment 444, 347–355. doi:10.1016/j.scitotenv.2012.12.010

Hu, S., Fruin, S., Kozawa, K., Mara, S., Winer, A.M., Paulson, S.E., 2009. Aircraft Emission Impacts in a Neighborhood Adjacent to a General Aviation Airport in Southern California. Environmental Science & Technology 43, 8039–8045. doi:10.1021/es900975f

Hubbell, B.J., Hallberg, A., McCubbin, D.R., Post, E., 2005. Health-Related Benefits of Attaining the 8-Hr Ozone Standard. Environ Health Perspect 113, 73–82. doi:10.1289/ehp.7186

IAWG, 2015. Technical Support Document:-Technical Update of the Social Cost of Carbon for Regulatory Impact Analysis-Under Executive Order 12866. Environmental Protection Agency.

ICAO, 2012. EASA - ICAO Aircraft Engine Emissions Databank [WWW Document]. URL http://easa.europa.eu/environment/edb/aircraft-engine-emissions.php (accessed 9.4.12).

Idris, H., Clarke, J.-P., Bhuva, R., Kang, L., 2002. Queuing model for taxi-out time estimation. Air Traffic Control Quarterly 10, 1–22.

Idris, H.R., Delcaire, B., Anagnostakis, I., Hall, W.D., Pujet, N., Feron, E., Hansman, R.J., Clarke, J.-P., Odoni, A., 1998. Identification of flow constraint and control points in departure operations at airport systems, in: Proceedings of the AIAA Guidance, Navigation and Control Conference. Reston, VA, pp. 947–956.

Jacob, D.J., 1999. Introduction to atmospheric chemistry. Princeton University Press, Princeton, N.J.

James, W., O'Dell, P., 2005. Derated Climb Performance In Large Civil Aircraft. Presented at the 2005 Boeing Performance and Flight Operations Engineering Conference.

Jerrett, M., Burnett, R.T., Pope, C.A., Ito, K., Thurston, G., Krewski, D., Shi, Y., Calle, E., Thun, M., 2009. Long-Term Ozone Exposure and Mortality. New England Journal of Medicine 360, 1085–1095. doi:10.1056/NEJMoa0803894

Jiang, Z., Worden, J.R., Jones, D.B.A., Lin, J.-T., Verstraeten, W.W., Henze, D.K., 2015. Constraints on Asian ozone using Aura TES, OMI and Terra MOPITT. Atmospheric Chemistry and Physics 15, 99–112. doi:10.5194/acp-15-99-2015

Jordan, N.S., Hoff, R.M., Bacmeister, J.T., 2010. Validation of Goddard Earth Observing System-version 5 MERRA planetary boundary layer heights using CALIPSO. J. Geophys. Res. 115, D24218. doi:10.1029/2009JD013777

JP Fleets, 2009. JP Airline Fleets International 2009/2010 (CD-ROM), 45th ed. Flightglobal, Reed Business Information, Ltd., Surrey, UK.

Jung, Y., Hoang, T., Montoya, J., Gupta, G., Malik, W., Tobias, L., Wang, H., 2011. Performance evaluation of a surface traffic management tool for Dallas/Fort Worth International Airport, in: Ninth USA/Europe Air Traffic Management Research and Development Seminar. pp. 1–10.

Khadilkar, H., Balakrishnan, H., 2011a. Estimation of Aircraft Taxi-out Fuel Burn using Flight Data Recorder Archives, in: Proceedings of the AIAA Guidance, Navigation and Control Conference. AIAA, Portland, OR.

Khadilkar, H., Balakrishnan, H., 2011b. A Multi-Modal Unscented Kalman Filter for Inference of Aircraft Position and Taxi Mode from Surface Surveillance Data. Presented at the American Institute of Aeronautics and Astronautics ATIO, AIAA.

King, D., Waitz, I.A., 2005. Assessment of the effects of operational procedures and derated thrust on American Airlines B777 emissions from London's Heathrow and Gatwick airports (No. PARTNER-COE-2005-001). Partnership for Air Transportation Noise and Emissions Reductions.

Kinosian, J.R., 1982. Ozone-precursor relationships from EKMA diagrams. Environmental Science & Technology 16, 880–883. doi:10.1021/es00106a011

Konovalov, I.B., 2003. Nonlinear relationships between atmospheric aerosol and its gaseous precursors: Analysis of long-term air quality monitoring data by means of neural networks. Atmospheric Chemistry and Physics 3, 607–621.

Koo, B., Yarwood, G., Cohan, D.S., 2008. Higher-Order Decoupled Direct Method (HDDM) for Ozone Modeling Sensitivity Analyses and Code Refinements (No. 582-7-84005-NaN-7). Environ International Corporation, Novato, California.

Koo, J., Wang, Q., Henze, D.K., Waitz, I.A., Barrett, S.R.H., 2013. Spatial sensitivities of human health risk to intercontinental and high-altitude pollution. Atmospheric Environment 71, 140–147. doi:10.1016/j.atmosenv.2013.01.025

Koornneef, J., Ramirez, A., van Harmelen, T., van Horssen, A., Turkenburg, W., Faaij, A., 2010. The impact of CO2 capture in the power and heat sector on the emission of SO2, NOx, particulate matter, volatile organic compounds and NH3 in the European Union. Atmospheric Environment 44, 1369–1385. doi:10.1016/j.atmosenv.2010.01.022

Kopacz, M., Jacob, D.J., Henze, D.K., Heald, C.L., Streets, D.G., Zhang, Q., 2009. Comparison of adjoint and analytical Bayesian inversion methods for constraining Asian sources of carbon monoxide using satellite (MOPITT) measurements of CO columns. J. Geophys. Res. 114, D04305. doi:10.1029/2007JD009264

Krewski, D., Jerrett, M., Burnett, R.T., Ma, R., Hughes, E., Shi, Y., Turner, M.C., Pope III, C.A., Thurston, G., Calle, E.E., Thun, M.J., 2009. Extended follow-up and spatial analysis of the American Cancer Society study linking particulate air pollution and mortality (No. 140). Health Effects Institute, Boston, MA.

Kumar, N., Russell, A.G., 1996. Development of a computationally efficient, reactive subgrid-scale plume model and the impact in the northeastern United States using increasing levels of chemical detail. J. Geophys. Res. 101, 16737–16744. doi:10.1029/96JD01372

Lack, D.A., Cappa, C.D., Langridge, J., Bahreini, R., Buffaloe, G., Brock, C., Cerully, K., Coffman, D., Hayden, K., Holloway, J., Lerner, B., Massoli, P., Li, S.-M., McLaren, R., Middlebrook, A.M., Moore, R., Nenes, A., Nuaaman, I., Onasch, T.B., Peischl, J., Perring, A., Quinn, P.K., Ryerson, T., Schwartz, J.P., Spackman, R., Wofsy, S.C., Worsnop, D., Xiang, B., Williams, E., 2011. Impact of Fuel Quality Regulation and Speed Reductions on Shipping Emissions: Implications for Climate and Air Quality. Environmental Science & Technology 45, 9052–9060. doi:10.1021/es2013424

Lam, Y.F., Fu, J.S., 2009. A novel downscaling technique for the linkage of global and regional air quality modeling. Atmospheric Chemistry and Physics 9, 9169–9185. doi:10.5194/acp-9-9169-2009

Lapina, K., Henze, D.K., Milford, J.B., Huang, M., Lin, M., Fiore, A.M., Carmichael, G., Pfister, G.G., Bowman, K., 2014. Assessment of source contributions to seasonal vegetative exposure to ozone in the U.S. J. Geophys. Res. Atmos. 119, 324–340. doi:10.1002/2013JD020905

Lebron, F., 1975. A comparison of weekend-weekday ozone and hydrocarbon concentrations in the Baltimore-Washington metropolitan area. Atmospheric Environment (1967) 9, 861–863. doi:10.1016/0004-6981(75)90046-3

Lee, D.S., Pitari, G., Grewe, V., Gierens, K., Penner, J.E., Petzold, A., Prather, M.J., Schumann, U., Bais, A., Berntsen, T., 2010. Transport impacts on atmosphere and climate: Aviation. Atmospheric Environment 44, 4678–4734. doi:10.1016/j.atmosenv.2009.06.005

Lee, H., Balakrishnan, H., 2010. Optimization of airport taxiway operations at Detroit metropolitan airport (DTW), in: Proceedings of the AIAA Aviation Technology, Integration, and Operations Conference (ATIO).

Lee, J.J., 2005. Modeling aviation's global emissions, uncertainty analysis, and applications to policy (Thesis). Massachusetts Institute of Technology.

Levine, B.S., Gao, H.O., 2007. Aircraft Taxi-Out Emissions at Congested Hub Airports and Implications for Aviation Emissions Reduction in the United States, in: Transportation Research Board 86th Annual Meeting. Washington, DC, pp. 1–15.

Levy, J.I., Carrothers, T.J., Tuomisto, J.T., Hammitt, J.K., Evans, J.S., 2001. Assessing the public health benefits of reduced ozone concentrations. Environ Health Perspect 109, 1215–1226.

Levy, J.I., Woody, M., Baek, B.H., Shankar, U., Arunachalam, S., 2012. Current and Future Particulate-Matter-Related Mortality Risks in the United States from Aviation Emissions During Landing and Takeoff. Risk Analysis 32, 237–249. doi:10.1111/j.1539-6924.2011.01660.x

Liang, J., Jacobson, M.Z., 2000. Effects of subgrid segregation on ozone production efficiency in a chemical model. Atmospheric Environment 34, 2975–2982. doi:10.1016/S1352-2310(99)00520-8

Lin, J.-T., McElroy, M.B., 2010. Impacts of boundary layer mixing on pollutant vertical profiles in the lower troposphere: Implications to satellite remote sensing. Atmospheric Environment 44, 1726–1739. doi:10.1016/j.atmosenv.2010.02.009

Lissys, 2008. Piano-x Aircraft Emissions and Performance User's Guide. Woodhouse Eaves, United Kingdom.

Lobo, P., Hagen, D.E., Whitefield, P.D., 2012. Measurement and analysis of aircraft engine PM emissions downwind of an active runway at the Oakland International Airport. Atmospheric Environment 61, 114–123. doi:10.1016/j.atmosenv.2012.07.028

Lyon, T.F., Dodds, W.J., Bahr, D.W., 1979. Determination of the Effects of Ambient Conditions on CFM56 Aircraft Engine Emissions (No. 460379011).

MacLean, H.L., Lave, L.B., 2000. Environmental Implications of Alternative-Fueled Automobiles: Air Quality and Greenhouse Gas Tradeoffs. Environmental Science & Technology 34, 225–231. doi:10.1021/es9905290

Mahashabde, A., Wolfe, P., Ashok, A., Dorbian, C., He, Q., Fan, A., Lukachko, S., Mozdzanowska, A., Wollersheim, C., Barrett, S.R.H., Locke, M., Waitz, I.A., 2011. Assessing the environmental impacts of aircraft noise and emissions. Progress in Aerospace Sciences 47, 15–52. doi:10.1016/j.paerosci.2010.04.003

Megaritis, A.G., Fountoukis, C., Charalampidis, P.E., Pilinis, C., Pandis, S.N., 2013. Response of fine particulate matter concentrations to changes of emissions and temperature in Europe. Atmospheric Chemistry and Physics 13, 3423–3443. doi:10.5194/acp-13-3423-2013

Menut, L., 2003. Adjoint modeling for atmospheric pollution process sensitivity at regional scale. J. Geophys. Res. 108, 8562. doi:10.1029/2002JD002549

Menut, L., Vautard, R., Beekmann, M., Honoré, C., 2000. Sensitivity of photochemical pollution using the adjoint of a simplified chemistry-transport model. J. Geophys. Res. 105, 15379–15402. doi:10.1029/1999JD900953

Mesbah, S.M., Hakami, A., Schott, S., 2013. Optimal Ozone Reduction Policy Design Using Adjoint-Based NO$_x$ Marginal Damage Information. Environmental Science & Technology 47, 13528–13535. doi:10.1021/es402531n

Mesbah, S.M., Hakami, A., Schott, S., 2012. Improving NOx Cap-and-Trade System with Adjoint-Based Emission Exchange Rates. Environ. Sci. Technol. 46, 11905–11912. doi:10.1021/es302406y

Milford, J.B., Russell, A.G., McRae, G.J., 1989. A new approach to photochemical pollution control: implications of spatial patterns in pollutant responses to reductions in nitrogen oxides and reactive organic gas emissions. Environ. Sci. Technol. 23, 1290–1301. doi:10.1021/es00068a017

Miyoshi, C., Mason, K.J., 2013. The damage cost of carbon dioxide emissions produced by passengers on airport surface access: the case of Manchester Airport. Journal of Transport Geography 28, 137–143. doi:10.1016/j.jtrangeo.2012.12.003

Myhre, G., Shindell, D., Bréon, F.M., Collins, W., Fuglestvedt, J., Huang, J., Koch, D., Lamarque, J.F., Lee, D., Mendoza, B., others, 2013. Anthropogenic and natural radiative forcing. Climate change 423.

Nakahara, A., Reynolds, T.G., White, T., Maccarone, C., Dunsky, R., 2011. Analysis of a surface congestion management technique at New York JFK airport, in: AIAA Aviation Technology, Integration and Operations (ATIO) Conference, Virginia Beach, VA.

Nikoleris, T., Gupta, G., Kistler, M., 2011. Detailed estimation of fuel consumption and emissions during aircraft taxi operations at Dallas/Fort Worth International Airport. Transportation Research Part D: Transport and Environment 16, 302–308. doi:10.1016/j.trd.2011.01.007

Pappin, A.J., Hakami, A., 2013a. Attainment vs Exposure: Ozone Metric Responses to Source-Specific NOx Controls Using Adjoint Sensitivity Analysis. Environ. Sci. Technol. 47, 13519–13527. doi:10.1021/es4024145

Pappin, A.J., Hakami, A., 2013b. Source Attribution of Health Benefits from Air Pollution Abatement in Canada and the United States: An Adjoint Sensitivity Analysis. Environmental Health Perspectives 121, 572–579. doi:10.1289/ehp.1205561

Park, R.J., Jacob, D.J., Field, B.D., Yantosca, R.M., Chin, M., 2004. Natural and transboundary pollution influences on sulfate-nitrate-ammonium aerosols in the United States: Implications for policy. J. Geophys. Res. 109, D15204. doi:10.1029/2003JD004473

Parrington, M., Palmer, P.I., Henze, D.K., Tarasick, D.W., Hyer, E.J., Owen, R.C., Helmig, D., Clerbaux, C., Bowman, K.W., Deeter, M.N., Barratt, E.M., Coheur, P.-F., Hurtmans, D., Jiang, Z., George, M., Worden, J.R., 2012. The influence of boreal biomass burning emissions on the distribution of tropospheric ozone over North America and the North Atlantic during 2010. Atmos. Chem. Phys. 12, 2077–2098. doi:10.5194/acp-12-2077-2012

Partanen, A.-I., Laakso, A., Schmidt, A., Kokkola, H., Kuokkanen, T., Pietikäinen, J.-P., Kerminen, V.-M., Lehtinen, K.E.J., Laakso, L., Korhonen, H., 2013. Climate and air

quality trade-offs in altering ship fuel sulfur content. Atmospheric Chemistry and Physics Discussions 13, 21989–22024. doi:10.5194/acpd-13-21989-2013

Patterson, J., Noel, G.J., Senzig, D.A., Roof, C.J., Fleming, G.G., 2009. Analysis of Departure and Arrival Profiles Using Real-Time Aircraft Data. Journal of Aircraft 46, 1094–1103. doi:10.2514/1.42432

Pereira, C.J., Amiridis, M.D., 1995. NOx Control from Stationary Sources, in: Reduction of Nitrogen Oxide Emissions, ACS Symposium Series. American Chemical Society, pp. 1–13.

Pinder, R.W., Dennis, R.L., Bhave, P.V., 2008. Observable indicators of the sensitivity of PM2.5 nitrate to emission reductions—Part I: Derivation of the adjusted gas ratio and applicability at regulatory-relevant time scales. Atmospheric Environment 42, 1275–1286. doi:10.1016/j.atmosenv.2007.10.039

Pope, C.A., Burnett, R.T., Thun, M.J., Calle, E.E., Krewski, D., Ito, K., Thurston, G., 2002. Lung cancer, cardiopulmonary mortality, and long-term exposure to fine particulate air pollution. JAMA 287, 1132–1141. doi:10.1001/jama.287.9.1132

Pujet, N., Delcaire, B., Feron, E., 1999. Input-output modeling and control of the departure process of congested airports, in: Proceedings of the AIAA Guidance, Navigation, and Control Conference. pp. 9–11.

Reynolds, S.D., Blanchard, C.L., Ziman, S.D., 2004. Understanding the Effectiveness of Precursor Reductions in Lowering 8-Hr Ozone Concentrations—Part II. The Eastern United States. Journal of the Air & Waste Management Association 54, 1452–1470. doi:10.1080/10473289.2004.10471003

Reynolds, T., Ren, L., Clarke, J.-P., Burke, A., Green, M., 2005. History, Development and Analysis of Noise Abatement Arrival Procedures for UK Airports. American Institute of Aeronautics and Astronautics. doi:10.2514/6.2005-7395

Rienecker, M.M., Suarez, M.J., Todling, R., Bacmeister, J., Takacs, L., Liu, H.C., Gu, W., Sienkiewicz, M., Koster, R.D., Gelaro, R., others, 2008. The GEOS-5 Data Assimilation System–Documentation of Versions 5.0. 1, 5.1. 0, and 5.2. 0. NASA Tech. Memo 104606, 2008.

Russell, A.R., Valin, L.C., Cohen, R.C., 2012. Trends in OMI NO2 observations over the United States: effects of emission control technology and the economic recession. Atmos. Chem. Phys. 12, 12197–12209. doi:10.5194/acp-12-12197-2012

Sandu, A., Daescu, D.N., Carmichael, G.R., Chai, T., 2005. Adjoint sensitivity analysis of regional air quality models. Journal of Computational Physics 204, 222–252. doi:10.1016/j.jcp.2004.10.011

Schichtel, B.A., Husar, R.B., 2001. Eastern North American transport climatology during high- and low-ozone days. Atmospheric Environment 35, 1029–1038. doi:10.1016/S1352-2310(00)00370-8

Schürmann, G., Schäfer, K., Jahn, C., Hoffmann, H., Bauerfeind, M., Fleuti, E., Rappenglück, B., 2007. The impact of NOx, CO and VOC emissions on the air quality of Zurich airport. Atmospheric Environment 41, 103–118. doi:10.1016/j.atmosenv.2006.07.030

Seemann, R., Langhans, S., Schilling, T., Gollnick, V., 2010. Modeling the Life Cycle Cost of Jet Engine Maintenance. Hamburg: Technische Universität Hamburg-Harburg.

Seinfeld, J.H., 1988. Ozone Air Quality Models. JAPCA 38, 616–645. doi:10.1080/08940630.1988.10466404

Seinfeld, J.H., Pandis, S.N., 2006. Atmospheric chemistry and physics: from air pollution to climate change, 2nd ed. John Wiley and Sons, Hoboken, NJ.

Sierra, A., Vanoye, A.Y., Mendoza, A., 2013. Ozone sensitivity to its precursor emissions in northeastern Mexico for a summer air pollution episode. Journal of the Air & Waste Management Association 63, 1221–1233. doi:10.1080/10962247.2013.813875

Sillman, S., 1999. The relation between ozone, NOx and hydrocarbons in urban and polluted rural environments. Atmospheric Environment 33, 1821–1845. doi:10.1016/S1352-2310(98)00345-8

Sillman, S., 1993. Tropospheric ozone: The debate over control strategies. Annual Review of Energy and the Environment 18, 31–56.

Simaiakis, I., Balakrishnan, H., 2012. Dynamic control of airport departures: Algorithm development and field evaluation, in: American Control Conference (ACC), 2012. IEEE, pp. 1695–1701.

Simaiakis, I., Balakrishnan, H., 2010a. Impact of Congestion on Taxi Times, Fuel Burn, and Emissions at Major Airports. Transportation Research Record: Journal of the Transportation Research Board 2184, 22–30. doi:10.3141/2184-03

Simaiakis, I., Balakrishnan, H., 2010b. Analysis and control of airport departure processes to mitigate congestion impacts. Transportation Research Record: Journal of the Transportation Research Board 22–30.

Simaiakis, I., Balakrishnan, H., 2009. Queuing models of airport departure processes for emissions reduction. American Institute of Aeronautics and Astronautics, 1801 Alexander Bell Dr., Suite 500 Reston VA 20191-4344 USA,.

Simaiakis, I., Balakrishnan, H., Khadilkar, H., Reynolds, T.G., Hansman, R.J., Reilly, B., Urlass, S., 2011. Demonstration of reduced airport congestion through pushback rate control, in: Proceedings of the 9th USA/Europe Air Traffic Management R&D Seminar. Berlin, Germany.

Simone, N.W., Stettler, M.E.J., Barrett, S.R.H., 2013. Rapid estimation of global civil aviation emissions with uncertainty quantification. Transportation Research Part D: Transport and Environment 25, 33–41. doi:10.1016/j.trd.2013.07.001

Singh, K., Eller, P., Sandu, A., Henze, D., Bowman, K., Kopacz, M., Lee, M., 2009. Towards the Construction of a Standard Adjoint GEOS-Chem Model, in: Proceedings of the 2009 Spring Simulation Multiconference, SpringSim '09. Society for Computer Simulation International, San Diego, CA, USA, p. 110:1–110:8.

Stadler, W., 1979. A survey of multicriteria optimization or the vector maximum problem, part I: 1776-1960. Journal of Optimization Theory and Applications 29, 1–52. doi:10.1007/BF00932634

Stettler, M.E.J., Boies, A.M., Petzold, A., Barrett, S.R.H., 2013. Global Civil Aviation Black Carbon Emissions. Environmental Science & Technology 130823150610008. doi:10.1021/es401356v

Stettler, M.E.J., Eastham, S., Barrett, S.R.H., 2011. Air quality and public health impacts of UK airports. Part I: Emissions. Atmospheric Environment 45, 5415–5424. doi:10.1016/j.atmosenv.2011.07.012

Tao, Z., Williams, A., Huang, H.-C., Caughey, M., Liang, X.-Z., 2007. Sensitivity of U.S. surface ozone to future emissions and climate changes. Geophysical Research Letters 34. doi:10.1029/2007GL029455

The Boeing Company, 2013. Boeing Current Market Outlook 2013–2032. Boeing, U.S.

Thielmann, A., Prévôt, A.S.H., Grüebler, F.C., Staehelin, J., 2001. Empirical ozone isopleths as a tool to identify ozone production regimes. Geophys. Res. Lett. 28, 2369–2372. doi:10.1029/2000GL012787

Thurston, G.D., Ito, K., 2001. Epidemiological studies of acute ozone exposures and mortality. J Expo Anal Environ Epidemiol 11, 286–294. doi:10.1038/sj.jea.7500169

Tonnesen, G.S., Dennis, R.L., 2000. Analysis of radical propagation efficiency to assess ozone sensitivity to hydrocarbons and NO_x : 1. Local indicators of instantaneous odd oxygen production sensitivity. Journal of Geophysical Research 105, 9213. doi:10.1029/1999JD900371

Tsimpidi, A.P., Karydis, V.A., Pandis, S.N., 2008. Response of fine particulate matter to emission changes of oxides of nitrogen and anthropogenic volatile organic compounds in the eastern United States. J Air Waste Manag Assoc 58, 1463–1473.

Tzimas, E., Mercier, A., Cormos, C.-C., Peteves, S.D., 2007. Trade-off in emissions of acid gas pollutants and of carbon dioxide in fossil fuel power plants with carbon capture. Energy Policy 35, 3991–3998. doi:10.1016/j.enpol.2007.01.027

Unal, A., Hu, Y., Chang, M.E., Talat Odman, M., Russell, A.G., 2005. Airport related emissions and impacts on air quality: Application to the Atlanta International Airport. Atmospheric Environment 39, 5787–5798. doi:10.1016/j.atmosenv.2005.05.051

US CENSUS, U.C.B., 2010. TIGER/Line® with Data [WWW Document]. URL https://www.census.gov/geo/maps-data/data/tiger-data.html (accessed 7.15.14).

US EIA, 2015. Weekly U.S. Gulf Coast Kerosene-Type Jet Fuel Spot Price FOB (Dollars per Gallon) [WWW Document]. URL http://www.eia.gov/dnav/pet/hist/LeafHandler.ashx?n=PET&s=EER_EPJK_PF4_RGC_DPG&f=W (accessed 10.18.15).

US EPA, 2015. About the AQS Database | AirData | US EPA [WWW Document]. URL http://www.epa.gov/air/data/aqsdb.html (accessed 7.9.11).

US EPA, 2014a. 2011 National Air Emissions Inventory.

US EPA, 2014b. SPECIATE [WWW Document]. URL http://www.epa.gov/ttnchie1/software/speciate/ (accessed 8.16.14).

US EPA, 2010. Guidelines for Preparing Economic Analyses (No. 240-NaN-10–1). United States Environmental Protection Agency, Washington, DC 20460.

US EPA, 2008a. Average In-Use Emissions from Heavy-Duty Trucks (No. EPA420-F-08-027).

US EPA, 2008b. Average Annual Emissions and Fuel Consumption for Gasoline-Fueled Passenger Cars and Light Trucks (No. EPA420-F-08-024). OTAQ.

USEPA, 2011. The Benefits and Costs of the Clean Air Act from 1990 to 2020. U.S. EPA Office of Air and Radiation.

Wagner, K.K., Wheeler, N., McNerny, D., 1992. The Effect of Emission Inventory Uncertainty on Urban Airshed Model Sensitivity to Emission Reductions. Presented at the Tropospheric Ozone: Nonattainment and Design Value Issues.

Walker, T.W., Jones, D.B.A., Parrington, M., Henze, D.K., Murray, L.T., Bottenheim, J.W., Anlauf, K., Worden, J.R., Bowman, K.W., Shim, C., Singh, K., Kopacz, M., Tarasick, D.W., Davies, J., von der Gathen, P., Thompson, A.M., Carouge, C.C., 2012. Impacts of midlatitude precursor emissions and local photochemistry on ozone abundances in the Arctic. J. Geophys. Res. 117, D01305. doi:10.1029/2011JD016370

Wang, H., Jacob, D.J., Le Sager, P., Streets, D.G., Park, R.J., Gilliland, A.B., van Donkelaar, A., 2009. Surface ozone background in the United States: Canadian and

Mexican pollution influences. Atmospheric Environment 43, 1310–1319. doi:10.1016/j.atmosenv.2008.11.036

West, J.J., Ansari, A.S., Pandis, S.N., 1999. Marginal PM25: Nonlinear Aerosol Mass Response to Sulfate Reductions in the Eastern United States. Journal of the Air & Waste Management Association 49, 1415–1424.

Westerdahl, D., Fruin, S., Fine, P., Sioutas, C., 2008. The Los Angeles International Airport as a source of ultrafine particles and other pollutants to nearby communities. Atmospheric Environment 42, 3143–3155. doi:10.1016/j.atmosenv.2007.09.006

Wey, C.C., Anderson, B.A., Wey, C., Miake-Lye, R.C., Whitefield, P., Howard, R., 2007. Overview on the Aircraft Particle Emissions Experiment (APEX). Journal of Propulsion and Power 23, 898–905. doi:10.2514/1.26406

Wey, C.C., Anderson, B.E., Hudgins, C., Wey, C., Li-Jones, X., Winstead, E., Thornhill, L.K., Lobo, P., Hagen, D., Whitefield, P., Yelvington, P.E., Herndon, S.C., Onasch, T.B., Miake-Lye, R.C., Joda Wormhoudt, Knighton, W.B., Howard, R., Bryant, D., Corporan, E., Moses, C., Holve, D., Dodds, W., 2006. Aircraft particle emissions experiment (APEX) (No. NASA/TM-2006-214382). NASA.

WHO, 2008. Health risks of ozone from long-range transboundary air pollution. World Health Organization, Regional Office for Europe, Copenhagen.

WHO, 2006. Health Risks of Particulate Matter from Long-range Transboundary Air Pollution; Joint WHO/Convention Task Force on the Health Aspects of Air Pollution (No. E88189). World Health Organization, Regional Office for Europe, Bonn.

Wolfe, P.J., Yim, S.H.L., Lee, G., Ashok, A., Barrett, S.R.H., Waitz, I.A., 2014. Near-airport distribution of the environmental costs of aviation. Transport Policy, Air Transportation and the Environment 34, 102–108. doi:10.1016/j.tranpol.2014.02.023

Woody, M., Haeng Baek, B., Adelman, Z., Omary, M., Fat Lam, Y., Jason West, J., Arunachalam, S., 2011. An assessment of Aviation's contribution to current and future fine particulate matter in the United States. Atmospheric Environment 45, 3424–3433. doi:10.1016/j.atmosenv.2011.03.041

Yantosca, B., Long, M., Payer, M., Cooper, M., 2012. GEOS–Chem v9–01–03 Online User's Guide. Atmospheric Chemistry Modeling Group, School of Engineering and Applied Sciences, Harvard University 29.

Yi, Y., Kimball, J.S., Jones, L.A., Reichle, R.H., McDonald, K.C., 2011. Evaluation of MERRA Land Surface Estimates in Preparation for the Soil Moisture Active Passive Mission. J. Climate 24, 3797–3816. doi:10.1175/2011JCLI4034.1

Yim, S.H.L., Lee, G.L., Lee, I.H., Allroggen, F., Ashok, A., Caiazzo, F., Eastham, S.D., Malina, R., Barrett, S.R.H., 2015. Global, regional and local health impacts of civil aviation emissions. Environ. Res. Lett. 10, 34001. doi:10.1088/1748-9326/10/3/034001

Yim, S.H.L., Stettler, M.E.J., Barrett, S.R.H., 2013. Air quality and public health impacts of UK airports. Part II: Impacts and policy assessment. Atmospheric Environment 67, 184–192. doi:10.1016/j.atmosenv.2012.10.017

Yu, K.., Cheung, Y.., Cheung, T., Henry, R.C., 2004. Identifying the impact of large urban airports on local air quality by nonparametric regression. Atmospheric Environment 38, 4501–4507. doi:10.1016/j.atmosenv.2004.05.034

Zavala, M., Lei, W., Molina, M.J., Molina, L.T., 2009. Modeled and observed ozone sensitivity to mobile-source emissions in Mexico City. Atmospheric Chemistry and Physics 9, 39–55.

Zaveri, R.A., Peters, L.K., 1999. A new lumped structure photochemical mechanism for large-scale applications. Journal of Geophysical Research 104, 30387. doi:10.1029/1999JD900876

Zhang, L., Jacob, D.J., Downey, N.V., Wood, D.A., Blewitt, D., Carouge, C.C., van Donkelaar, A., Jones, D.B.A., Murray, L.T., Wang, Y., 2011. Improved estimate of the policy-relevant background ozone in the United States using the GEOS-Chem global model with $1/2° \times 2/3°$ horizontal resolution over North America. Atmospheric Environment 45, 6769–6776. doi:10.1016/j.atmosenv.2011.07.054

Zhang, L., Jacob, D.J., Knipping, E.M., Kumar, N., Munger, J.W., Carouge, C.C., van Donkelaar, A., Wang, Y.X., Chen, D., 2012. Nitrogen deposition to the United States: distribution, sources, and processes. Atmospheric Chemistry and Physics 12, 4539–4554. doi:10.5194/acp-12-4539-2012

Zhang, Y., Wu, S.-Y., 2013. Fine Scale Modeling of Agricultural Air Quality over the Southeastern United States Using Two Air Quality Models. Part II. Sensitivity Studies and Policy Implications. Aerosol and Air Quality Research. doi:10.4209/aaqr.2012.12.0347

Zhao, B., Wang, S.X., Xing, J., Fu, K., Fu, J.S., Jang, C., Zhu, Y., Dong, X.Y., Gao, Y., Wu, W.J., Wang, J.D., Hao, J.M., 2015. Assessing the nonlinear response of fine particles to precursor emissions: development and application of an extended response surface modeling technique v1.0. Geosci. Model Dev. 8, 115–128. doi:10.5194/gmd-8-115-2015

Zhu, L., Henze, D.K., Cady-Pereira, K.E., Shephard, M.W., Luo, M., Pinder, R.W., Bash, J.O., Jeong, G.-R., 2013. Constraining U.S. ammonia emissions using TES remote sensing observations and the GEOS-Chem adjoint model. J. Geophys. Res. Atmos. 118, 3355–3368. doi:10.1002/jgrd.50166